SCUOLA DI DOTTORATO
UNIVERSITÀ DEGLI STUDI DI MILANO-BICOCCA

Department of

Environmental and Earth Sciences (DISAT)

PhD program: **Marine Sciences, Technology, and Management (MTM)** Cycle: **XXXVIII**

Poly(lactic) acid Microplastics: From Production and Characterization to Biological Interactions and Degradation

Surname: **FERRARI** Name: **Giorgia**

Registration number: **822781**

Tutor: **ATHANASSIOU Athanassia**

Supervisor: **FRAGOULI Despina**

Coordinator: **GALLI Paolo**

ACADEMIC YEAR

2024/2025

Table of Contents

Summary

Since the early twentieth century, the rapid development of polymer science and the massive expansion of plastic production have profoundly transformed human society. However, in recent decades, the uncontrolled growth of plastic manufacturing has also resulted in severe environmental consequences, including widespread pollution of water, air, and soil. Among the most concerning emerging pollutants are microplastics (MPs) and nanoplastics (NPs), defined as contaminants that are not routinely monitored yet possess the potential to enter ecosystems and exert adverse ecological and biological effects. Their environmental relevance is largely linked to their high bioavailability and the limited knowledge about their impact on living organisms.

This thesis focuses on poly(lactic acid) (PLA), a biopolymer that is increasingly recognized as one of the most important thermoplastic alternatives to petroleum-based plastics. PLA is already applied in a variety of industrial sectors, and its production and demand are rapidly growing (**Chapter 1**). Consequently, PLA-derived waste is expected to rise, raising concerns that it may contribute to pollution in a manner comparable to conventional plastics. Although PLA is marketed as a biodegradable polymer, its degradation occurs only under strictly controlled industrial composting conditions. In natural environments, by contrast, PLA tends to persist and behave similarly to traditional, non-biodegradable polymers. This suggests that the environmental release of PLA MPs and NPs will likely increase in the coming years, reinforcing the need to evaluate their fate and potential impacts.

Due to the lack of standard protocols in performing sampling, separation, concentration, and identification of real MPs and NPs environmental samples, studies on their environmental fate and on their interactions with living organisms require the use of model engineered particles, so particles that are formed in the laboratory through chemical and physical processes. In this thesis, we focus on

the top-down production of poly(lactic acid) (PLA) NPs and MPs (**Chapter 2**) using mechanical grinding and ball milling techniques under different conditions. Particles obtained through ball milling exhibited average sizes in the range of a few hundred nanometers, whereas grinding generated a much broader size distribution, spanning from several millimeters down to particles smaller than 50 µm. Following their characterization, PLA MPs were employed to evaluate potential physiological stress and alterations in oxidative balance in the coral *Pocillopora damicornis*. As described in **Chapter 3**, the mechanically ground MPs, after an appropriate size fractionation, displayed a broad size distribution, with 90% of the particles measuring ≤ 370 µm and 50% ≤ 192 µm. These particles exhibited irregular morphologies and rough surfaces, together with decreased crystallinity and molecular weight compared to the initial pellets. Coral colonies were then exposed for 72 hours to three MPs concentrations (5, 15, and 50 mg/L). No mortality or bleaching was detected under any treatment. However, colonies subjected to the highest concentration showed enhanced activity of the antioxidant enzyme glutathione reductase, although lipid peroxidation analysis indicated that the exposure did not induce significant oxidative damage. To obtain a more comprehensive understanding of PLA MPs interactions with corals, we also investigated the role of mucus secretion and ciliary movement in *Porites lutea* in capturing and interacting PLA MPs with a size ≤ 50 µm (**Chapter 4**). To carry out this study, a particle image velocimetry (PIV) setup combining light-sheet microscopy with a laminar flow chamber was used, allowing high-resolution visualization from both lateral and en face perspectives. The observations showed that the coral actively secreted mucus filaments and, through coordinated ciliary beating, generated vortical structures in the surrounding water. These processes facilitated the capture and aggregation of MPs, which could subsequently be either retained by the coral or released back into the water column. The results demonstrate that corals actively contribute to the capture of PLA MPs from the surrounding water.

Moreover, the growing concern about plastic pollution has prompted increasing attention to remediation strategies aimed at mitigating the persistence of these materials in natural environments. A major challenge remains the management of plastics at their end-of-life, since their accumulation and slow degradation contribute significantly to environmental concerns. In this context, understanding the degradation pathways of bioplastics such as poly(lactic acid) (PLA) is essential for evaluating their potential as more sustainable alternatives. **Chapter 5** investigates how different fabrication methods of PLA MPs influence their enzymatic degradation by a commercial lipase from *Aspergillus oryzae*. Mechanical fragmentation of industrial PLA pellets yielded particles with distinct physicochemical characteristics, which in turn affected their susceptibility to enzymatic attack. Degradation was associated with increased surface porosity and crystallinity, reduced molecular weight, and the formation of oxidized organic groups, confirming the lipase's effectiveness in breaking down PLA. These findings highlight that the biodegradation performance of PLA MPs is influenced by the fabrication method, emphasizing the need to consider particle production procedures when assessing MPs degradation.

1

General Introduction

Plastics are integral to modern society, yet their environmental impact is profoundly detrimental. The origin of plastics can be traced back to naturally occurring polymers, such as rubber and shellac, which served as precursors to synthetic alternatives. A major milestone was the invention of the first semi-synthetic plastic, Parkesine, by Alexander Parkes in 1862. Derived from cellulose treated with nitric acid, Parkesine exhibited versatile molding and shaping properties (Seymour and Kauffman, 1992). Another important breakthrough occurred in the early 20th century with the creation of Bakelite in 1907, the first fully synthetic plastic. Produced from phenol and formaldehyde, Bakelite possessed unique characteristics, including non-conductivity and heat resistance, which made it particularly suitable for electrical applications (Baker, 2018). The foundations laid in polymer chemistry during the 1930s and 1940s, exemplified by the development of nylon, polystyrene (PS), and polyethylene (PE), provided the basis for the modern plastics era. Yet, the true breakthrough in terms of production scale and societal impact occurred in the following decades. In the 1950s and 1960s, plastics underwent rapid industrial growth and became deeply embedded in everyday life. This expansion was largely sustained by the advent of advanced polymerization technologies and the industrial introduction of new polymers, including polypropylene (PP), high-density polyethylene (HDPE), and low-density polyethylene (LDPE), which profoundly transformed applications in packaging, household products, and the textile industry (Hossain et al., 2024). This development marked the advent of single-use plastics in the 20th century, representing a pivotal shift in consumer behavior. The widespread adoption of disposable items led to a substantial increase in plastic waste generation and raised growing concerns regarding their environmental impact. The same properties that make plastics durable also create significant challenges for end-of-life management, particularly

regarding marine pollution and the accumulation of non-biodegradable waste (Auta et al., 2017). Their production, largely dependent on fossil resources, contributes to increasing atmospheric CO_2 levels and intensifies climate change. Furthermore, the widespread use of petrochemical-based plastics poses substantial risks to biodiversity and human health due to pollution (Chowdhury et al., 2023). Despite their versatility, conventional plastics are inherently non-biodegradable, resulting in long-term accumulation in both terrestrial landfills and marine ecosystems (Provencher et al., 2019). These environmental pressures are further aggravated by the continuous growth in global plastic production, which reached 413.8 million tons in 2023 (Statista, 2023), combined with the fact that only 9% of plastic materials are recycled (OECD, 2022b). Each year, an estimated 1.7 million tons of plastic debris enter the oceans from river and coastline, further complicating global waste management strategies and posing additional threats to terrestrial resource production (OECD, 2022a). In response, the plastics industry has increasingly highlighted its commitment to the development of bioplastics and advanced recycling technologies as potential strategies to mitigate environmental impacts (Yadav et al., 2024).

Bioplastics have emerged as a sustainable alternative to conventional petroleum-based plastics within material science. According to European Bioplastics, a plastic material is defined as a bioplastic if it is either biobased, biodegradable, or features both properties. Bio-based polymers are produced from renewable resources and may consist entirely or only partially of bio-based content (Phadke and Rawtani, 2023), while biodegradable polymers are defined by their ability to undergo microbial degradation, ultimately converting into water, carbon dioxide, and biomass under appropriate environmental conditions (Souza and Fernando, 2016).

According to the classification system proposed by European Bioplastics (European bioplastics, 2019), bioplastics can be categorized into three main groups: i) biobased or partially biobased non-biodegradable plastics (e.g., biobased polyethylene, polypropylene, or polyethylene terephthalate), ii) biobased and biodegradable plastics (e.g., polylactic acid (PLA) and polyhydroxyalkanoates

(PHA)), and iii) petroleum-based biodegradable plastics (e.g., polybutylene adipate terephthalate (PBAT)). The importance of bioplastics lies in their potential to mitigate environmental problems associated with conventional plastics. Moreover, their versatility and adaptability allow for their application across diverse sectors, including food packaging, pharmaceuticals, and textiles (Bidari et al., 2023).

Most biodegradable bioplastics are polyesters, among which PLA and PHA stand out. Due to their versatility and compliance with international composting certification standards, these polymers are among the most widely used bioplastics and, together with PP exhibit the highest relative growth rates in industrial production (Naser et al., 2021). Furthermore, owing to its favorable mechanical properties, ease of processing, renewability, and non-toxicity, PLA is currently considered one of the most commercially promising thermoplastic bioplastics (Naser et al., 2021). In fact, as of 2024, global PLA production reached 2.4 million tons annually, with projections of 5.7 million tons by 2029 (Ishimwe, 2024).

PLA is produced through the fermentation of renewable feedstocks such as corn, cassava, potato, and sugarcane (Qi et al., 2017). Although it is classified and marketed as a biodegradable polymer, its biodegradability is largely restricted to industrial composting conditions. In natural environments—and particularly in marine ecosystems—PLA is expected to degrade much more slowly (DiGregorio, 2009).

Overall, the main challenge associated with both synthetic and biodegradable plastics lies in their inadequate management during and at the end of their life cycle. Given the vast scale of global plastic production, this issue represents a major environmental concern. Indeed, a significant portion of this waste ultimately enters marine environment where biotic and abiotic degradation processes break down plastic into micro- and nanofragments (Andrady et al., 2011; Arthur et al., 2009). In recent years, the widespread occurrence of MPs (plastic particles smaller than 5 mm) and NPs (fragments smaller than 100 nm) (Gewert et al., 2015) has emerged as a significant environmental concern due

to their high bioavailability and the largely unknown effects they may have on living organisms (Wright et al., 2020). Numerous studies have demonstrated that MPs, mostly derived from synthetic polymers, are widely distributed not only in natural environments but also in drinking water (Schymanski et al., 2018), seafood (Rummel et al., 2016), sea salt (Yang et al., 2015), and even honey (Mühlschlegel et al., 2017). More recently, MPs originating from PLA have been identified in sediments (Bancin et al., 2019), marine habitats (Kazour et al., 2019), and wastewater streams (Huang et al., 2023), raising increasing concerns about the consequences of PLA degradation in the environment (Liao and Chen, 2021). Such particles can interact with pollutants and organisms, thereby posing potential ecological and environmental threats (Ainali et al., 2022).

To address the environmental risks of MPs, different remediation strategies have been explored, including physical, chemical, and biochemical approaches. Methods like rapid sand filtration, dissolved air flotation, and membrane bioreactors achieve high removal rates (Ahmed et al., 2024), but their large-scale use is limited by high energy requirements, low selectivity, and reduced efficiency in capturing the smallest particles (Badola et al., 2022). As a more sustainable alternative, enhanced biodegradation is gaining attention as an effective solution. This process, mainly suited for bioplastics but also applicable to conventional plastics, exploits the ability of microorganisms such as bacteria, fungi, and algae to break down polymer chains (Chen et al., 2020). Enzymes like hydrolases, esterases, depolymerases, and lipases cleave chemical bonds in insoluble polymers, producing shorter chains that microorganisms can assimilate and transform into CO_2, H_2O, biomass, and energy (Yuan et al., 2020).

Considering the issues discussed, the aim of this thesis is to investigate and better understand the challenges related to the study and pollution of the marine environment by PLA fragments and to explore potential solutions through bioremediation.

To this end (**Chapter 2**), model engineered PLA MPs and NPs were produced using grinding and ball milling techniques. These particles were chemically and physically characterized prior to being employed in subsequent experiments. PLA MPs were then employed to assess potential physiological stress and disturbances in oxidative homeostasis in the coral *Pocillipora damicornis* (**Chapter 3**). To obtain a more comprehensive understanding of PLA MPs interactions, we also investigated the role of mucus secretion and ciliary movement in *Porites lutea* in capturing and interacting with these particles (**Chapter 4**). Finally, we reveal critical issues on the MPs biodegradation studies by evaluating how variations in the PLA MPs fabrication methods affect their enzymatic degradation process utilizing a commercial lipase enzyme from Aspergillus oryzae (**Chapter 5**).

1.1 Research questions of the thesis

The aim of this thesis is to investigate the potential effects of polylactic acid (PLA) microplastics across two main areas. The first focuses on the interactions between PLA microplastics (MPs) and corals, examining their impact on coral health as well as their interactions with coral mucus and cilia. The second area explores how different manufacturing processes of PLA MPs can influence their enzymatic biodegradation, providing insights into how production methods may affect the environmental persistence of these particles. By addressing both the biological interactions and the material-specific properties of PLA microplastics, this work aims to provide a comprehensive understanding of their ecological implications and degradation dynamics, leading to the following research questions:

1. What are the effects of PLA microplastics on overall coral health, including mortality, bleaching, and oxidative response?
2. Can PLA microplastics interact with coral mucus and cilia? Can corals actively remove PLA microplastics from the surrounding water?
3. Do different PLA MPs fabrication methods affect their susceptibility to enzymatic degradation?
4. Which particle characteristics resulting from different fabrication processes determine the efficiency of enzymatic degradation?

In order to answer these questions four main objectives are proposed:

1. Produce and characterize different types of PLA particles using a top-down approach (**Chapters 2–5**).
2. Assess the effects of laboratory-produced PLA microplastics on corals, evaluating their impact on coral health (**Chapter 3**).
3. Investigate the role of coral cilia and mucus in the removal of PLA microplastics from the surrounding water (**Chapter 4**).
4. Address existing knowledge gaps by examining how variations in microplastic fabrication methods applied to industrial PLA pellets can generate particles with distinct physicochemical properties, even when processing methods appear similar, and evaluate their enzymatic biodegradation (**Chapter 5**).

1.2 Manuscript outlines

Chapter 3: Unraveling the Impact of Bio-Based Poly(lactic) Acid Microplastics on *Pocillopora damicornis* (Cnidaria, Scleractinia)

Giorgia Ferrari, Enrico Montalbetti, Davide Seveso, Valerio Isa, Lavorano Silvia, Sergio Marras, Stefania Sganga, Riccardo Carzino, Athanassia Athanassiou, Despina Fragouli

Manuscript submitted

Chapter 4: Ciliary Dynamics and Mucus Mechanisms of Microplastic Trapping in *Porties lutea* (Cnidaria, Scleractinia)

Giorgia Ferrari, Cesar O. Pacherres, Michael Kühl, Despina Fragouli

Manuscript in preparation

Chapter 5: Enzymatic Degradation of Poly(lactic) Acid Microplastics: Influence of the Fabrication Method

Giorgia Ferrari, Christina N. Economou, Sergio Marras, Stefania Sganga, Nicola Tirelli, Athanassia Athanassiou, Despina Fragouli

Manuscript submitted

1.3 References

Ahmed, S. F., Islam, N., Tasannum, N., Mehjabin, A., Momtahin, A., Chowdhury, A. A., Almomani, F., Mofijur, M. (2024). Microplastic removal and management strategies for wastewater treatment plants. Chemosphere, 347, 140648. https://doi.org/10.1016/j.chemosphere.2023.140648

Ainali, N. M., Kalaronis, D., Evgenidou, E., Kyzas, G. Z., Bobori, D. C., Kaloyianni, M., Yang, X., Bikiaris, D. N., Lambropoulou, D. A. (2022). Do poly(lactic acid) microplastics instigate a threat? A perception for their dynamic towards environmental pollution and toxicity. Sci. Total Environ., 832, 155014. https://doi.org/10.1016/j.scitotenv.2022.155014

Andrady, A. L. (2011). Microplastics in the Marine Environment. Mar. Pollut. Bull., 62(8), 1596–1605. https://doi.org/10.1016/j.marpolbul.2011.05.030

Arthur, C., Baker, J. E., & Bamford, H. A. (2009). Proceedings of the International Research Workshop on the Occurrence, Effects, and Fate of Microplastic Marine Debris, September 9-11, 2008, University of Washington Tacoma, Tacoma, WA, USA.

Ashrafy, A., Liza, A. A., Islam, M. N., Billah, M. M., Arafat, S. T., Rahman, M. M., Rahman, Sk. M. (2022). Microplastics Pollution: A Brief Review of Its Source and Abundance in Different Aquatic Ecosystems. J. Hazard. Mater. Adv., 9, 100215. https://doi.org/10.1016/j.hazadv.2022.100215

Auta, H. S., Emenike, C. U., & Fauziah, S. H. (2017). Distribution and importance of microplastics in the marine environment: A review of the sources, fate, effects, and potential solutions. Environ. Int., 102, 165–176. https://doi.org/10.1016/j.envint.2017.02.013

Badola, N., Bahuguna, A., Sasson, Y., Chauhan, J. S. (2021). Microplastics removal strategies: A step toward finding the solution. Front. Environ. Sci. Eng., 16(1). https://doi.org/10.1007/s11783-021-1441-3

Bancin, L. J., Walther, B. A., Lee, Y.-C., Kunz, A. (2019). Two-dimensional distribution and abundance of micro- and mesoplastic pollution in the surface sediment of Xialiao Beach, New Taipei City, Taiwan. Mar. Pollut. Bull., 140, 75–85. https://doi.org/10.1016/j.marpolbul.2019.01.028

Baker, I. (2018). Bakelite. Fifty Materials That Make the World, 15–17. https://doi.org/10.1007/978-3-319-78766-4_4

Bidari, R., Abdillah, A. A., Ponce, R. A. B., & Charles, A. L. (2023). Characterization of Biodegradable Films Made from Taro Peel (Colocasia esculenta) Starch. Polymers, 15(2), 338. https://doi.org/10.3390/polym15020338

Cheng, J., Jacquin, J., Conan, P., Pujo-Pay, M., Barbe, V., George, M., Fabre, P., Bruzaud, S., Ter Halle, A., Meistertzheim, A.-L., Ghiglione, J.-F. (2021). Relative Influence of Plastic Debris Size and Shape, Chemical Composition and Phytoplankton-Bacteria Interactions in Driving Seawater Plastisphere Abundance, Diversity and Activity. Front. Microbiol., 11. https://doi.org/10.3389/fmicb.2020.610231

Chowdhury, M. A., Hossain, N., Badrudduza, M. D., & Rana, M. D. (2023). Development and characterization of natural sourced bioplastic for food packaging applications. Heliyon, 9(2), e13538. https://doi.org/10.1016/j.heliyon.2023.e13538

DiGregorio, B. E. (2009). Biobased Performance Bioplastic: Mirel. Chem. Biol., 16(1), 1–2. https://doi.org/10.1016/j.chembiol.2009.01.001

European bioplastics. (2019). Bioplastics. European Bioplastics E.V. https://www.european-bioplastics.org/bioplastics/

Gewert, B., Plassmann, M. M., & MacLeod, M. (2015). Pathways for degradation of plastic polymers floating in the marine environment. Environ. Sci.: Processes Impacts, 17(9), 1513–1521. https://doi.org/10.1039/c5em00207a

Hossain, M. T., Shahid, A., Mahmud, N., Habib, A., Rana, M. M., Khan, S., & Hossain, M. D. (2024). Research and application of polypropylene: a review. Discov. Nano, 19(1). https://doi.org/10.1186/s11671-023-03952-z

Huang, M., Wang, D., Zhang, S., Weng, Y., Li, K., Huang, R., Guo, Y., Jiang, C., Wang, Z., Wang, H., Meng, H., Lin, Y., Fang, M., & Li, J. (2023). Impacts of Polylactic Acid Microplastics on

Performance and Microbial Dynamics in Activated Sludge System. Sustain., 15(19), 14332–14332. https://doi.org/10.3390/su151914332

Ishimwe, S. (2024). *BIOPLASTICS MARKET DEVELOPMENT UPDATE 2024*. European Bioplastics E.V. https://www.european-bioplastics.org/bioplastics-market-development-update-2024/

Kazour, M., Jemaa, S., Issa, C., Khalaf, G., Amara, R. (2019). Microplastics pollution along the Lebanese coast (Eastern Mediterranean Basin): Occurrence in surface water, sediments and biota samples. Sci. Total Environ., 696, 133933. https://doi.org/10.1016/j.scitotenv.2019.133933

Lackner, M., Mukherjee, A., & Koller, M. (2023). What Are "Bioplastics"? Defining Renewability, Biosynthesis, Biodegradability, and Biocompatibility. Polymers, 15(24), 4695–4695. https://doi.org/10.3390/polym15244695

Liao, J., Chen, Q. (2021). Biodegradable plastics in the air and soil environment: Low degradation rate and high microplastics formation. J. Hazard. Mater., 418, 126329. https://doi.org/10.1016/j.jhazmat.2021.126329

Mühlschlegel, P., Hauk, A., Walter, U., Sieber, R. (2017). Lack of evidence for microplastic contamination in honey. Food Addit. Contam. Part A, 34(11), 1982–1989. https://doi.org/10.1080/19440049.2017.1347281

Naser, A. Z., Deiab, I., & Darras, B. M. (2021). Poly(lactic acid) (PLA) and polyhydroxyalkanoates (PHAs), green alternatives to petroleum-based plastics: a review. RSC Adv., 11(28), 17151–17196. https://doi.org/10.1039/D1RA02390J

OECD. (2022a). Global Plastics Outlook: Economic Drivers, Environmental Impacts and Policy Options. OECD. https://doi.org/10.1787/de747aef-en

OECD. (2022b, February 22). Plastic pollution is growing relentlessly as waste management and recycling fall short, says OECD. OECD. https://www.oecd.org/en/about/news/press-releases/2022/02/plastic-pollution-is-growing-relentlessly-as-waste-management-and-recycling-fall-short.html

Phadke, G., & Rawtani, D. (2023). Bioplastics as polymeric building blocks: Paving the way for greener and cleaner environment. Eur Polym. J., 199, 112453–112453. https://doi.org/10.1016/j.eurpolymj.2023.112453

Provencher, J. F., Ammendolia, J., Rochman, C. M., & Mallory, M. L. (2019). Assessing plastic debris in aquatic food webs: what we know and don't know about uptake and trophic transfer. Environ. Rev., 27(3), 304–317. https://doi.org/10.1139/er-2018-0079

Regulation - 2023/2055 – EN – EUR Lex. (2023). Europa.eu. http://data.europa.eu/eli/reg/2023/2055/oj

Schymanski, D., Goldbeck, C., Humpf, H.-U., Fürst, P. (2018). Analysis of microplastics in water by micro-Raman spectroscopy: Release of plastic particles from different packaging into mineral water. Water Res., 129, 154–162. https://doi.org/10.1016/j.watres.2017.11.011

Seymour, R. B., & Kauffman, G. B. (1992). The rise and fall of celluloid. J. Chem. Educ., 69(4), 311. https://doi.org/10.1021/ed069p311

Souza, V. G. L., & Fernando, A. L. (2016). Nanoparticles in food packaging: Biodegradability and potential migration to food—A review. Food Packaging and Shelf Life, 8, 63–70. https://doi.org/10.1016/j.fpsl.2016.04.001

Statista. (2025, February 28). Annual Production of Plastics Worldwide from 1950 to 2020. Statista. https://www.statista.com/statistics/282732/global-production-of-plastics-since-1950/

Wright, R. J., Erni-Cassola, G., Zadjelovic, V., Latva, M., & Christie-Oleza, J. A. (2020). Marine Plastic Debris: A New Surface for Microbial Colonization. Environ. Sci. Technol., 54(19), 11657–11672. https://doi.org/10.1021/acs.est.0c02305

Wright, S. L., Thompson, R. C., & Galloway, T. S. (2013). The Physical Impacts of Microplastics on Marine organisms: a Review. Environ. Pollut., 178, 483–492. https://doi.org/10.1016/j.envpol.2013.02.031

Yadav, K., & Nikalje, G. C. (2024). Comprehensive analysis of bioplastics: life cycle assessment, waste management, biodiversity impact, and sustainable mitigation strategies. PeerJ, 12, e18013–e18013. https://doi.org/10.7717/peerj.18013

Yuan, J., Ma, J., Sun, Y., Zhou, T., Zhao, Y., & Yu, F. (2020). Microbial degradation and other environmental aspects of microplastics/plastics. Sci. Total Environ., 715, 136968

2

Micro- and nanoplastic fabrication protocols

Microplastic (MPs) and nanoplastic (NPs) particles have emerged as a major environmental concern due to their widespread occurrence, persistence, and potential impacts on ecosystems and human health. Despite their ubiquity, understanding of their environmental fate and biological effects remains limited, largely because of the analytical challenges associated with detecting and characterizing MPs and NPs in complex environmental and biological matrices. Laboratory-produced reference particles are therefore essential for controlled experimental studies, as commercially available MPs and NPs often fail to represent the irregular morphologies and size distributions found in the environment. In this context, top-down mechanical techniques, such as grinding and ball milling, represent a feasible strategy to produce PLA-derived micro- (MPs) and nanoplastics (NPs) with environmentally relevant characteristics. In this thesis, novel experimental protocols were established and optimized for the generation of MPs and NPs from PLA pellets via this approach. These protocols enable reproducible fabrication of polydisperse particles of irregular shape, closely mimicking secondary plastic fragments found in natural environments. The resulting reference materials provide tools for investigating the environmental behavior and biological interactions of MPs and NPs, addressing a critical gap in the current understanding of plastic pollution.

2.1 Introduction

Microplastic particles represent one of the major environmental challenges of our time. Their widespread occurrence and interactions with surrounding ecosystems have raised significant environmental and health concerns. Owing to their persistence and high mobility, micro- and nanoplastics (MPs and NPs) have been detected across nearly all environmental compartments. Moreover, recent studies have confirmed their presence in plants (Li et al., 2020), animals (Zolotova et al., 2022), and even in human biological samples such as blood (Leslie et al., 2022), lungs (Jenner et al., 2022), and placenta (Ragusa et al., 2021). Despite the growing awareness of their ubiquity, a comprehensive understanding of the environmental fate and effects of MNPs remains limited. This knowledge gap largely arises from the considerable challenges associated with their detection and quantification in different environmental matrices. Because MNPs generally occur at very low concentrations, their identification and characterization require concentration and separation from environmental or biological matrices through complex analytical protocols involving multiple digestion and filtration steps—procedures that can easily result in particle loss or contamination (Dimante-Deimantovica et al., 2022; Koelmans et al., 2019). The difficulty of isolating MPs and NPs from environmental samples, combined with the limited selection of commercially available reference materials, has driven many researchers to produce laboratory reference particles to overcome these analytical constraints. However, when relying on commercially available MPs and NPs for experimental studies, several limitations arise. Among them, the most important one relies on the fact that these materials are often pristine, spherical, and monodisperse, and therefore may not accurately represent the fragmented and weathered particles commonly found in natural environments (Rozman et al., 2022; Gouin et al., 2022).

Therefore, a growing number of research groups focus on the development of their own test and reference MPs and NPs. In this context, two main production strategies are commonly adopted: chemical bottom-up and physical top-down approaches, each characterized by specific advantages and drawbacks in terms of the range and properties of the resulting particles.

Bottom-up methods rely on the controlled synthesis of MPs and NPs from smaller precursors, commonly through monomer polymerization (Ali et al., 2023) or by inducing precipitation from polymer solutions (Benzo et al., 2025). These chemical approaches provide greater control over particle size and composition (Abid et al., 2022), typically producing nano- or low micrometer-range particles, in contrast to the broader distributions obtained with top-down processes. Their high yield and reproducibility make them particularly suitable for large-scale MPs and NPs production. Nevertheless, a major limitation of bottom-up techniques is that the resulting particles are generally spherical, differing from the irregular morphologies observed in environmentally derived MPs and NPs. Additionally, incomplete removal of surfactants, solvents, precursors, or initiators used during synthesis may introduce contaminants that can bias subsequent analyses (Reynaud et al., 2022).

Top-down approaches rely on mechanical and thermal processes that physically fragment plastics into smaller particles, leading to the formation of MPs and NPs (Song et al., 2018; Enfrin et al., 2020). Common techniques within this category include grinding, milling, sonication, laser ablation, and sanding. Among these, grinding and milling are the most frequently applied, as they use mechanical forces to reduce the size of macroscopic plastics—typically through rotary blades (Jiménez-Arroyo et al., 2023) or spheres operating within a sealed chamber (McColley et al., 2023) (Figure 2.1). The random orientation of the applied stresses during fragmentation produces irregular and polydisperse particles, offering a more realistic representation of environmentally relevant MPs and NPs, making them well suited for producing reference materials and for studies on their environmental and biological fate.

Grinding includes a variety of techniques that rely on shear, compression, or cutting forces. One common example is the use of blade-based instruments, such as knife or cutting mills (Arce et al., 2025; Kristen et al., 2016), in which rotating blades interact with stationary edges to achieve controlled particle size reduction. This approach is particularly suitable for tough or elastic materials, including polymer pellets. Another category of grinders is the impact-shear type, exemplified by high-speed rotor mills, which combine centrifugal acceleration and shearing forces to efficiently reduce particle size (Lionetto et al., 2021).

On the one hand, grinder equipped with multiple blades can process thick and hard polymers and are widely used for rough and medium size reduction (Macko, 2012). These grinders rely solely on shearing and cutting forces, and decreasing the mesh size typically results in a narrower particle size distribution (Kristen et al., 2016).

In contrast, high-speed rotor mills utilize centrifugal force to propel particles outward from the grinding chamber at high energy, causing initial fragmentation upon impact with the wedge-shaped rotor teeth rotating at high speed. Subsequently, the polymer particles are further reduced in size through the shearing action occurring between the rotor and the surrounding ring sieve (Lionetto et al., 2021). However, to achieve particle sizes in the nanometer range, additional processing steps such as ball milling are required.

Ball milling consists in mixing granules with inorganic beads, either in the presence of a liquid medium (wet ball milling) or in its absence (dry ball milling). The mechanical agitation that follows promotes rupture and fragmentation of the particulate material, leading to particle size reduction into the micro- submicron and nano range. However, the mechanical action of the milling balls generates friction and localized temperature increases within the milling chamber, leading to several limitations such as excessive heat buildup due to particle–media friction, as well as polymer melting, softening, or agglomeration (Astner et al., 2019; Caldwell et al., 2021).

These effects hinder control over particle size and morphology and make it difficult to obtain fine and homogeneous powders.

To overcome these drawbacks, several mitigation strategies have been developed, such as cryomilling and wet milling. In cryomilling, the polymer is pre-cooled to very low temperatures (e.g., using liquid nitrogen) before or during the milling process. Cooling the material below its glass transition temperature (Tg) makes the polymer brittle, facilitating more efficient fragmentation (Ducoli et al., 2025). However, this approach requires specialized equipment, the handling of cryogenic fluids, and involves higher operational costs.

In wet milling, the process is carried out in the presence of a liquid medium—typically water, ethanol, or another inert solvent. The liquid acts as a heat sink, dissipating from the thermal energy generated by mechanical forces and thereby preventing thermal degradation or melting of the plastic polymers (Astner et al., 2019).

Moreover, to enhance the production yield of MPs and NPs, multi-step milling strategies are often employed. These typically begin with a coarse grinding or pre-milling of bulk plastics to produce MPs, which subsequently serve as the feedstock for further size reduction processes (El Hadri et al., 2020; Astner et al., 2019; Ji et al., 2020).

The mechanical stress induced during milling can cause polymer chain scission, leading to a decrease in molecular weight and partial degradation—phenomena comparable to those observed during natural weathering and environmental degradation (Ravishankar et al., 2018). Moreover, the physicochemical characteristics of the resulting particles, including size distribution, molecular weight, and biodegradability, largely depend on the pretreatment applied to the starting material prior to milling. Because this method does not rely on complex chemical reactions or sophisticated instrumentation, it represents a highly versatile approach applicable to a wide range of polymers.

Importantly, ball milling achieves particle size reduction without compromising the chemical structure of the original material. Finally, by combining the process with post-milling size separation techniques, such as sieving and filtration, it is possible to obtain plastic particle fractions distributed across different size ranges.

For these reasons, top-down approaches—specifically grinding as well as wet and dry ball milling—were chosen for the production of PLA particles in this study. To this end, novel experimental protocols were developed for their production through the mechanical fragmentation, generating irregular morphologies that closely resemble those of environmentally derived MPs and NPs, formed through the breakdown of larger plastic debris.

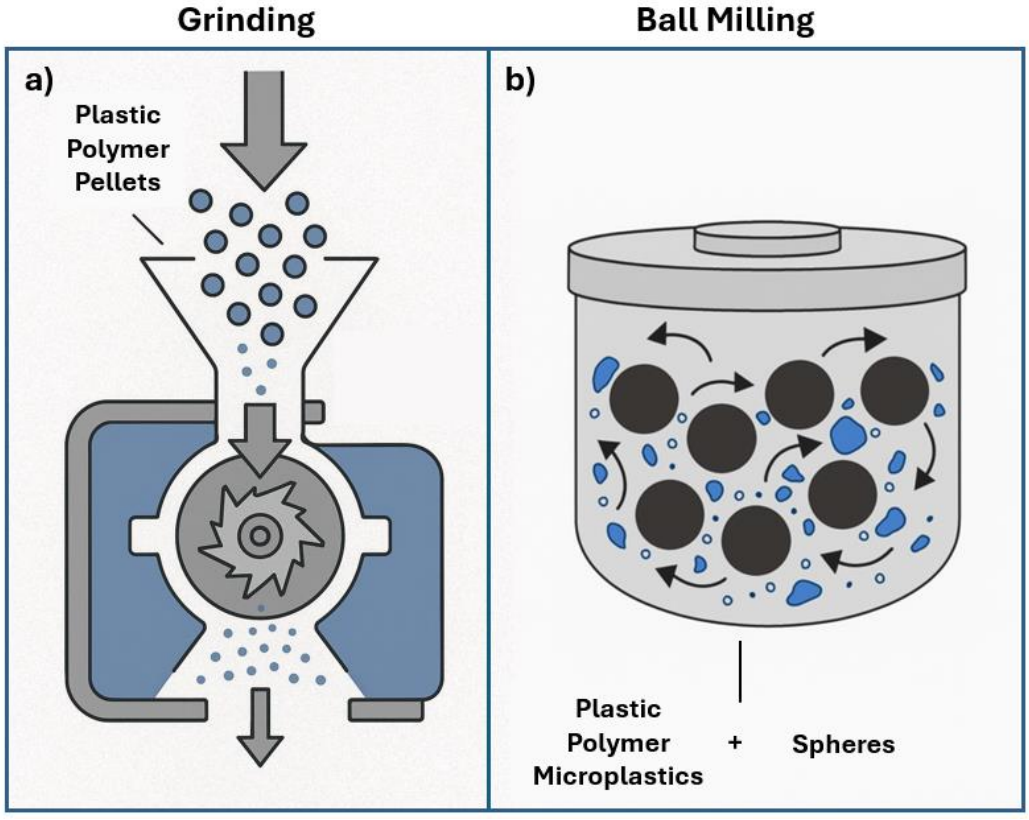

Figure 2.1. Schematic representation of the **a)** grinding and **b)** ball milling processes. In the right illustration, blue particles represent the PLA MPs, while black spheres indicate the milling spheres used during the ball milling procedure.

2.2 Materials and Methods

2.2.1 Materials

Semi-crystalline poly (lactic acid) (PLA) in the form of pellets with 4 mm average size was purchased by NatureWorks LLC (U.S.A) (commercial name: PLA4043D, Mn = 160.000 g/mol, density:1.24 g/cm^3). Deionized water was obtained from Milli-Q Advantage A10 purification system.

2.2.2 Particles Preparation and Characterization

PLA particles of various sizes were produced by using Dry mill – IKA – PILOTINA MC, electrical sieves with VWR Test Sieve 200x50 mm (mesh size 300 µm, 150 µm, and 50 µm) and Retsch Ball mill – Planetary ball mill – PM 100.

The particle size distribution of PLA microplastics was determined using a Particle Analyzer SYNC (Microtrac Retsch GmbH, Germany). The instrument operates on laser diffraction technology (780 nm red laser), which estimates particle size based on the light scattering pattern generated by particles dispersed in a liquid medium. Samples were prepared by suspending the ground particles in Milli-Q water, ensuring homogeneous dispersion prior to measurement. Analyses were performed at room temperature, with three replicate measurements for each sample. The system provides particle size distribution data within a measurable range of [specify range, e.g., 0.1–1000 µm]. The principal size parameters reported include D_{50} and D_{90}, representing the particle diameters at the 50th and 90th percentiles of the cumulative volume distribution, respectively. Data acquisition and processing were performed using Microtrac software, and the resulting distributions were further analyzed and plotted using OriginPro 2022.

Z-Potential (ζ-potential) of the formed NPs was performed using Zetasizer Nano ZS (Malvern Instruments) spectrometer.

Morphological analysis on the surface of the MPs was conducted by scanning electron microscopy (SEM, JEOL JSM-6490LA) at an acceleration voltage of 10 kV after coating the samples with a 10-nm Au layer using a high-resolution sputter coater (Cressington 208 HR). The morphology of the NPs was examined using a field emission scanning electron microscope (*ZEISS Gemini SEM 560*, Carl Zeiss Microscopy GmbH, Germany). Images were acquired in high-vacuum mode using an InLens detector, with an accelerating voltage of 2.0 kV and a working distance of 2.5 mm.

The size distribution and concentration of PLA nanoplastics (NPs) were determined using a Nanoparticle Tracking Analyzer (NTA, NanoSight, Malvern Instruments Ltd., UK) equipped with NTA software version 3.4 Build 3.4.4. The suspensions were gently sonicated for a few minutes to prevent particle aggregation before analysis. Measurements were performed at room temperature (approximately 25 °C) using a 488 nm laser and a sCMOS camera. For each sample, three replicate videos were recorded under identical settings. Video data were analyzed with the NTA 3.4 Build 3.4.4 software, which tracks the Brownian motion of individual particles to calculate their hydrodynamic diameter using the Stokes–Einstein equation. Results are expressed as the mean particle diameter (nm) and particle concentration (particles/mL). Between each sample, the system was thoroughly flushed with Milli-Q water to prevent cross-contamination.

2.2.3 PLA MPs and NPs production

PLA MPs were produced through a grinding process using an IKA–PILOTINA MC mill, followed by sieving with an electrical sieve shaker (VWR Test Sieve, 200 × 50 mm) equipped with meshes of 300, 150, and 50 µm, depending on the desired particle size range.

Initially, PLA pellets with a diameter of approximately 4 mm were ground using the dry mill operating at 1500 rpm and equipped with a 1 mm sieve, resulting in grains smaller than 1 mm.

The resulting powder was then further processed through a finer sieve (750 µm) to obtain particles below 750 µm in size. Initially, an additional grinding step was carried out using a 500 µm sieve. The particles obtained from this process were used as feeding material for the first ball milling procedure (Procedure A). However, due to the considerable material loss observed during this step, the procedure was discontinued. Instead, PLA particles with size lower that 750 µm were subsequently sieved with an electrical sieve to obtain the MPs with different size fractions employed in the following experiments.

Specifically, to separate particles into distinct size fractions according to the intended experimental application, multiple electrical sieving steps were performed. For the MPs used in **Chapter 3**, which required particles within the 150–300 µm size range, the pre-ground powder (≤750 µm) was electrically sieved sequentially using 300 µm and 150 µm meshes. Particles retained on the final, 150 µm, sieve were collected for subsequent use.

For the MPs employed in **Chapter 4**, which required a finer fraction (≤50 µm), the same pre-ground powder (≤750 µm) was subjected to three consecutive electrical sieving steps with 300 µm, 150 µm, and 50 µm meshes. In this case, particles that passed through the final 50 µm sieve were collected and used for further analyses. Finally, for the experiments described in **Chapter 5**, three distinct types of PLA MPs were prepared, one by grinding and two by ball milling. The first type produced through a grinding process resulted in MPs with a particle size of ≤ 300 µm. To obtain this fraction, the pre-ground PLA powder (≤ 750 µm) was sieved using the electrical sieve shaker equipped with a 300 µm mesh. The particles that passed through the mesh were collected and used as one of the MPs types in the study.

The two remaining MPs types were obtained through ball milling procedures. In particular, the PLA MPs (≤ 300 µm) obtained from the grinding process previously described were subsequently used to produce two additional types of PLA MPs, designated as MPs_{Wet} (Procedure B) and MPs_{Dry} (Procedure D), depending on whether water was present or absent during their production. Moreover, further processing of the material obtained through Procedure B and D led to NPs fraction production.

Procedure D – MPs_{Dry} (Dry Ball Milling)

The production of PLA MPs through dry ball milling (Procedure D) was performed using a PM100 Retsch® planetary ball mill. A total of 2 g of PLA MPs (≤ 300 µm, obtained from the grinding process) were placed in a 50 mL zirconia (ZrO_2) jar together with 50 g of zirconia spheres (⌀ = 1 mm). Milling was carried out at 650 rpm for 5 hours, applying a 3 min milling / 7 min pause cycle to prevent excessive temperature increase inside the jar and, consequently, polymer melting.

After milling, the zirconia spheres were separated from the PLA MPs using an electrical sieve (VWR Test Sieve, 200 × 50 mm) equipped with a 300 µm mesh. The PLA MPs obtained were collected and stored for subsequent experiments.

Procedure B – MPs_{Wet} (Wet Ball Milling)

The wet ball milling procedure (Procedure B) was performed under the same operating conditions as the dry one, but in the presence of water. Specifically, 2 g of PLA MPs (≤ 300 µm) were placed in a 50 mL zirconia jar together with 50 g of zirconia spheres (⌀ = 1 mm) and 6 mL of Milli-Q water. Milling was conducted at 650 rpm for 5 hours, following the same 3 min milling -7 min pause cycle used for the dry process, to control temperature and avoid polymer melting.

At the end of milling, additional Milli-Q water was added to the mixture, which was then filtered through a hydrophilic cellulose acetate membrane (5 µm cutoff). This step produced two fractions: Solution A, containing water and PLA MPs ≤ 5 µm; Solid B, composed of zirconia spheres and PLA MPs > 5 µm.

Solid B was dried to remove residual water completely, and the dried material was subsequently sieved using the same procedure adopted for the dry milling process to recover the MPs_{Wet} fraction.

Further Processing for Both Procedures (B and D)

The ball milling technique, applied under both dry and wet conditions, was also used to produce NPs. The material obtained from both dry and wet milling was suspended in water and sequentially filtered through hydrophilic cellulose acetate filters, first with a 5 µm pore size and then with a 0.2 µm pore size, yielding a solution containing PLA NPs. To increase NP concentration, multiple milling cycles and filtered suspensions were combined and concentrated by rotary evaporation (water bath at 40 °C, 10 mbar).

2.3 Results and Discussion

Since the aim of the ball milling processes was to obtain both MPs and NPs, the optimization of the procedures was designed to account for the production of both fractions. As the generation of NPs through ball milling inherently produces a large amount of MPs, the yield of NPs significantly influenced the overall optimization process. he wet and dry ball milling processes were refined to ensure reproducibility and precise control over particle size distribution. This optimization led to the development of four distinct procedures, two of which (Procedures B and D) were subsequently selected as the standard protocols for producing MPs and NPs via ball milling (see Section 2.2.3).The optimization process aimed to identify conditions that maximize particle fragmentation while minimizing processing time and energy consumption, with particular attention to achieving a suitable balance between processing duration, material input, and yield. Several milling parameters were evaluated, including the material the number and size of the milling spheres, milling time, powder amount, and the presence or absence of liquid medium. Although longer milling times generally led to a higher yield of smaller particles, excessively prolonged runs were found to be inefficient in terms of both time and energy use. Therefore, the final set of parameters (as described above) was chosen as a compromise between efficiency, reproducibility, and practicality, ensuring the production of sufficient amounts of MPs and NPs within a reasonable time frame.

ZrO_2 was chosen as the material for both the jar and the milling spheres due to its excellent mechanical and chemical properties. This material is considerably hard (7.5 Mohs, approximately 1200 HV), ensuring minimal wear during milling and preserving both the spheres and the sample integrity. Although hard and brittle, zirconium oxide provides sufficient toughness for prolonged milling operations. Its chemical resistance and thermal stability make it ideal for grinding materials sensitive to moisture or chemical reactions, without contaminating the sample.

Overall, zirconium oxide offers efficiency, durability, and sample purity, making it the optimal choice for ball milling applications. The size of the spheres was selected based on the size of the starting polymer grains, as generally the spheres should be approximately three times larger than the largest particle. Regarding the overall milling time, based on previous studies (Lionetto et al., 2021; Caldwell et al., 2020), the process was initially set to alternate 3 minutes of milling with 7 minutes of pause, for a total duration of 5 hours (corresponding to 90 minutes of effective milling and 210 minutes of rest). The pause intervals were introduced to prevent overheating inside the milling jar.

In defining the remaining milling parameters, particular attention was given to the proportion of material and spheres inside the jar. According to the Retsch manual (Retsch, 2025, GmbH), for dry milling it is recommended to divide the jar contents into three equal portions of spheres, material, and air, whereas for wet milling, approximately 60% of the jar should be filled with spheres and 30% with the material to be milled. However, applying these proportions would have resulted in excessive material consumption. In fact, obtaining around 10 g of PLA particles of 300 µm through grinding and sieving required approximately 500 g of starting pellets. Therefore, processing about 20 g of PLA per session — approximately corresponding to one-third (or about 30%) of the jar volume — following the manufacturer's guidelines would have led to an unreasonably high use of both material and energy. For this reason, a reduced amount of material was used in each milling session to optimize efficiency while minimizing waste.

The amount of spheres used was based on the value recommended in the Retsch manual for dry ball milling and was extended to the wet milling procedure as well.

In light of this, four distinct ball milling procedures, labeled A, B, C, and D, were developed by varying process parameters.

Ball Milling Procedures – (A, B, C, and D)

Procedure A consisted of milling 5 g of PLA (500 µm) using 50 g of ZrO_2 spheres (3 mm diameter) in the presence of 6 mL of Milli-Q at 650 rpm. Based on previous literature (e.g., Lionetto et al., Caldwell et al.), the milling process was initially set to alternate 3 minutes of milling and 7 minutes of pause, for a total duration of 5 hours (corresponding to 90 minutes of effective milling and 210 minutes of rest). The pause intervals were introduced to prevent overheating inside the milling jar. The obtained materials was filtered through hydrophilic cellulose acetate filters, first with a 5 µm pore size and then with a 0.2 µm pore size, yielding a solution containing PLA NPs. As shown in Table 2.1, this protocol yielded 2.51×10^8 particles/mL with a mean size of 101.7 nm. Procedure A effectively reduced the PLA microparticles to the nanometric range within 90 minutes of cumulative milling.

Procedure B used the same milling time and pause ratio and filtration steps of Procedure A but modified other parameters: 50 g of 1 mm ZrO_2 spheres, 2 g of PLA (300 µm), and 6 mL of Milli-Q water, operated at 650 rpm for 5 h. Smaller PLA particles were used, (≤300 µm), obtained by sieving 750 µm PLA MPs using the electrical sieve, as the starting material. This choice not only increased the number of NPs produced but also reduced the overall amount of polymer required for each milling experiment. The smaller feeding material improved the milling efficiency. As reported in Table 2.1, this procedure resulted in an approximately two orders of magnitude increase (1.14×10^{10} particles/mL) in nanoplastic concentration compared to Procedure A.

Procedure C maintained the same experimental conditions as Procedure B but extended the total duration to 6 hours, preserving the 3min – 7min milling-to-pause ratio. This resulted in a total of 108 minutes of active milling and 360 minutes overall. Although a slight increase in nanoplastic yield was observed (Table 2.1) , the improvement was considered marginal relative to the additional time and energy consumption required.

Procedure D was performed under dry conditions, using 50 g of 1 mm ZrO_2 spheres and 2 g of PLA (≤300 μm) for 5 hours (3 min of milling – 7 min of pause) at 650 rpm, without the addition of water. To obtain the NP fraction, the material produced by dry milling was suspended in 50 mL of Milli-Q water and sequentially filtered through hydrophilic cellulose acetate filters, first with a 5 μm pore size and subsequently with a 0.2 μm pore size. As shown in Table 2.1, the resulting yield (1.88×10^8 particles/mL) confirmed that the presence of a liquid medium significantly enhances milling efficiency, leading to higher nanoplastic production within the same time frame.

To conclude, all the milling procedures effectively reduced the PLA MPs to the nanometric range. However, Procedures B and D were selected as final protocols both for the production of specific MPs used in the experiments described in **Chapter 5** and for achieving the most efficient generation of NPs.

Table 2.1. Experimental parameters and results of different ball milling procedures

Procedure	A	B	C	D
Starting material (µm)	500	300	300	300
ZrO_2 spheres (mm)	3	1	1	1
Milling condition	wet	wet	wet	dry
Milling parameters (min)	3 milling – 7 pause	3 milling – 7 pause	3 milling – 7 pause	3 milling – 7 pause
Milling time (min)	90	90	108	90
Overall milling time (h)	5	5	6	5
Concentration of NPs fractions (part./mL)	$2.51 \times 10^8 \pm 6.87 \times 10^6$	$1.14 \times 10^{10} \pm 7.88 \times 10^8$	$1.29 \times 10^{10} \pm 2.52 \times 10^8$	$1.88 \times 10^8 \pm 3.98 \times 10^6$
Mean size of NPs (nm)	101.8 ± 1.8 nm	121.9 ± 5.5 nm	130.6 ± 1.4 nm	106.0 ± 2.9
D90 (nm)	152.4 ± 4.7 nm	197.0 ± 7.5 nm	190.8 ± 9.0 nm	157.1 ± 4.7 nm

Grinding and milling represent a *top-down* mechanical approach, starting from bulk polymer materials and progressively breaking them down into smaller fragments through the application of shear, abrasion, or impact forces. In the context of plastic materials, grinding reduces macro-scale particles (pellets) into micro- and submicron particles by physically disrupting their structure without the need for chemical reagents. In summary, grinding is a widely used top-down process for producing polymeric particles with reduced dimensions and serves as a preliminary step before more energy-intensive methods such as ball milling. Figure 2.1a exemplarily shows particle size distributions of ground PLA MPs after both grinding and electrical sieving steps. In particular, the fabricated MPs have 90% (D90) of particles with a size ≤ 415 µm and 50% (D50) of particles with a size ≤ 189 µm.

Therefore the PLA MPs obtained after the grinding process exhibited high polydispersity, while their morphology was irregular with a broad size distribution range (Figure 2.1b). For a more detailed characterization of the MPs obtained through grinding and electrical sieving steps, see **Chapter 3 and 4**.

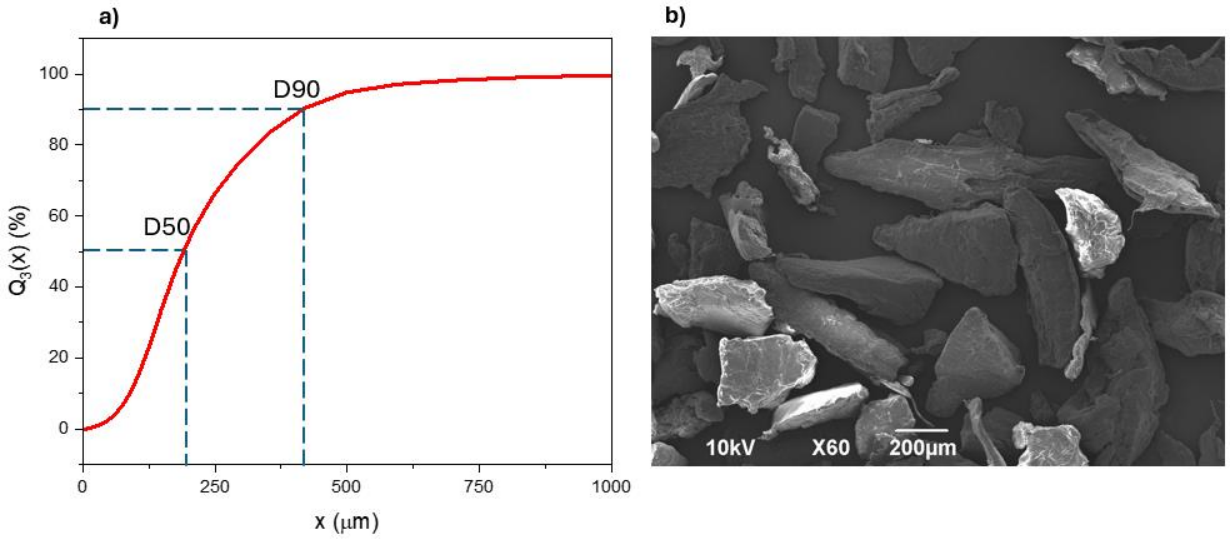

Figure 2.2. Particle size distribution curve of PLA MPs obtained after the grinding process (750 µm sieve) and the first sieving step using an electrical sieve with a 300 µm mesh size measured by granulometry. The plot shows the cumulative volumetric percentage $Q_3(x)$ (%) of particles with diameters less than or equal to x (µm). The red curve represents the average of three replicates. **b)** SEM image showing the irregular morphology of PLA MPs obtained after the grinding process.

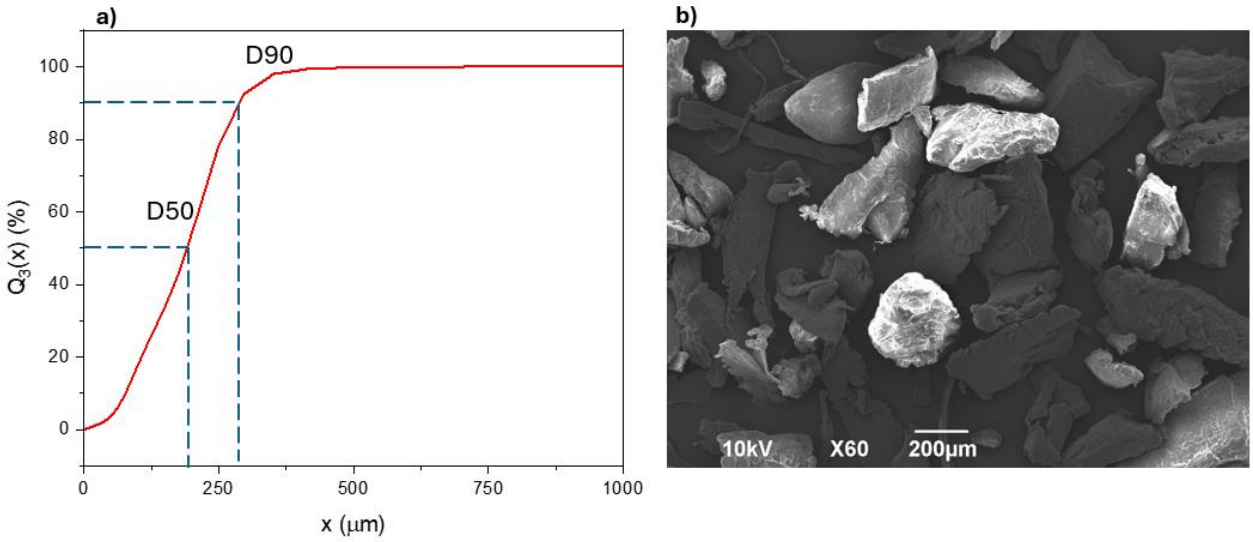

Figure 2.3. Particle size distribution curve of PLA MPs obtained after the ball milling process (exemplary wet) measured by granulometry. The plot shows the cumulative volumetric percentage $Q_3(x)$ (%) of particles with diameters less than or equal to x (μm). The red curve represents the average of three replicates. **b)** SEM image showing the irregular morphology of PLA MPs obtained after the ball milling process.

Figure 2.2a illustrates representative particle size distributions of PLA microplastics (MPs) produced by wet ball milling. Specifically, 90% (D90) of the particles have sizes ≤ 285 μm, while 50% (D50) are ≤ 191 μm. Thus, the PLA MPs obtained through ball milling also displayed high polydispersity, characterized by irregular shapes and a broad size distribution range (Figure 2.2b).

The surface morphology of the PLA MPs obtained after both wet and dry milling processes (MPs obtained through Procedure B and D) was characterized by SEM analysis. As illustrated in Figure 2.3b, the particles appeared either as thin, flake-like fragments or as more compact, rounded particles with uneven contours. Furthermore, the SEM images revealed that the PLA MPs possessed a heterogeneous and rough surface texture (Figure 2.4A-B), consistent with the mechanical fragmentation of larger polymer pieces during milling.

This process induced surface fractures, grooves, and cavities, typical features associated with the mechanical stress and shear forces exerted during grinding and milling. For a more detailed characterization of the MPs obtained through the dry and wet milling protocols, see **Chapter 5**.

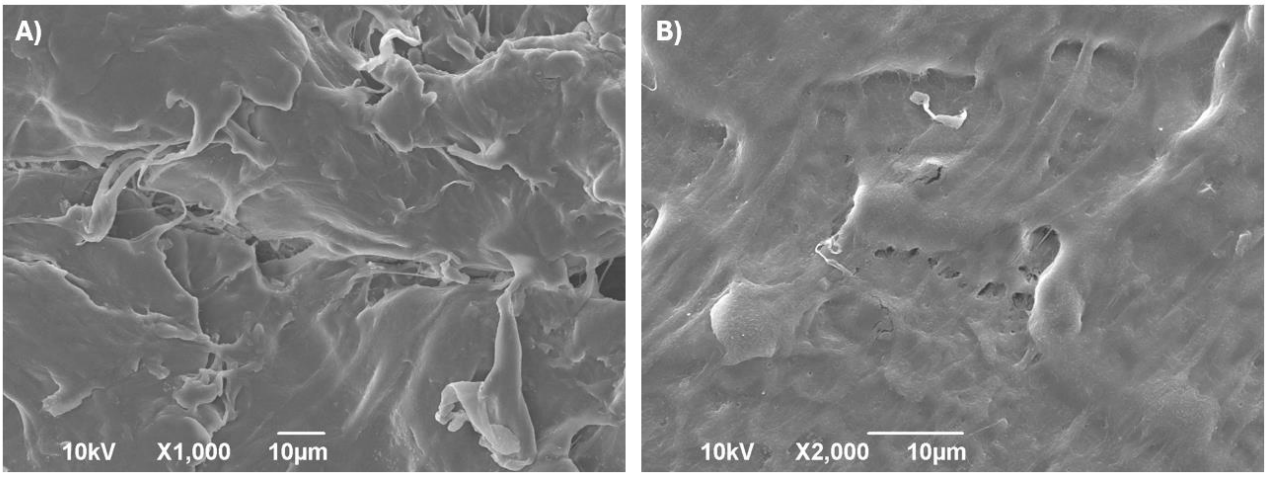

Figure 2.4 (A-B). Exemplary SEM images of PLA MPs obtained after the milling process at different magnifications, showing detailed surface features of the particles.

In addition to producing PLA MPs, the ball milling process also led to the formation of a nanosized fraction. To characterize and quantify these NPs generated during ball milling NTA was performed on the resulting suspension. As shown in Figure 2.5a and Table 2.2, the NTA results revealed that the majority of PLA NPs were smaller than 400 nm, with most of them falling within the sub-100 nm range. The analysis was conducted on a 40 mL sample prepared by pooling the suspensions produced in five independent wet ball milling runs. Overall, the nanoparticle suspension exhibited a concentration of $3.97\times10^{12} \pm 7.46\times10^{10}$ particles per mL, with an average particle diameter of 100.5 ± 0.4 nm.

These findings are consistent with the morphological observations obtained through SEM analysis (Figure 2.5b), which similarly revealed the presence of nanosized PLA particles within the same size range detected by NTA.

To assess the colloidal stability of the synthesized PLA NPs, their surface charge was measured. After the wet ball milling process, the NPs dispersed in water exhibited a zeta potential of −14.1 ± 1.1 mV at a pH around 6, as the mean value obtained from four independent samples (Figure 2.6), indicating that the suspension was relatively unstable due to the low magnitude of the zeta potential (ζ-potential) (Mo et al., 2016). Specifically, ζ-potential is a critical parameter that reflects the electrical properties at the interface of charged particles. Its value depends on both the characteristics of the nanoparticles and the properties of the surrounding medium. It is widely recognized that ζ-potential provides a useful estimate of the electrostatic interactions between dispersed particles (Pochapski et al., 2021) and is frequently employed as a quantitative indicator of charge-mediated colloidal stability (Sharaf et al., 2020). Accordingly, ζ-potential measurements are commonly used to evaluate the potential for aggregation or dispersion of nanoparticle suspensions (Kowalczyk et al., 2020; Zhu et al., 2020). Generally, nanoparticles with ζ-potential values between ±30 and ±40 mV are considered moderately stable. Taken together, the relatively low ζ-potential measured for our PLA NPs confirms that they are not particularly stable in aqueous suspension.

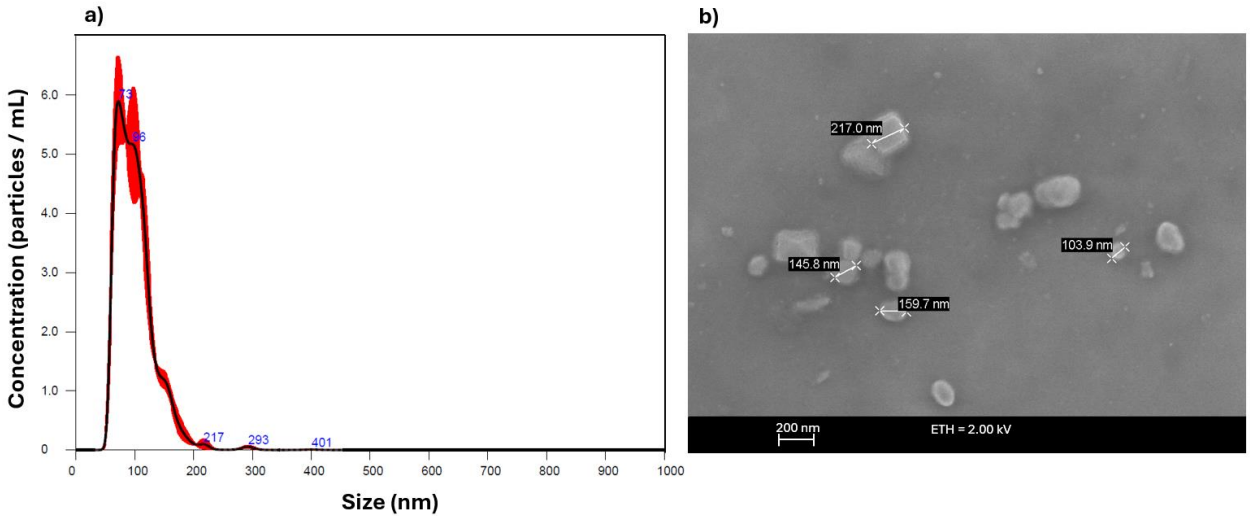

Figure 2.5. a) Average of 3 measurements of FTLA Concentration / size and **b)** SEM image of PLA NPs obtained after wet ball milling process.

Table 2.2. Sample statistics: average, mode and (10%, 50% and 90%) percentiles of the particles' size.

STATS: MEAN +/- STANDARD ERROR	
MEAN	100.5 +/- 0.4 nm
MODE	80.6 +/- 8.8 nm
D10	66.2+/- 0.6 nm
D50	94.5 +/- 1.3 nm
D90	142.8 +/- 2.6 nm
CONCENTRATION	3.97e+12 +/- 7.46e+10 particles/ml

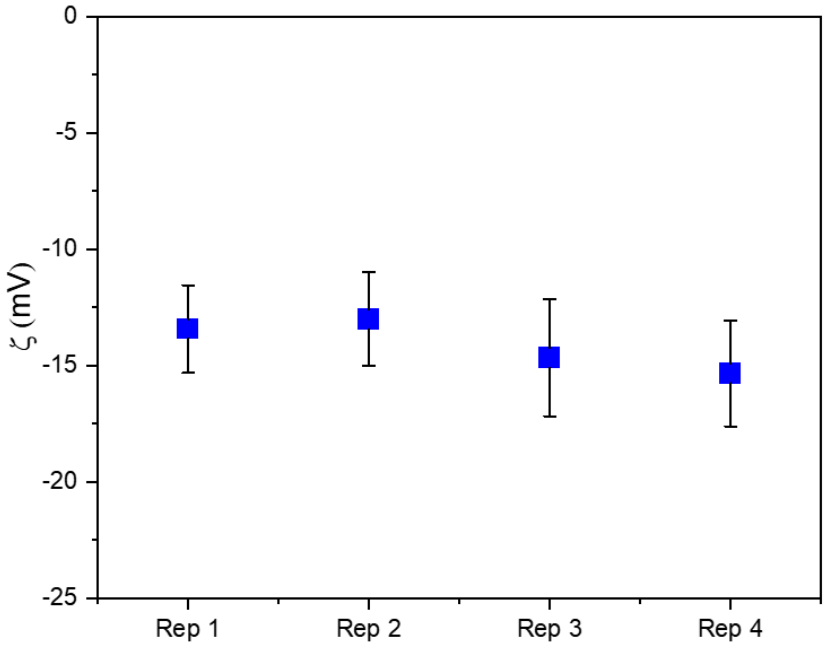

Figure 2.6. Scatter plot of the mean zeta potential values for four independent replicates (Rep1–Rep4), each calculated from three measurements. Individual points represent the mean of each replicate, and vertical error bars indicate the standard deviation (±SD) of the three measurements.

2.4 Conclusions

Given the challenges associated with sampling MPs and NPs directly from the environment for experimental studies, this work developed efficient and reproducible protocols (Procedure B and D) for the laboratory production of PLA MPs and NPs. This standardized approach allows for better control over particle characteristics, ensuring consistency across experimental applications. The specific characterization of the different PLA MPs produced and employed throughout this study is presented in detail in the following chapters, in relation to their respective experimental uses.

2.5 References

Abid, N., Khan, A. M., Shujait, S., Chaudhary, K., Ikram, M., Imran, M., Haider, J., Khan, M., Khan, Q., & Maqbool, M. (2022). Synthesis of nanomaterials using various top-down and bottom-up approaches, influencing factors, advantages, and disadvantages: A review. Adv. Colloid Interface Sci., 300(102597), 102597. https://doi.org/10.1016/j.cis.2021.102597

Ali, W., Ali, H., Gillani, S., Zinck, P., & Souissi, S. (2023). Polylactic acid synthesis, biodegradability, conversion to microplastics and toxicity: a review. Environ. Chem. Lett., 21. https://doi.org/10.1007/s10311-023-01564-8

Arce, C., & Krátký, L. (2025). Comparing the Impact of Knife and Ball Milling of Beech Chips on the Particle Size Characteristics. Waste Biomass Valorization, 1–14. https://doi.org/10.1007/s12649-025-03119-0

Astner, A. F., Hayes, D. G., O'Neill, H., Evans, B. R., Pingali, S. V., Urban, V. S., & Young, T. M. (2019). Mechanical formation of micro- and nano-plastic materials for environmental studies in agricultural ecosystems. Sci. Total Environ., 685, 1097–1106. https://doi.org/10.1016/j.scitotenv.2019.06.241

Benzo, M., Pérez Barthaburu, M. E., Pérez-Parada, A., Olivera, Á., & Fornaro, L. (2025). Developing environmentally relevant micro- and nanoplastics to assess removal efficiencies in wastewater treatment processes. Environ. Sci. Nano, 12(1), 748–761. https://doi.org/10.1039/d4en00250d

Caldwell, J., Lehner, R., Balog, S., Rhême, C., Gao, X., Septiadi, D., Weder, C., Petri-Fink, A., & Rothen-Rutishauser, B. (2021). Fluorescent plastic nanoparticles to track their interaction and fate in physiological environments. Environ. Sci. Nano, 8(2), 502–513. https://doi.org/10.1039/d0en00944j

Dimante-Deimantovica, I., Suhareva, N., Barone, M., Putna-Nimane, I., & Aigars, J. (2022). Hide-and-seek: Threshold values and contribution towards better understanding of recovery rate in microplastic research. MethodsX, 9, 101603. https://doi.org/10.1016/j.mex.2021.101603

Ducoli, S., Rani, M., Marchesi, C., Speziani, M., Zacco, A., Gavazzi, G., ... & Depero, L. E. (2025). Comparison of different fragmentation techniques for the production of true-to-life microplastics. Talanta, 283, 127106. https://doi.org/10.1016/j.talanta.2024.127106

El Hadri, H., Gigault, J., Maxit, B., Grassl, B., & Reynaud, S. (2020). Nanoplastic from mechanically degraded primary and secondary microplastics for environmental assessments. Nanoimpact, 17, 100206. https://doi.org/10.1016/j.impact.2019.100206

Enfrin, M., Lee, J., Gibert, Y., Basheer, F., Kong, L., & Dumée, L. F. (2020). Release of hazardous nanoplastic contaminants due to microplastics fragmentation under shear stress forces. J. Hazard. Mater., 384, 121393. https://doi.org/10.1016/j.jhazmat.2019.121393

Gouin, T., Ellis-Hutchings, R., Thornton Hampton, L. M., Lemieux, C. L., & Wright, S. L. (2022). Screening and prioritization of nano- and microplastic particle toxicity studies for evaluating human health risks – development and application of a toxicity study assessment tool. Microplast. Nanoplast., 2(1). https://doi.org/10.1186/s43591-021-00023-x

Jenner, L. C., Rotchell, J. M., Bennett, R. T., Cowen, M., Tentzeris, V., & Sadofsky, L. R. (2022). Detection of Microplastics in Human Lung Tissue Using μFTIR Spectroscopy. Sci. Total Environ., 831, 154907. https://doi.org/10.1016/j.scitotenv.2022.154907

Ji, Y., Wang, C., Wang, Y., Fu, L., Man, M., & Chen, L. (2020). Realistic polyethylene terephthalate nanoplastics and the size- and surface coating-dependent toxicological impacts on zebrafish embryos. Environ. Sci. Nano, 7(8), 2313–2324. https://doi.org/10.1039/d0en00464b

Jiménez-Arroyo, C., Tamargo, A., Molinero, N., Reinosa, J. J., Alcolea-Rodriguez, V., Portela, R., Bañares, M. A., Fernández, J. F., & Moreno-Arribas, M. V. (2023). Simulated gastrointestinal digestion of polylactic acid (PLA) biodegradable microplastics and their interaction with the gut microbiota. Sci. Total Environ., 902, 166003. https://doi.org/10.1016/j.scitotenv.2023.166003

Koelmans, A. A., Mohamed Nor, N. H., Hermsen, E., Kooi, M., Mintenig, S. M., & De France, J. (2019). Microplastics in freshwaters and drinking water: Critical review and assessment of data quality. Water Res., 155(1), 410–422. https://doi.org/10.1016/j.watres.2019.02.054

Kowalczyk, D., & Kamińska, I. (2020). Effect of pH and surfactants on the electrokinetic properties of nanoparticles dispersions and their application to the PET fibres modification. J. Mol. Liq., 320, 114426–114426. https://doi.org/10.1016/j.molliq.2020.114426

Kirsten, C., Lenz, V., Schröder, H. W., & Repke, J. U. (2016). Hay pellets—The influence of particle size reduction on their physical–mechanical quality and energy demand during production. Fuel Process. Technol., 148, 163–174. https://doi.org/10.1016/j.fuproc.2016.02.013

Leslie, H. A., van Velzen, M. J. M., Brandsma, S. H., Vethaak, D., Garcia-Vallejo, J. J., & Lamoree, M. H. (2022). Discovery and quantification of plastic particle pollution in human blood. Environ. Int., 163(107199), 107199. https://doi.org/10.1016/j.envint.2022.107199

Li, L., Luo, Y., Li, R., Zhou, Q., Peijnenburg, W. J. G. M., Yin, N., Yang, J., Tu, C., & Zhang, Y. (2020). Effective uptake of submicrometre plastics by crop plants via a crack-entry mode. Nat. Sustain., 3(11), 929–937. https://doi.org/10.1038/s41893-020-0567-9

Lionetto, F., Corcione, C. E., Rizzo, A., & Maffezzoli, A. (2021). Production and Characterization of Polyethylene Terephthalate Nanoparticles. Polymers (Basel), 13(21), 3745. https://doi.org/10.3390/polym13213745

Macko, M. (2012). Size reduction by grinding as an important stage in recycling. Post-Consum. Waste Recycl. Optimum Prod., 273–294.

McColley, C. J., Nason, J. A., Harper, B. J., & Harper, S. L. (2023). An assessment of methods used for the generation and characterization of cryomilled polystyrene micro- and nanoplastic particles. Microplast. Nanoplast., 3(1). https://doi.org/10.1186/s43591-023-00069-z

Mo, S., Shao, X., Chen, Y., & Cheng, Z. (2016). Increasing entropy for colloidal stabilization. Sci. Rep., 6(1), 36836. https://doi.org/10.1038/srep36836

Pochapski, D. J., Carvalho dos Santos, C., Leite, G. W., Pulcinelli, S. H., & Santilli, C. V. (2021). Zeta Potential and Colloidal Stability Predictions for Inorganic Nanoparticle Dispersions: Effects of Experimental Conditions and Electrokinetic Models on the Interpretation of Results. Langmuir, 37(45), 13379–13389. https://doi.org/10.1021/acs.langmuir.1c02056

Ragusa, A., Svelato, A., Santacroce, C., Catalano, P., Notarstefano, V., Carnevali, O., Papa, F., Rongioletti, M. C. A., Baiocco, F., Draghi, S., D'Amore, E., Rinaldo, D., Matta, M., & Giorgini, E. (2021). Plasticenta: First evidence of microplastics in human placenta. Environ. Int., 146(106274), 106274. https://doi.org/10.1016/j.envint.2020.106274

Ravishankar, K., Ramesh, P. S., Sadhasivam, B., & Raghavachari, D. (2018). Wear-induced mechanical degradation of plastics by low-energy wet-grinding. Polym. Degrad. Stab., 158, 212–219. https://doi.org/10.1016/j.polymdegradstab.2018.10.026

Retsch. (2025). Retsch.com. https://www.retsch.com/products/milling/ball-mills/planetary-ball-mill-pm-100/downloads/

Reynaud, S., Aynard, A., Grassl, B., & Gigault, J. (2022). Nanoplastics: From model materials to colloidal fate. Curr. Opin. Colloid Interface Sci., 57, 101528. https://doi.org/10.1016/j.cocis.2021.101528

Rozman, U., & Kalčíková, G. (2022). Seeking for a perfect (non-spherical) microplastic particle – The most comprehensive review on microplastic laboratory research. J. Hazard. Mater., 424, 127529. https://doi.org/10.1016/j.jhazmat.2021.127529

Sharaf, O. Z., Taylor, R. W., & Eiyad Abu-Nada. (2020). On the colloidal and chemical stability of solar nanofluids: From nanoscale interactions to recent advances. Phys. Rep., 867, 1–84. https://doi.org/10.1016/j.physrep.2020.04.005

Song, Y. K., Hong, S. H., Jang, M., Han, G. M., Jung, S. W., & Shim, W. J. (2018). Corrections to "Combined Effects of UV Exposure Duration and Mechanical Abrasion on Microplastic Fragmentation by Polymer Type." Environ. Sci. Technol., 52(6), 3831–3832. https://doi.org/10.1021/acs.est.8b00172

Zhu, H., Prince, E., Narayanan, P., Liu, K., Nie, Z., & Kumacheva, E. (2020). Colloidal stability of nanoparticles stabilized with mixed ligands in solvents with varying polarity. Chem. Commun., 56(58), 8131–8134. https://doi.org/10.1039/d0cc02592e

Zolotova, N., Kosyreva, A., Dzhalilova, D., Fokichev, N., & Makarova, O. (2022). Harmful Effects of the Microplastic Pollution on Animal health: a Literature Review. PeerJ, 10(10). https://doi.org/10.7717/peerj.13503

3

Unraveling the Impact of Bio-Based Poly(lactic) Acid Microplastics on *Pocillopora damicornis* (Cnidaria, Scleractinia)

Giorgia Ferrari[1,2], Enrico Montalbetti[2,3], Davide Seveso[2,3], Valerio Isa[2,3,4], Lavorano Silvia[4] Sergio Marras[5], Stefania Sganga[6,7], Riccardo Carzino[8], Athanassia Athanassiou[1] , Despina Fragouli[1*]

[1] Smart Materials, Istituto Italiano di Tecnologia (IIT), Genoa, Italy

[2]Department of Earth and Environmental Science, University of Milano Bicocca, Milano, Italy

[3] MaRHE Center (Marine Research and High Education Center), Magoodhoo Island, Faafu Atoll, Maldives

[4] Costa Edutainment SpA - Acquario di Genova, Area Porto Antico, Genoa, Italy

[5] Materials Characterization Facility, Istituto Italiano di Tecnologia (IIT), Genova, Italy

[6] Polymers and Biomaterials, Istituto Italiano di Tecnologia (IIT), Genova, Italy

[7] Nanobiointeractions & Nanodiagnostics, Istituto Italiano di Tecnologia (IIT), Genova, Italy

[8] Materials Characterization Facility, Istituto Italiano di Tecnologia (IIT), Genova 16163, Italy

Manuscript submitted

3.1 Abstract

Microplastics are widespread and persistent environmental pollutants that pose a significant threat to marine ecosystems such as tropical coral reefs. While the harmful effects of synthetic microplastics on reef-building corals are well documented, the impacts of their bio-based counterparts remain largely understudied. In this study, we investigate the chemical and physical properties of mechanically grounded polylactic acid microplastics and assess their short-term effects on the physiology and cellular oxidative state of the widespread scleractinian coral P. damicornis. The fabricated microplastics, obtained by mechanical grinding, exhibit a wide size distribution, with 90% of particles ≤ 370 µm and 50% ≤ 192 µm. They display irregular sizes and rough surfaces, along with reduced crystallinity and molecular weight compared to the original pellets. Coral colonies were exposed to three microplastic concentrations (5 mg/L, 15 mg/L, and 50 mg/L) for 72 hours, and no mortality or signs of bleaching were observed in all cases. Although colonies exposed to the higher concentration exhibited an increase in the activity of the antioxidant enzyme glutathione reductase, no significant cellular oxidative damage was caused by the microplastics, as the lipid peroxidation analysis indicated. This study provides a preliminary assessment of the physiological effects of polylactic acid microplastics on stony corals, emphasizing the need for further research on bio-based contaminants and their impacts on marine benthic organisms.

3.2Introduction

Although plastic has improved human life, its accumulation in the environment has become a major concern, with around 70% of global debris composed of plastic (Avio et al., 2017; Conkle et al., 2018). A significant portion enters marine ecosystems, where degradation processes generate micro- and nanoplastics (Andrady et al., 2011; Arthur et al., 2009). These particles are now widespread and represent a growing environmental issue due to their high bioavailability and largely unknown effects on organisms (Gewert et al., 2015; Wright et al., 2020).

Among them, sessile benthic organisms are at great risk of harmful interactions with MPs, as plastic particles tend to sink over time (Kowalski et al., 2016; Wang et al., 2016). The MPs surfaces attract microbial colonization, which reduces their buoyancy and leads to their eventual deposition on the sea floor (Zettler et al., 2013; Kaiser et al., 2017; Wright et al., 2020). Indeed, MPs have been shown to significantly impact marine sessile benthic organisms, by disrupting various key physiological functions, affecting their overall physiological homeostasis. Exposure to MPs can impair immune system functionality, leading to a reduction in hemocyte count, disturbances in oxidative balance, altered respiration, and increased energy consumption due to MP and associated chemical additives ingestion (Mkuye et al., 2022).

These findings highlight the complex and multifaceted impact of MPs on marine sessile benthic organisms, emphasizing the need for further research on their ecological consequences. So far most of the studies have been focused on MPs with synthetic polymer nature (Wright et al. 2013). However, in the recent years, bioplastics are continuously gaining space in the commercial field, as a promising alternative to conventional plastic, with polylactic acid (PLA), to be a key thermoplastic biopolymer.

Although PLA is considered biodegradable, its degradation occurs mainly in controlled environments like industrial composting, and in natural ecosystems it behaves similarly to conventional plastics. With increasing PLA production and use, the release of PLA-derived micro- and nanoplastics into the environment is expected to rise (Ainali et al., 2022)

Coral reefs contribute significantly to the global economy by providing coastal protection, food resources, tourism opportunities, and other goods and services (Costanza et al., 2014; Spalding et al., 2017). Central to these ecosystems are scleractinian corals, which form three-dimensional structures that support a wide variety of reef species underscoring the role of coral reefs as biodiversity hotspots (Graham and Nash, 2012). Soft corals are also essential components of coral reef benthic communities, representing the second most abundant group after hard corals and playing a significant role in supporting the high biodiversity characteristic of these ecosystems (Hutchings 2019; Garra et al., 2020.).

While research has highlighted the potential negative impacts of MPs on corals, the precise mechanisms driving these effects remain unclear. Specifically, toxicological studies on petroleum-based microplastics (MPs), ranging in size from a few micrometers to several hundred micrometers, have revealed significant biological effects. Polymers such as high-density polyethylene (HDPE) (Reichert et al., 2019), polyethylene (PE) (Martin et al., 2019), and polystyrene (PS) (Tang et al., 2018) have been shown to impair growth, elevate antioxidant enzyme activity, and stimulate mucus production. Montalbetti et al. (2022) conducted multivariate analyses on the soft coral Coelogorgia palmosa that revealed significant differences in the responses of corals to varying concentrations of PE MPs ranging from 180 to 212 µm. Corals exposed to high concentrations (50 mg/L and 70 mg/L) showed notable changes in superoxide dismutase (SOD), catalase (CAT), and lipid peroxidation (LPO) when compared to the lower concentration (10 mg/L) and control groups, revealing that oxidative stress is caused by the presence of these particles.

Vencato et al. (2021) reported that Coelogorgia palmosa can interact with PE MPs (180-212 µm) through both ingestion and adhesion. Additionally, an overproduction of mucus was observed, suggesting that mucus-mediated adhesion is the primary mechanism for trapping MPs.

Another study conducted by Isa et al. (2024) suggested also that PE MPs (180-212 µm) could exacerbate thermal stress effects on coral cellular homeostasis, even at environmental relevant concentration (1 mg/L). This study indicated that the synergistic interaction between elevated ocean temperatures and PE MPs led to significant disruptions in cellular homeostasis in P. damicornis also modifying the cell oxidative status. Previous studies have also demonstrated that petroleum-based MPs exposure induces the production of reactive oxygen species (ROS) at the cellular level in various benthic organisms (Jeong et al. 2016; Sutton et al. 2016; Rocha et al. 2020), including corals (Tang et al., 2018; Soriano-Santiago et al., 2013). These studies clearly show that oxidative stress is one of the main effects triggered in corals by exposure to plastic fragments. However, despite extensive research on the impact of synthetic materials and MPs on corals, the potential effects of bio-based polymers are still largely unknown.

In this study, we focus on the development of MPs derived from PLA, and on the assessment of their potential impact on coral physiology and health. Since MPs ranging from 150 to 500 µm are the most predominant in the environment (Alfaro-Núñez et al., 2021), PLA MPs were produced by mechanically grinding PLA pellets resulting in particles with 90% of the size distribution ≤ 370 µm and 50% ≤ 192 µm.. These MPs were then chemically and physically characterized, to highlight differences with the original material. To create more ecologically relevant exposure conditions, the MPs were pretreated in Artemia sp. enriched seawater before coral exposure. The reef-building coral P. damicornis, a widespread and ecologically significant species, was then exposed to three MPs concentrations (5 mg/L, 15 mg/L, and 50 mg/L) to evaluate potential physiological stress and disruptions of the oxidative homeostasis.

To assess oxidative stress, the activity of key antioxidant enzymes involved in ROS detoxification and neutralization, such as SOD, CAT, GR and GST, was measured. Additionally LPO was analyzed to determine cellular oxidative damage Coral bleaching was evaluated by quantifying chlorophyll a and c2 concentrations within coral tissues. This research provides a preliminary evaluation of the effects of PLA MPs on a specific hard coral species, providing valuable insights into the physiological and ecological consequences of biobased plastic exposure. By examining the interactions between PLA MPs and corals, this study established a foundation for future investigations into the broader impacts of bioplastics in marine ecosystems.

3.3 Materials and Methods

3.3.1 Materials

Semi-crystalline poly (lactic acid) (PLA) in the form of pellets with 4 mm average size was supplied by NatureWorks LLC (U.S.A) (commercial name: PLA4043D, Mn = 160.000 g/mol, density:1.24 g/cm^3). Artemia salina water medium was collected from the Genoa Aquarium in June 2024. Upon collection, the medium, containing an average concentration of 250 individuals/mL was filtered (5 µm nylon sieve) to remove the living organisms. All reagents and chemicals used were purchased from Sigma-Aldrich. Deionized water was obtained from Milli-Q Advantage A10 purification system.

3.3.2 MPs production

PLA MPs were produced by using Dry mill – IKA – PILOTINA MC and an electrical siever with VWR Test Sieve 200 x 50 mm (mesh size 300 and 150 µm). Initially, the 4 mm pellets were reduced to grains with size lower than 1 mm by the dry mill operating at 1500 rpm, equipped with a 1 mm sieve. The obtained powder was further processed through a finer sieve to obtain powder grain size lower than 750 mm. To isolate particles mostly in the 150–300 µm size range, the powder was subsequently sieved using an electrical siever (VWR Test Sieve, 200 x 50 mm) with a 300 µm mesh size, followed by a second sieving step with a 150 µm mesh size. Particles that did not pass through the final sieve were collected for further use. PLA MPs were exposed for 1 hour to Artemia salina water medium. Subsequently the treated PLA MPs were removed from the medium, rinsed using Milli-Q water, and allowed to dry at ambient conditions.

3.3.3 MPs characterization

Morphological analysis on the surface of the MPs was conducted by scanning electron microscopy (SEM) (JEOL JSM-6490LA SEM) using the secondary electrons detector with a 10 kV accelerating voltage and a load current of 78 μA. The MPs were attached to aluminum stubs by using carbon tape and coated with a 10 nm gold layer through a high-resolution sputter coater (Cressington 208 HR). Particle size and shape analysis was performed through laser diffraction and dynamic image analysis using the Particle Analyzer SYNC (wet operation Flowsync, Microtrac Retsch GmbH) assuming spherical geometry of the particles. The MPs were suspended in distilled water and the suspensions were sonicated in the equipment at 40 kHz at 100% of power for 120 s before analysis, to prevent any aggregation. The refractive indices of PLA MPs and water were 1.50 and 1.33 respectively. Diameters at the 50th percentile, D50, and at the 90th percentile, D90, were reported. Data analysis was performed with Microtrac and OriginPro 2022 software. Measurements were conducted at room temperature, and the samples were analyzed in triplicate.

A differential scanning calorimeter (DSC) (Discovery DSC 250 TA Instruments) was used to determine the thermal properties of the polymeric fragments. PLA MPs and reference pellets (3-5 mg) were placed in a Tzero aluminum pans and, after their accurate weighing, the measurements were performed under N_2 flow (50 mL min^{-1}) using conventional heating-cooling-heating scan cycles (from -20 °C to 200 °C) with a heating-cooling rate of 10 °C min^{-1}.

X-ray diffraction analyses were carried out on a Malvern-PANalytical 3rd generation Empyrean X-ray powder diffractometer. The instrument was equipped with a 1.8kW CuKα ceramic X-ray tube operating at 45 kV and 40 mA, iCore and dCore automated PreFIX optical modules, motorized Eulerian Cradle (chi, phi,x,y and z movements) and solid-state hybrid pixel PIXcel^{3D} area detector operating in 0D mode.

The XRD patterns were collected from 5° to 35° with a step size of 0.05°. A parallel beam configuration, including 0.04 rad soller slits and 0.28° parallel plate collimator on the diffracted beam and specific for samples characterized by an extremely irregular surface, was used. The acquisition was carried out in air at room temperature, using a zero-diffraction silicon substrate.

The degree of crystallinity $X_{c_{XRD}}$ was calculated using the equation:

$$X_{C_{XRD}} = \frac{A_c}{A_c + A_a} 100\% \qquad \text{Equation 3.1}$$

where $\mathbf{A_c}$ and $\mathbf{A_a}$ denote the integrated intensity of crystalline peaks and amorphous halo respectively, on the X-ray diffractograms. Data analysis was performed using HighScore Plus 5.2 software from Malvern Panalytical.

Gel permeation chromatography (GPC) was performed using an integrated OMNISEC system (Malvern Panalytical Ltd., UK) equipped with a PLgel 5 µm MIXED-D column in series with a PLgel 3 µm MIXED-E operating online at 35 °C and connected to a refractive index and light scattering detectors (Omnisec reveal, Malvern, UK). As eluent, tetrahydrofuran (THF) with 250 ppm of butylated hydroxytoluene (BHT) is used. The instrument is calibrated using PS (PolyCal standards, Malvern Panalytical Ltd., UK) 105 kDa narrow standard of known dispersity, intrinsic viscosity, and dn/dc. Before measurements, the PLA MPs were dissolved in chloroform for 4 h and then diluted 4 times in THF with 250 ppm of BHT to reach a concentration of 10 mg/mL. The samples were then mixed in a thermoshaker at 35 °C for 24 h and finally filtered with a 0.2 µm pore size PTFE filter. The analysis was conducted by injecting three times with a flow rate of 0.8 mL/min for 35 min. Data analysis was performed using OMNISEC software V11.32.

Infrared spectra of the PLA pellets and MPs were acquired with a Fourier Transform Infrared (FTIR) spectrometer (Vertex 70v FT-IR, Bruker) coupled to a single-reflection attenuated total reflection (ATR) accessory (MIRacle ATR, PIKE Technologies) (ATR-FTIR).

All the spectra presented were the average of 32 repetitive scans in the range of 4000-600 cm^{-1} at a resolution of 2 cm^{-1}. The changes in the carbonyl band, characteristic of the degradation of the PLA polymer chain, were explored through the calculation of the carbonyl index (CI) (Gomes et al., 2024), i.e. the ratio between the intensity of the carbonyl (C═O) peak at 1750 cm^{-1} and that of the methylene (C-H) peak at 1452 cm^{-1} as expressed in the following equation:

$$CI = \frac{I_{C=O}}{I_{C-H}} \qquad \text{Equation 3.2}$$

Raman spectra were collected using Renishaw in Via confocal Raman microscope with 785 nm excitation wavelength. The spectral measurements were conducted with 10 s exposure time, laser power of 100% and 50 x of magnification. The spectrometer provides raman spectra in the range of 200 to 3600 cm^{-1} . All spectra represented in this study were baseline corrected.

Surface chemical composition and the presence of specific functional groups of the samples were investigated by means of X-ray Photoelectron spectroscopy (XPS, Kratos, Axis UltraDLD). The samples were prepared through drop casting of 40 µl of the MPs water dispersions on indium oxide substrates. Both survey spectra and high-resolution ones were acquired, using a monochromatic Al kα source operated at 20 mA and 15 kV. Survey spectra were acquired at pass energy of 160 eV, energy step of 1 eV and over an analysis area of 300 × 700 µm. High resolution spectra were acquired on the same area, at pass energy of 20 eV and with an energy step of 0.1 eV. The Kratos charge neutralizer system was used on all samples; binding energy scale calibration was performed by setting the position of the main C1s component at 285 eV (for C-C bonds). Casa xps software were used to analyze the experimental data.

3.3.4 PLA MPs effects on corals: oxidative stress and bleaching assessment

3.3.4.1 Experimental setup

At the Genoa Aquarium, 24 nubbins (8-10 cm in length) of *P. damicornis* were collected from 6 different donor colonies. Nubbins were fixed on supports made of epoxy resin and transferred to two 50 L experimental flow-through tanks for 7 days of acclimatation at the temperature of 25 °C, with a light/dark cycle of 11/13 h respectively. The irradiation was equal to 250 PAR (µmol photons m^{-2} s^{-1}). After acclimation, each nubbin was placed in 2 L glass beaker with an air pump used in each chamber to keep the MPs in constant motion, simulating the water turbulence typically experienced in natural reef environments (Martin et al., 2019) following the procedure previously adopted (Isa et al., 2024). Beakers were placed in water baths to maintain a constant temperature of 25 °C. Nubbins (n = 6) were randomly assigned to one of four treatments, consisting of the three different experimental concentrations of MPs and one control group (without MPs). The PLA MPs concentrations were equal to 5 mg/L, 15 mg/L and 50 mg/L. The MPs exposures were performed at 25 °C for 72 h. At the conclusion of the experiment, coral fragments from each of the four previously described conditions were collected and immediately stored at −80°C for subsequent analysis.

3.3.4.2 Protein extraction

The extraction of the total protein content for the enzymatic assays was performed as previously reported (Montalbetti et al., 2021; Montalbetti et al., 2023). Specifically, coral nubbins were ground using a pre-chilled mortar and pestle and homogenized in 750 µl lysis buffer (Tris-HCl 50 mM, pH 7.4, NaCl 150 mM, glycerol 10%, NP40 detergent 1%, EDTA 5 mM) containing 1mM phenylmethylsulfonylfluoride. After the first centrifugation step (5 min, 3000 rpm) to remove skeletal components, cells were sonicated (6×10 s pulse on ice, amplitude 10 µm, Soniprep 150, Sanyo).

Samples were then subjected to a second centrifugation step (15 min, 14,000 rpm, 4°C), and the supernatant was immediately frozen (− 80 °C) until subsequent assays. The total protein content of each sample was determined through the Bradford method using bovine serum albumin (BSA) as a calibration curve.

3.3.4.3 Superoxide dismutase (SOD) activity assay

SOD activity was assessed according to Vance et al. (1972). As SOD competes with ferricytochrome c for oxygen radicals, the enzyme activity was detected as the ability to inhibit the reduction of ferricytochrome c by O_2 generated from the xanthine/xanthine oxidase system. For the reaction, the following reagents were utilized in a final volume of 1 ml: ferricytochrome c 0.01 mM, EDTA 0.1 mM, xanthine 0.01 mM, and xanthine oxidase 0.0061 U. Different volumes of each sample were tested and added to the reaction mix to determine the 50% inhibition of the reaction rate. The ferricytochrome c reduction rate was followed spectrophotometrically at 550 nm, 25°C, through a Varian Cary 50 Scan Spectrophotometer (Agilent Technologies). Under the above conditions, one unit of SOD was defined as the amount of enzyme inhibiting the reduction of ferricytochrome c by 50%. Results are expressed as units (U) of enzyme per mg of proteins.

3.3.4.4 Catalase (CAT) activity assay

CAT activity was assessed by considering the peroxidative function of the enzyme based on the degradation of hydrogen peroxide. The method, described by Bergmeyer and Grassl (1983), relies on the degradation of hydrogen peroxide (H_2O_2) by the enzyme. The reaction mix contained 50 mM sodium phosphate buffer pH 7.5 and 12 mM H_2O_2) and 12 mMH_2O_2. This solution was mixed in a 1 ml cuvette with different volumes, and the decrease of H_2O_2 was measured spectrophotometrically at 240 nm (Varian Cary 50 Scan spectrophotometer, Agilent Technologies). Results are expressed as units (U) of enzyme per mg of proteins, and in this case, U refers to k, the first-order kinetic constant (min^{-1}), as previously described (Aebi 1984).

3.3.4.5 Glutathione reductase (GR) activity assay

The enzymatic assay of GR was analyzed following the procedure described by Wang et al. (2001). The activity of GR was assessed through the spectrophotometric detection of the absorbance at 340 nm (Varian Cary 50 Scan spectrophotometer, Agilent Technologies) of NADPH oxidation to NADP+ reaction, which occurs in conjunction with the glutathione reduction and is proportional to the decrease in absorbance over time. NADPH reaction was first measured in the reaction mix (containing 0.1 M potassium phosphate buffer pH 7.6, 0.16 mM NADPH, 1 mg ml^{-1} BSA, and 4.6 mM oxidized glutathione) and then adding different sample volumes. GR activity was obtained from the difference of the two absorbance values. One unit of GR activity is defined as the oxidation of 1 nmol NADPH/min at 25°C. Results are expressed as units (U) of enzyme per mg of proteins.

3.3.4.6 Glutathione S-transferase (GST) activity assay

GST activity was measured by considering the reaction of the enzyme with the 1-Chloro-2,4-dinitrobenzene (CDNB) substrate, according to Hayes and Strange (2000). The solution (containing 200 mM potassium phosphate buffer pH 6.5, 20 mM CDNB dissolved in 95 % ethanol, and 20 mM reduced glutathione) was mixed in a 1 mL cuvette with different volumes of samples. The formation of CDNB-oxidized glutathione conjugate was followed spectrophotometrically at 340 nm (Varian Cary 50 Scan spectrophotometer, Agilent Technologies). GST activity is expressed as units (U) of enzyme per mg of protein and is proportional to the increase in absorbance caused by conjugated product formation.

3.3.4.7 Lipid peroxidation (LPO)

Lipid peroxidation levels were assessed by measuring malondialdehyde (MDA) content using an MDA assay kit (Bioxytech LPO-586, Oxis International, USA). This method involves a reaction between a chromogenic reagent, N-methyl-2-phenylindole, and MDA at 45 °C. To prepare the samples, frozen coral apexes (approximately 1 g each) were ground using a pre-chilled mortar and pestle and homogenized in 1 ml of 20 mM phosphate buffer at pH 7.4. To prevent oxidation of the

samples, 10 µl of 0.5 M butylated hydroxytoluene in acetonitrile was added to the 1 ml tissue homogenate. Afterwards, the samples were centrifuged at 3000 x g for 10 min at 4 °C, and an aliquot of the supernatant was taken for protein determination using the Bradford method. The subsequent assay (using the hydrochloric acid solvent procedure) was performed following the manufacturer's instructions. The resulting blue product was quantified by measuring absorbance at 586 nm (Gérard-Monnier et al., 1998). The results are expressed as µmol of MDA per µg of protein.

3.3.4.8 Quantification of chlorophyll a and c2

The coral bleaching status of corals was assessed through analysis of the concentration of chlorophyll (Chl) a and c2. Coral tissue was removed from frozen coral fragments by using airflow from a 1,000 µL pipette tip, which was connected via a rubber hose to a benchtop filtered air pressure valve. This process was carried out using 5 mL of ice-cold phosphate-buffered saline (PBS) (Voolstra et al., 2020). The resulting tissue slurry was homogenized and then centrifuged at 3,600 g for 4 min. After centrifugation, the supernatant was discarded, and the remaining pellet was incubated in 100% acetone for 24 h in the dark at 4 °C. Following this extraction, the sample underwent re-centrifugation at 3,600 g for another 4 min. The supernatant obtained was used to measure concentrations of Chl a and c2 using fluorescence readings at 630, 663, and 750 nm, applying dinoflagellate-specific equations and normalizing the results to the coral surface area (Jeffrey and Humphrey 1975). The remaining coral skeletons were soaked in 10% bleach and allowed to dry for 48 h. The surface area of each fragment was measured using the paraffin wax dipping method (Veal et al. 2010). The change in weight due to the addition of wax was compared against a standard curve of dipped clay cylinders with known surface areas to calculate the skeletal surface area of each coral fragment.

3.3.5 Statistical analyses

The normality of the data was assessed using the Shapiro-Wilk test. When the assumptions of normality were not met, data transformations were applied. To evaluate significant differences in antioxidant enzyme activities, malondialdehyde (MDA) levels, and concentrations of chlorophyll a and c2 at various MP concentrations, we conducted separate one-way ANOVAs followed by Tukey's

HSD post hoc tests. The analyses were performed using SPSS version 29 (IBM). Statistical significance was set at $p < 0.05$, and all data are presented as arithmetic means ± standard error (SE) with $n = 5$ for each biomarker analysed, unless otherwise noted.

3.4Results and Discussion

3.4.1 PLA MPs properties

After the grinding process, MPs of specific size range were formed as shown in the granulometer analysis provided in Figure 1a. In particular, the fabricated MPs have D90 ≤ 370 µm and D50 ≤ 192 µm. The shape analysis (Table 3.1) indicates that the particles have an irregular shape with a mean sphericity of 0.73. SEM analysis confirms these observations, as evident in Figure 3.1 (b-d) with particles exhibiting irregular morphology and broad size distribution, as well as rough surface, in agreement with the morphological characteristics of environmental MP samples (Kefer et al., 2021).

Table 3.1. Imaging-derived parameters of particle morphology: mean sphericity and total particle count.

Imaging Data	
Mean Sphericity	**0.73**
Total Particle Count	**2963**

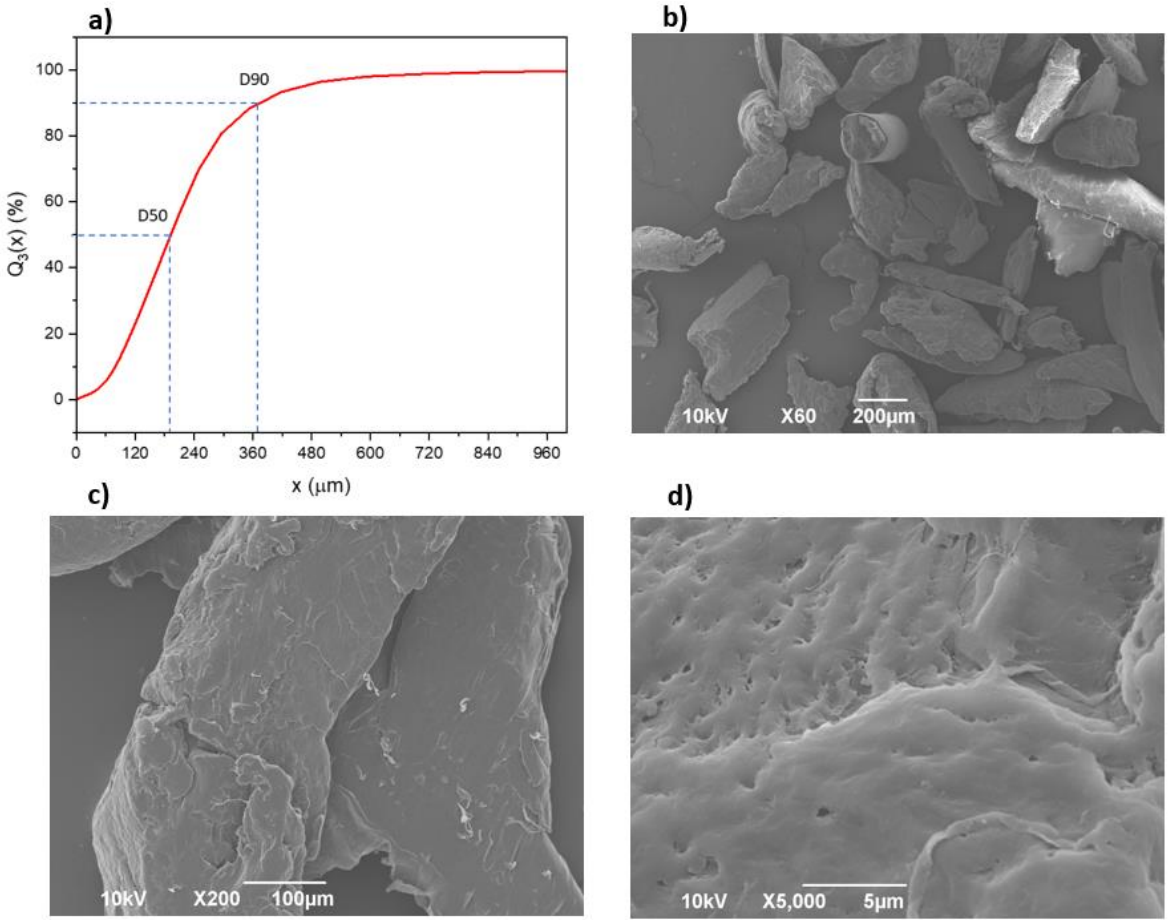

Figure 3.1 (a-b). a) Particle size distribution of the PLA MPs measured by granulometer. The plot represents the cumulative volumetric percentage Q3(x) (%) of particles as a function of their diameter x (µm).The red curve represents the average of three replicates. **b-d)** SEM images showing the irregular morphology and surface details of the MPs at different magnifications.

To evaluate the changes in PLA MPs following the grinding process and provide valuable insights into potential polymer degradation both crystallinity and molecular weight variations were assessed. The crystal structure was examined using XRD and, as shown in Figure 3.2, both, unprocessed pellets and MPs present typical semi-crystalline diffraction patterns with amorphous halo and crystalline peaks. The prominent diffraction peaks at 2θ ~ 16.6° (200/110 plane) and ~18.9° (203 plane) as well as the smaller peaks at 2θ ~ 14.78° (010) and ~22.2° (015) indicate the characteristic orientation of the α-phase orthorhombic crystals of the PLA structure (Pan et al., 2007) as indexed by the ICDD 00-064-1624 database (Babichuk et al., 2022).

The $X_{C_{XRD}}$ of the samples was calculated following Eq. 3.1, indicating that PLA pellets exhibit a value of 44.7% while the $X_{C_{XRD}}$ of the MPs decreases to 20.6% (Table 3.2). This is in agreement with a recent study on semicrystalline MPs which proved that prolonged marine weathering results in the decrease of their crystallinity. (Maddison et al., 2023)

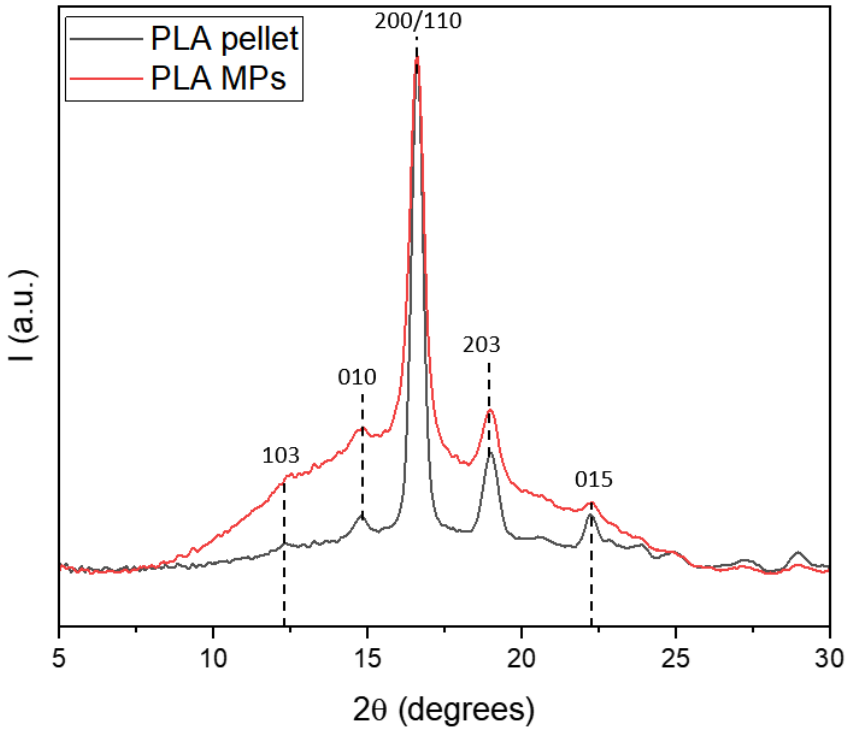

Figure 3.2. XRD diffractograms of pellets and PLA MPs.

The chemical changes induced upon the mechanical processing of the PLA pellets were analyzed by using ATR-FTIR spectroscopy (Figure 3.3). As shown, both spectra of the pellets and MPs present peaks characteristic of the PLA, indicating that the grinding process did not alter significantly the chemical structure of the polymer. In both cases the characteristic peaks at 1750 cm^{-1} and 1080 cm^{-1}, correspond to the stretching vibrations of the carbonyl group (C=O) and of the C–O bonds, respectively.

The spectral region between 1500 cm^{-1} and 1330 cm^{-1} is associated with C–H stretching vibrations (Boonme et al., 2016), while the symmetric scissoring vibration of the CH_3 group is observed at 1452 cm^{-1}. The C – CH_3 stretching band appears at 1042 cm^{-1}; and for C – COO, the stretching band appears at 867 cm^{-1} (Cesur et al., 2020; Cam et al., 2020). However, variations in the intensity of the peaks characteristic of the polymer's crystallinity are observed. Specifically, the contribution of the absorption band at 921 cm^{-1}, associated with the rocking vibration of the CH_3 group [rCH_3] of the α crystal form, becomes weaker at the PLA MPs spectrum, while the contribution of the peak at 956 cm^{-1}, assigned to the stretching vibration of the C_α-C backbone [$v(C_\alpha\text{-}C)$] of the amorphous phase, (Zhu et al., 2022) gets stronger. Moreover, the distinct peak observed at 1210 cm^{-1} in the PLA pellet—associated with the ester C–O stretching vibration and characteristic of the crystalline domains of PLA (Meaurio et al., 2006)—indicates a higher degree of crystallinity compared to the MPs, in which this feature appears only as a small shoulder. Such variations confirm that the grinding process causes a decrease of the crystalline phase of the PLA polymer in agreement with the XRD observations.

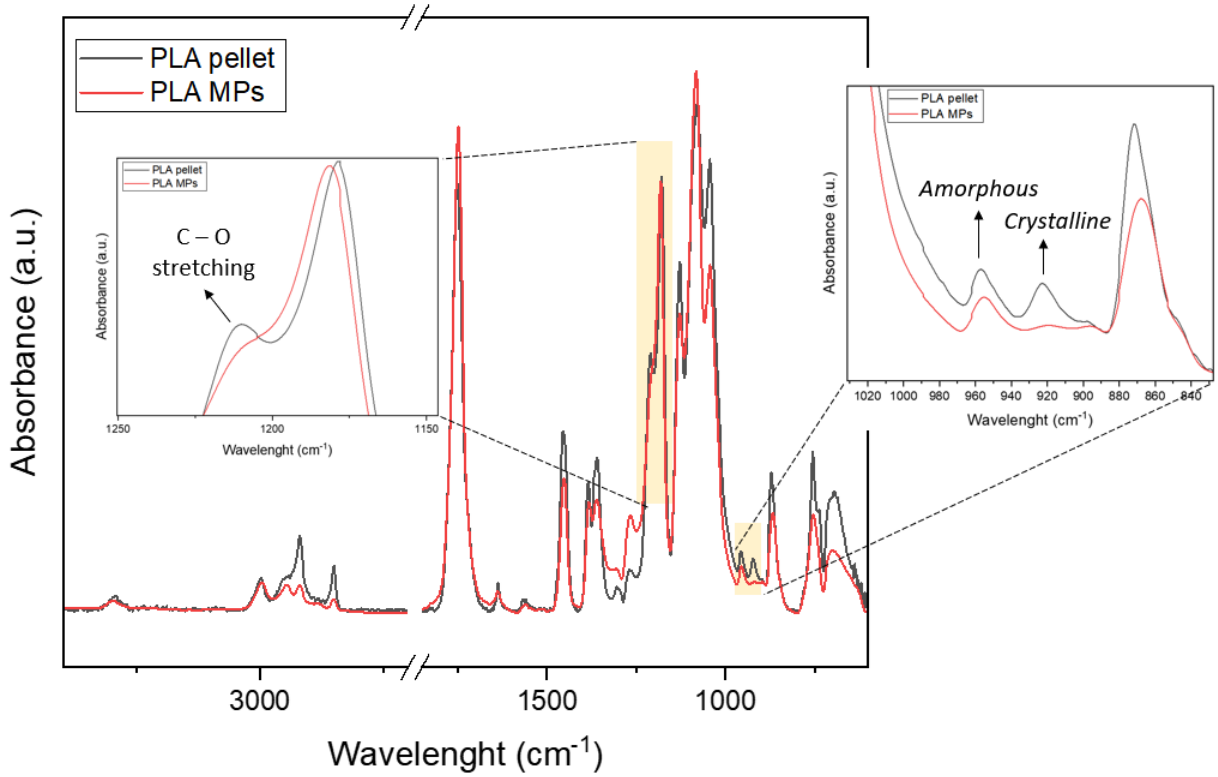

Figure 3.3. FTIR spectra of PLA pellet and MPs. Inset: magnified region of specific wavenumber range.

In the present study, changes in crystallinity may indicate a mechanical degradation process of the PLA molecular chain structure during the formation of the MPs. In fact, the mechanical stress applied during grinding disrupts the crystalline regions of PLA, enhancing its amorphous character (Cha et al., 2024). Such degradation is attributed to the action of shear forces that can lead to the rupture of bonds along the polymer backbone, resulting in polymer chain scission and, consequently, in a molecular weight reduction (Niaounakis, 2015; Lucas et al., 2008). This is also supported by the CI, calculated before and after the grinding process, with an increase of approximately 54% after the mechanical fragmentation (Figure 3.4), likely reflecting the onset of polymer degradation induced by the MP production process.

The overall degradation and macromolecular chain scission during the mechanical processing of the pellets is further supported by the molecular weight evaluation of the polymer before and after the mechanical processing. As shown in Table 3.2, in the case of MPs both the number- and weight-average molecular weights are decreased, confirming the PLA degradation, specifically triggered by mechanical stress induced during the grinding process.

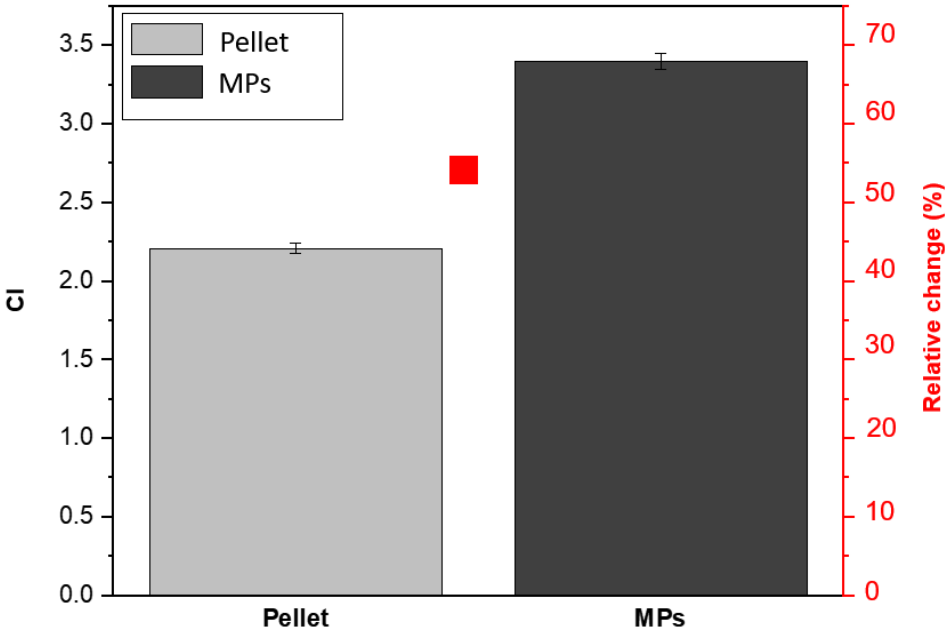

Figure 3.4. Plot shows the modification of the peaks of interest for PLA pellet and MPs before and after the grinding process. Carbonyl index (bars) and the relative percentage change (scatter).

Table 3.2. Summary of the weight-average (Mw) and number-average (Mn) molecular weights, molar-mass dispersity (Đ), and crystallinity of PLA pellets and MPs.

Sample	$\overline{M_w}$ **(kDa)**	$\overline{M_n}$ **(kDa)**	$\overline{Đ}$	$X_{c_{XRD}}$(%)
Pellet	**124.33 ± 18.03**	**92.66 ± 3.05**	**1.33 ± 0.15**	**44.73**
MPs	**102.66 ± 7.57**	**83.66 ± 2.51**	**1.27 ± 0.15**	**20.63**

The thermal analysis (Figure 3.5 and 3.6) of the PLA pellet and MPs shows the presence of a glass transition (T_g) event around 58.0 °C in both cases, corresponding to the transition of the amorphous fraction, while a melting event at T_m 152.5°C for the pellets and 150.7 °C for the MPs. The fact that the T_m of the unprocessed pellets is slightly higher than that of the PLA MPs, indicates a molecular weight reduction upon the mechanical fragmentation process, due to chain scissions, which disrupt the polymer's crystalline structure and lower its thermal stability (Pan et al., 2007; Lim et al., 2008). Based on the so far presented results, we may conclude that although environmental occurring MPs have been subjected to natural weathering/aging which is an extremely complicated process, the herein developed MPs may be considered as a valuable environmental relevant model in terms of morphology, structure and chemistry, to be used for further studies.

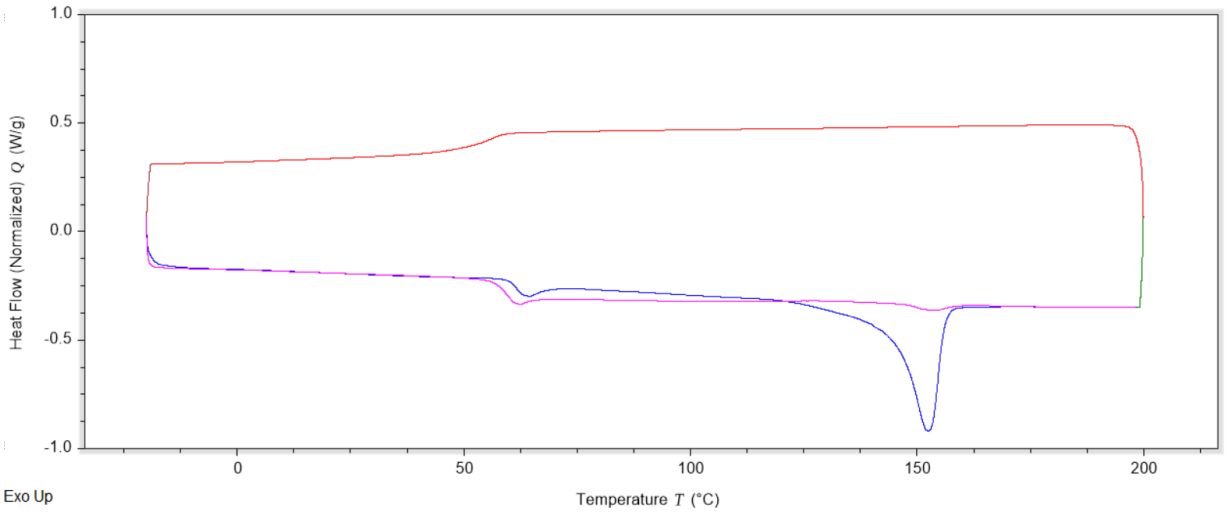

Figure 3.5. DSC thermogram of PLA pellet. Blue curve represents the first heating, a distinct melting peak at around 152°C is present suggesting the presence of a crystalline fraction. Pink curve represents the second heating, near absence of melting peak indicates that recrystallization does not occur during cooling at a rate of 10 °C/min.

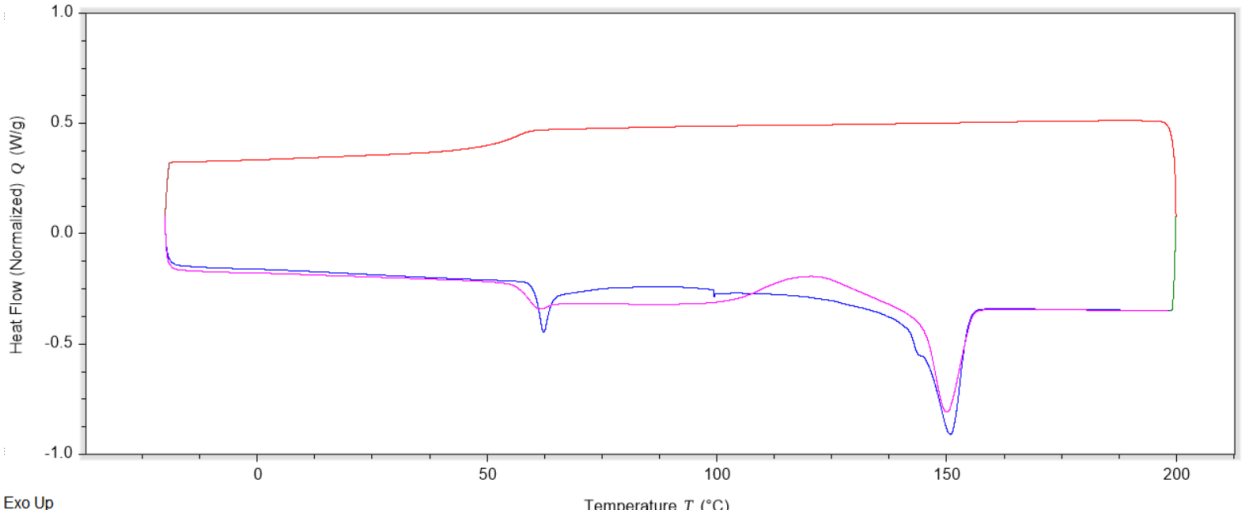

Figure 3.6. DSC thermogram of PLA MPs. Blue curve represents the first heating, a distinct melting peak at around 150°C is present suggesting the presence of a crystalline fraction. Pink curve represents the second heating, a distinct cold crystallization peak at around 120°.

3.4.2 PLA MPs and Artemia's exposure

PLA MPS were dipped for 1 hour in Artemia salina medium, to promote early-stage biofilm formation, thereby simulating the initial biofouling process that typically occurs when plastic debris enters the marine environment (Ramsperger et al., 2020). In the exposure medium it is expected to be present various organic compounds released by Artemia salina but not the living organisms. This can alter both the physical and chemical surface properties of the MPs, making them more attractive to marine filter feeders such as corals (Feng et al. 2020). This strategy also allows for the standardization of a realistic yet controlled system in the laboratory, avoiding the use of raw seawater, which is more variable and difficult to reproduce consistently across experiments.

Based on SEM analysis, the exposure to filtered Artemia salina water medium did not result in significant alterations to the surface morphology of PLA MPs.

In fact, as shown in Figure 3.7, the surface of the exposed MPs before and after being throughly rinsed with deionized water to remove any non-adhered matter, did not present any noticeable modifications compared to the pristine MPs. This type of pre-treatment did not also evidently affect the chemical properties of the MPs.

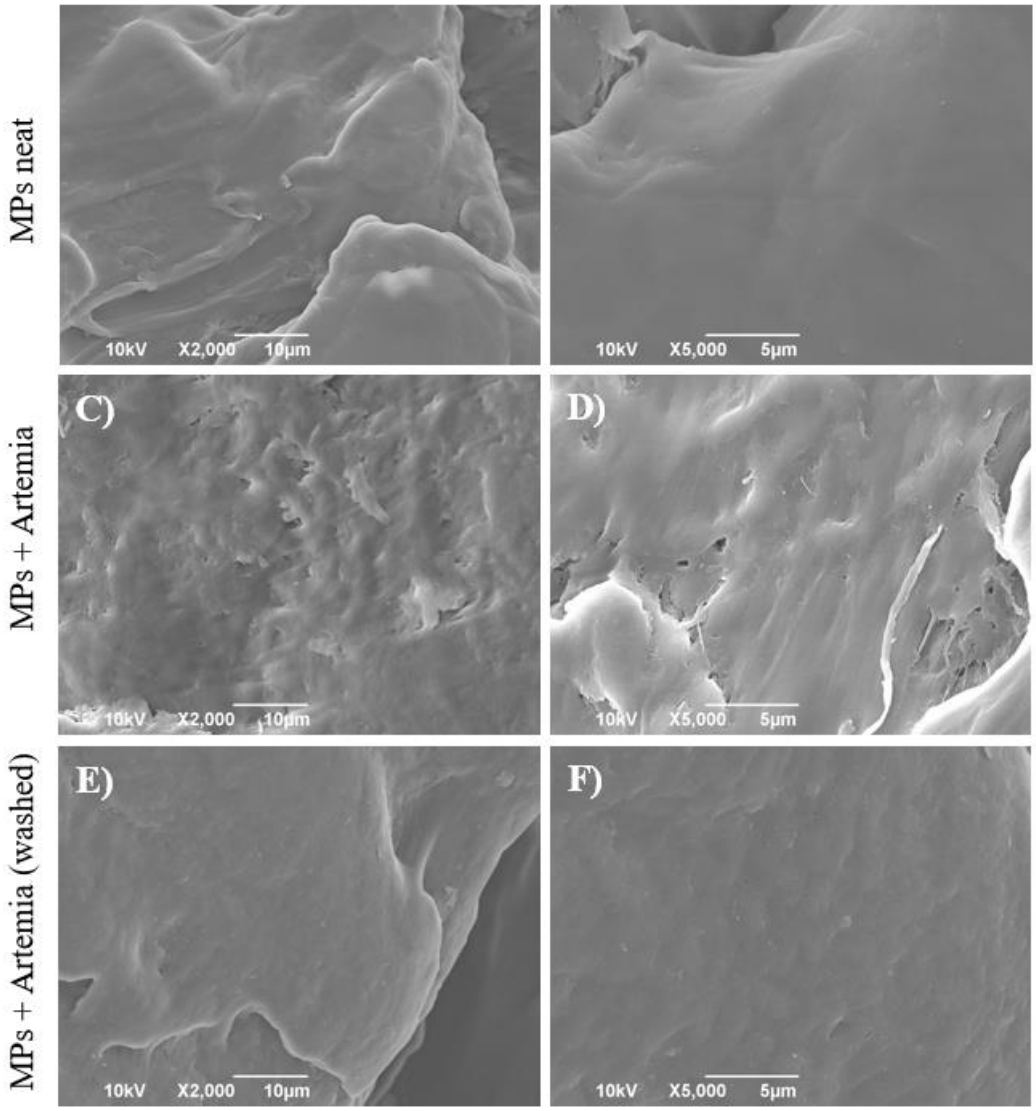

Figure 3.7. SEM images at different magnifications of PLA MPs **(A-B)** before (MPs neat), **(C-D)** after 1h of incubation in *Artemia salina* water medium (MPs + Artemia), and **(E-F)** after 1h of incubation in *Artemia salina* water medium and washed with deionized water (MPs + Artemia washed).

In particular, as shown in Figure 3.8 of the supporting information file, for both the exposed and for the deionized water rinsed after exposure MPs, the Raman bands observed at 1218, 1181, and 1095 cm^{-1}, attributed to the vibrational modes of the O-C-O ester groups, as well as the band at 518 cm^{-1}, associated with crystalline PLA, exhibit no changes compared to the signals before treatment. Similarly, the bands at 1768 and 1451 cm^{-1}, attributed to the carbonyl group and the methyl in-plane asymmetric wagging of the ester group, remain unchanged (Qin and Kean, 1998). The band around 397 cm^{-1} is indicative of amorphous PLA structures, while the band near 409 cm^{-1} corresponds to crystalline PLA (Smith et al., 2001). Consequently, the intensity ratio of these two peaks, which reflects the degree of crystallinity did not present any significant variation. Based on the results, it can be concluded that exposure to the *Artemia salina* water medium did not affect the overall chemical structure of PLA MPs.

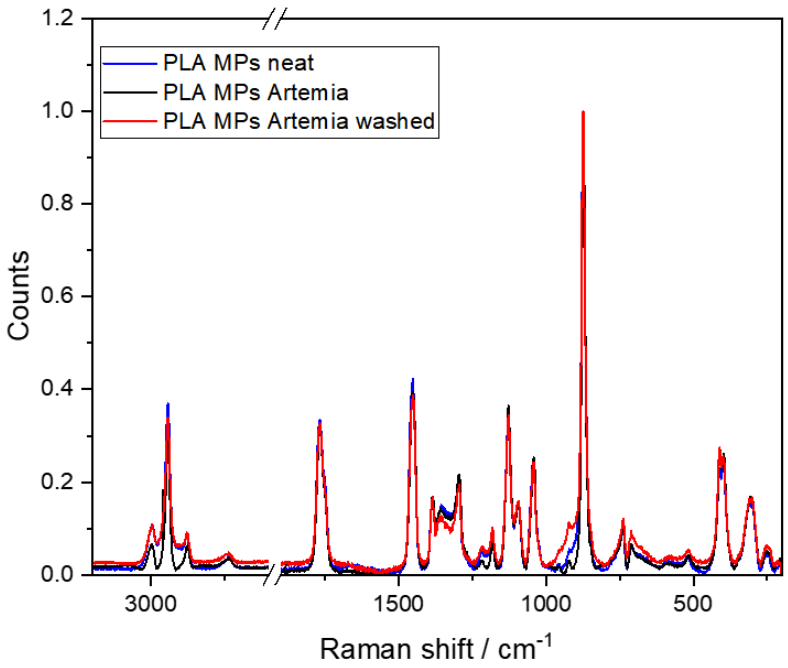

Figure 3.8. Comparison of Raman spectra of PLA MPs neat (blue), PLA MPs + Artemia (not washed) (black), and PLA MPs + Artemia (washed) (red).

Nonetheless, a closer look to the surface chemistry by XPS analysis of these MPs indicates modifications in their surface chemistry.-As shown in the wide scan spectra, the MPs present the main O and C elements representative of the organic nature of the polymer, and small traces of other elements such as In, representative of the substrate, and N possibly attributed to adsorbed contaminants. After exposure to the *Artemia salina* water medium, additional elemental traces were detected on the surface of the MPs attributed to seawater salts and other components adhered to the MP surface (Figure 3.9), together with the O/C ratio increase. To explore how well these components are adhered on the surface of the MPs, the samples were thoroughly rinsed with deionized water. Although the major part of the inorganic components were removed, subsequent XPS analysis still revealed the presence of some additional elements (Table S1) such as sulfur and nitrogen, indicating the occurrence of organic material, together with an O/C ratio higher than that of the pristine counterpart. Specifically, the O/C ratio increased from 0.10 to 0.13 (~30%) in MPs exposed to and subsequently washed after incubation in the *Artemia salina* water medium (Table S3.1), indicating the persistence of oxygen-containing species on their surface. Overall, these findings suggest that the rise in the O/C ratio after incubation results from the adsorption of external species, which alters the atomic balance and the distribution of oxygen components. MPs have the potential to act as carriers for a variety of organic substances (Hartman et al., 2017). When a material is introduced into an aqueous environment, its surface rapidly interacts with organic components initiating the formation of a conditioning film, formed through the adsorption of dissolved and suspended molecules (Loeb and Neihof, 1975; Rittle et al., 1990; Lawrence et al., 2016). Such films can comprise diverse organic constituents, including glycoproteins (Baier, 1980), lipids, nucleic acids, ions, polysaccharides, and proteins (Baier, 1980; Rittle et al., 1990; Taylor et al., 1997; Compère et al., 2001; Bakker et al., 2004) which largely originate from the metabolic by-products of aquatic organisms.

Despite this, detailed knowledge of how plastics interact at the microscale with the surrounding chemical milieu in marine systems—particularly how exposure to seawater alters their surface properties—remains limited (Bhagwat et al., 2021). In the present context, it is reasonable to hypothesize that the observed increase in the O/C ratio of PLA MPs may stem from their interaction with oxygen-rich organic matter released by Artemia species, leading to surface chemical modifications that render these particles more comparable to MPs naturally present in marine environments.

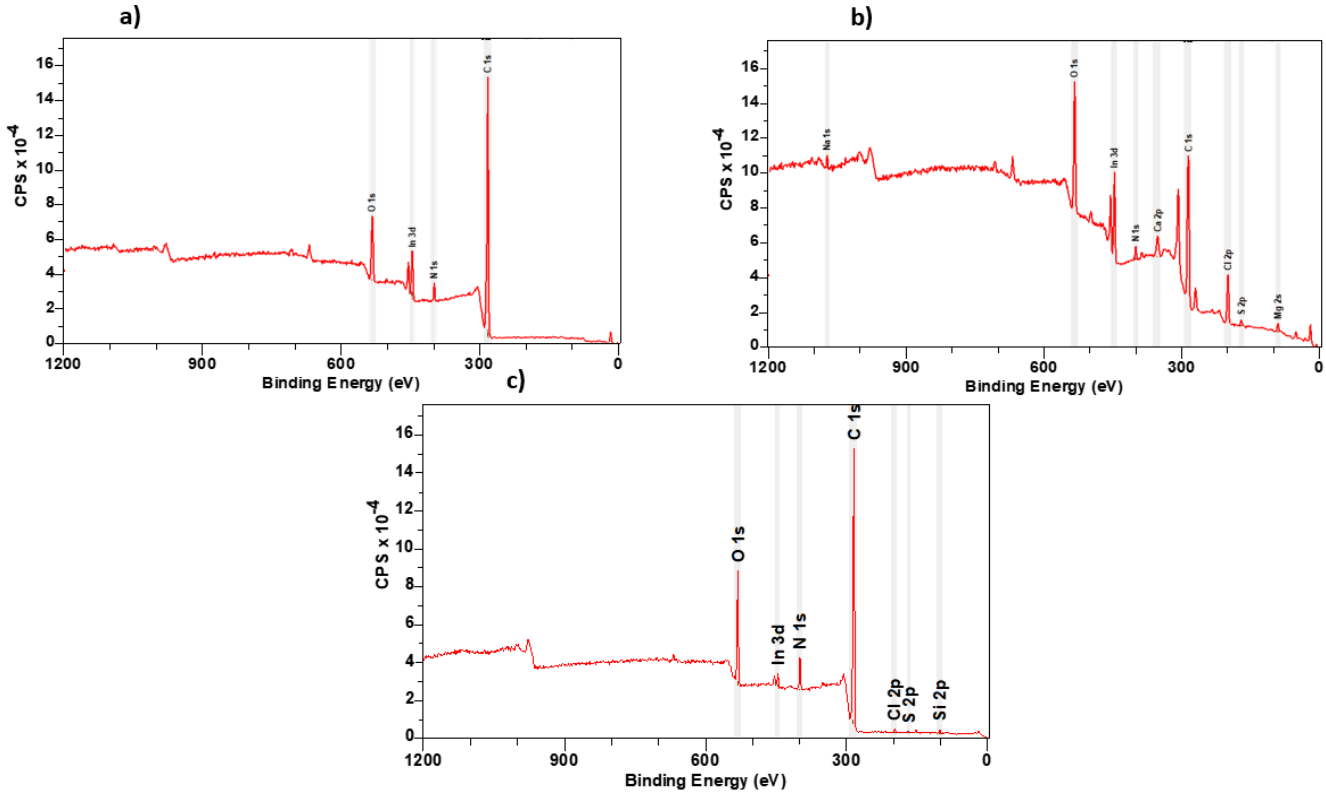

Figure 3.9. XPS wide scan spectra of **a)** before the incubation in *Artemia salina* water medium (MPs neat) **(b)** after 1h of incubation in *Artemia salina* water medium (MPs + Artemia) **c)** after 1h of incubation in *Artemia salina* water medium and washed with deionized water (MPs + Artemia washed).

3.4.3 Oxidative stress and coral bleaching assessment

The antioxidant activities of SOD, CAT, GR and GST were analyzed in *P. damicornis* samples exposed to varying concentrations of PLA MPs in order to assess their effects on the coral cellular oxidative homeostasis.

First, it is important to highlight that no partial or total mortality was observed in any of the coral nubbins across all treatments. Furthermore, neither mucus production nor polyp retraction was observed during the exposure period. Our results indicate that the only antioxidant enzyme that displayed a variation in activity in corals exposed to PLA MPs was GR. Specifically at the highest concentration of PLA MPs, GR activity significantly increased compared to the other tested conditions (Figure 3.10). In particular, after 72 h of exposure to PLA MPs, significant differences in GR activity were observed across treatments (one-way ANOVA, $F(3, 16) = 5{,}156$, $p = 0{,}011$). In detail, *P. damicornis* nubbins exposed to 50 mg L^{-1} of MPs exhibited higher GR activity compared to those in the control tank and those exposed to 15 and 5 mg L^{-1} concentrations (Figure 3.10). GR plays a key role in maintaining and restoring the redox balance between oxidized and reduced glutathione, a tripeptide that interacts with different ROS (Lesser 2006; Krueger et al. 2015, cited in Montalbetti et al. 2022).

Apart from GR, no other significant alterations were observed as SOD and CAT activities indicating that the exposure to MPs did not affect their activity (one-way ANOVA, $F(3, 16) = 1{,}430$, $p = 0{,}271$ and $F(3, 16) = 0{,}104$, $p = 0{,}95$, respectively). SOD and CAT are key enzymes involved in the direct detoxification of ROS, targeting superoxide anions (O_2^-) and hydrogen peroxide (H_2O_2), respectively (Vance et al. 1972; Bergmeyer and Grassl 1983).

These enzymes work synergistically to neutralize superoxide radicals ($\bullet O_2^-$) and hydrogen peroxide (H_2O_2), preventing the formation of highly reactive hydroxyl radicals (•OH) and subsequent cellular damage (Fridovich 1986). SOD, a critical antioxidant in coral physiology, acts as the first line of defense against ROS by catalyzing the disproportionation of O_2^- into H_2O_2 and molecular oxygen (O_2) (Gardner et al. 2016), and is found in various cellular compartments (Verma et al. 2019). CAT, another key antioxidant in the coral redox system, converts H_2O_2 into H_2O and O_2 (Levy et al. 2006). This is also the case for the GST activity, as no significant changes were observed after exposure to PLA MPs (one-way ANOVA, $F(3, 15) = 1{,}625$, $p = 0{,}226$). GST is central to Phase II biotransformation, facilitating the conjugation of intermediary metabolites produced during xenobiotic exposure with glutathione (Hayes & McLellan 1999; Limón-Pacheco & Gonsebatt 2009). The GST antioxidant enzyme system also aids in the conversion of peroxides and hydroxyl radicals into water, mitigating intracellular damage from ROS (Doyotte et al. 1997; Jiang et al. 2017).

Taken together, our results show that exposure to mechanically ground PLA MPs does not induce mortality and evident antioxidant response in *P. damicornis*. In fact, although a significant increase in GR activity was observed at the highest concentration (50 mg L^{-1}), we hypothesized that this response could be part of an adaptive antioxidant mechanism rather than a sign of overt oxidative damage. Indeed, GR, while not a classical antioxidant enzyme, plays an essential role in maintaining the proper ratio between GSH and its oxidized form, glutathione disulfide (GSSG), and thereby preserving the intracellular redox status in marine organisms (Regoli and Giuliani, 2014), fundamental for their health status. These outcomes appear to be in contrast to previous findings observed exposing corals to synthetic polymers/MPs although of different sizes.

For instance, Tang et al. (2018) reported that acute exposure of *P. damicornis* to 50 mg L^{-1} of 1µm PS MPs for 24 h led to a significant increase in the activities of SOD and CAT, alongside a significant decrease in GST activity, suggesting that, although of different size range, PLA MPs induces a less negative effect compared to PS MPs at similar concentrations. Similarly, exposure of Zoanthus sociatus to PVC MPs (size range 63-125 µm and concentration of 10 mg L^{-1}) for 96 h led to a marked increase in CAT activity and LPO, indicating oxidative stress (Rocha et al.2020). Analogously, Tubastraea aurea exhibited elevated CAT activity following polyvinyl chloride (PVC) (size range 5-10 µm and concentration of 30 mg L^{-1}) exposure after 72 h (Xiao et al., 2021). Chen et al. (2022) also reported short-term negative effects in Goniopora columna exposed to PE MPs with a diameter of 40-48 µm at concentrations of 5, 10, 50, 100, and 300 mg L^{-1}. Specifically, they observed a significant increase in antioxidant enzymes: SOD after 1 day of exposure at all concentrations; CAT after 5 days at 5, 10, 50, and 100 mg L^{-1}; and both GSH and GST after 5 days at all tested concentrations. Xiao et al. (2021) observed an increase of SOD and GSH after 96h of exposure to three different synthetic polymer, PET, PA66, and PET (size range 10-40 µm), at a concentration of 50 mg L^{-1}. Another study conducted on soft corals (Protopalythoa sp.) demonstrated that acute exposure (96 h) to 50 mg L^{-1} of different types of microplastics (PE, PVC, and PMMA) ranging in size from 1 to 20 µm induces significant alterations in antioxidant enzymes activity. Specifically, SOD increased significantly only following exposure to PVC MPs, whereas both GST and GSH showed significant increases in response to all tested MPs types (Jiang et al., 2020).

These comparisons suggest that PLA, a bio-based polymer, may elicit a less severe oxidative response in coral species compared to more persistent synthetic plastics such as PVC, PS or PE.

This was confirmed also by the analysis of the LPO levels which are indicative of the oxidative damage generated by PLA MPs in corals. In fact, although a slight, non-significant, increase was observed in corals exposed to PLA concentrations of 15 and 50 mg L^{-1} compared to controls (Figure 3.11), this was not statistically significant and in general, no significant changes were observed in LPO levels between all treatments (one-way ANOVA, $F(3, 16) = 0{,}323$, $p = 0.809$), (Figure 11).

In contrast, several studies have reported a significant increase in lipid peroxidation (LPO) following exposure to synthetic plastics. For instance, Rocha et al. (2020) found that short-term exposure (96 h) to PVC microplastics (size range 63-125 µm and concentration of 10 mg L^{-1}) induced a significant increase in peroxidative damage in Zoanthus sociatus. Similarly, short-term (96 h) Protopalythoa sp. exposure to PVC, PE and PMMA (size range 1-20 µm and concentration of 50 mg L^{-1}) can increase LPO (Jiang et al., 2020). A similar pattern was observed in Goniopora columna exposed to various concentrations of PE MPs (5, 10, 50, 100, and 300 mg L^{-1}) with a diameter of 40-48 µm, where lipid peroxidation levels significantly increased after 7 days at all tested concentrations (Chen et al., 2022). Based on the results obtained and comparison with similar studies, it can be inferred that PLA MPs induce a lower oxidative stress response compared to their synthetic counterparts. This suggests that biopolymers such as PLA may pose a reduced risk in terms of oxidative damage in marine invertebrates, although further studies are needed to fully assess their long-term biological effects and environmental persistence.

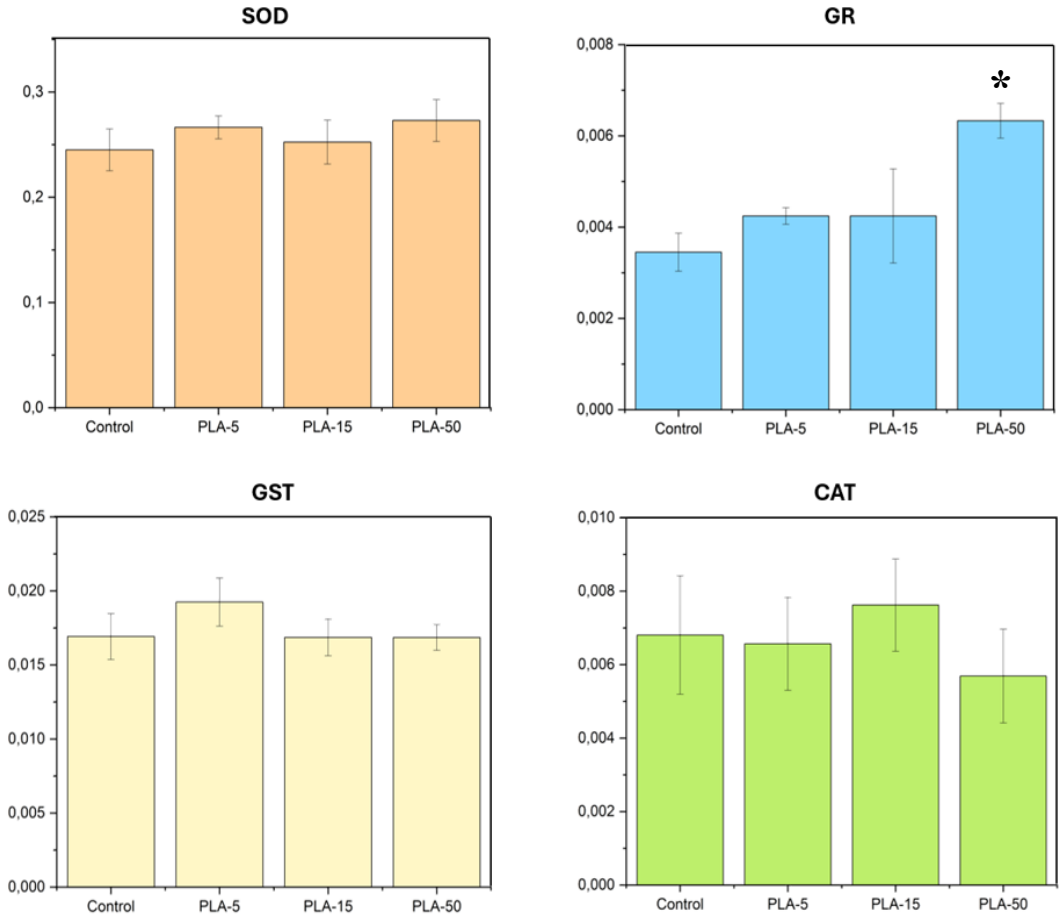

Figure 3.10. Enzymatic activity of SOD, GR, CAT, and GST detected in samples of *P. damicornis* exposed to different microplastic concentration treatments (Control; PLA 5 mg/L, 15 mg/L, and 50 mg/L) after 72 h. Lower case letters indicate significant differences between corals maintained under different treatments. Data are expressed as mean ± SD (n = 5 per treatment).

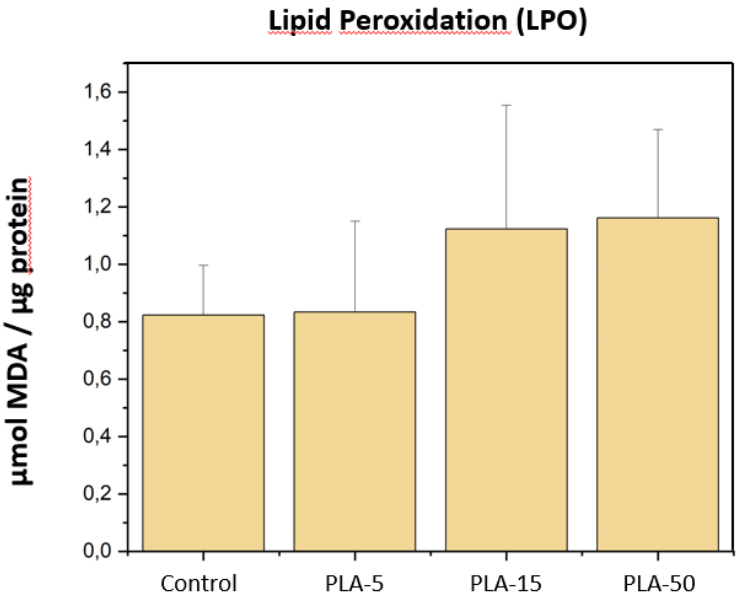

Figure 3.11. Levels of LPO in *P. damicornis* nubbins following 72 h of exposure to different PLA MPs concentrations. Data are expressed as µmol of MDA per mg of proteins and as mean ± SD (n = 5 per treatment).

3.4.4 Coral bleaching assessment

Finally, we analyzed the concentration of Chl a and c2 to assess the possible coral bleaching triggered by the exposition to different concentrations of PLA MPs. Chl a and c2 concentration showed no significant differences among the various treatments tested (one-way ANOVA, $F(3, 16) = 0{,}564$, $p = 0{,}647$ and $F(3, 16) = 1{,}890$, $p = 0{,}172$, respectively) (Figure 3.12). Therefore, no signs of bleaching were observed in corals subjected to any concentration of PLA MPs, suggesting that they do not affect the maintenance of the coral symbiosis.

On the contrary, Xiao et al. (2021) reported that exposure of *Acropora* sp. to synthetic microplastics (PET, PA66, and PE) with a size range from 20 to 40 µm at 50 mg L^{-1} for 96 h resulted in a significant reduction in chlorophyll content. Another study showed that a short-term exposure (24 h) of *Protopalythoa* sp. to PE and PMMA MPs (from 1 to 20 µm) at the same concentration induced a significant increase in chlorophyll ($a + c_2$) content; however, prolonged exposure (28 days) led to a significant decrease in chlorophyll ($a + c_2$) content (Jiang et al., 2020). Similarly to the short-term

condition of the above-mentioned study , Tang et al. (2018) found a significant increase of chlorophyll content after 12 h of exposure to 50 mg L^{-1} of PS MPs (1 µm).

Table S3.2 provides a comprehensive and visually accessible summary of the differential effects of synthetic MPs reported in previous studies compared to the effects of biobased MPs, specifically PLA, investigated in the present study. The table highlights variations in antioxidant enzymes, LPO responses, and chlorophyll (a+c2) content, emphasizing both inter-study differences and the distinctive outcomes observed for PLA MPs.

In conclusion, based on the results obtained from both oxidative stress and bleaching-related biomarkers, it can be suggested that PLA MPs produced through mechanical grinding do not induce detectable cellular or physiological damage in corals.

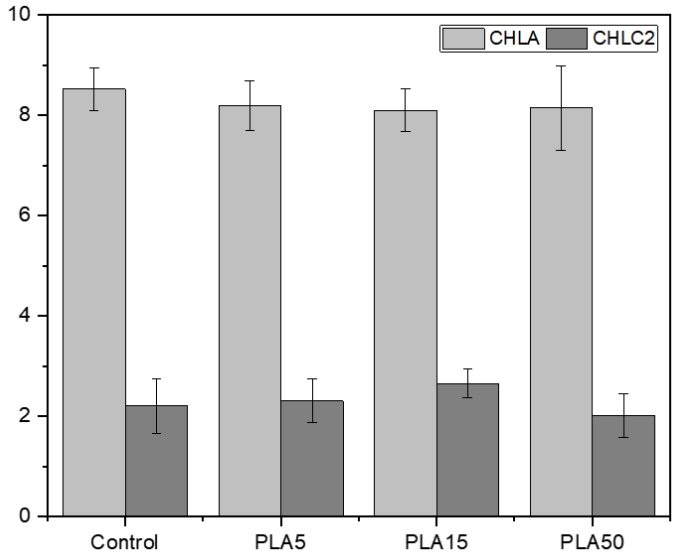

Figure 3.12. Concentration of chlorophyll a (CHLA) and c2 (CHLC2) in *P. damicornis* nubbins following 72 h of exposure to different microplastics concentration treatments (Control; PLA 5 mg/L, 15 mg/L, and 50 mg/L). Data are expressed as mean ± SD (n = 5 per treatment).

3.5Conclusions

This study aims to evaluate the effects of bio-based MPs on corals, in contrast to the majority of existing research that has focused primarily on synthetic MPs. Mechanically ground PLA MPs treated in Artemia salina water medium, were used to simulate plastic fragments commonly encountered in marine environments, thereby providing a more ecologically realistic exposure scenario than those involving commercially available MPs. The resulting MPs exhibited chemical and structural properties distinct from the original PLA pellets, specifically showing reduced crystallinity, lower molecular weight and higher carbonyl index. These features resemble those of environmentally weathered MPs, suggesting that our mechanically ground PLA MPs may more accurately represent the partially degraded particles typically present in natural marine settings. To access potential impacts, the effects of these PLA MPs were assessed on *P. damicornis*. After 72 hours of exposure to three different MPs concentrations, coral fragments showed no signs of mortality, visible stress responses, or bleaching. These findings contrast with numerous studies that have reported adverse effects of synthetic plastic fragments, of various size ranges, exposure on coral health. Overall, the results indicate that, at the specific size ranges, short-term exposure to PLA MPs does not cause detectable physiological alterations in corals. Nevertheless, further research is essential to investigate the long-term impacts of biobased MPs, and to develop a more comprehensive, ecologically relevant, understanding of their effects on coral reef ecosystems.

3.6 References

Aebi, H. (1984). Catalase in vitro. Methods Enzymol., 105, 121–126. https://doi.org/10.1016/s0076-6879(84)05016-3

Ainali, N. M., Kalaronis, D., Evgenidou, E., Kyzas, G. Z., Bobori, D. C., Kaloyianni, M., Yang, X., Bikiaris, D. N., & Lambropoulou, D. A. (2022). Do poly(lactic acid) microplastics instigate a threat? A perception for their dynamic towards environmental pollution and toxicity. Sci. Total Environ., 832, 155014. https://doi.org/10.1016/j.scitotenv.2022.155014

Alfaro-Núñez, A., Astorga, D., Cáceres-Farías, L., Bastidas, L., Soto Villegas, C., Macay, K., & Christensen, J. H. (2021). Microplastic pollution in seawater and marine organisms across the Tropical Eastern Pacific and Galápagos. Sci. Rep., 11(1), 6424. https://doi.org/10.1038/s41598-021-85939-3

Andrady, A. L. (2011). Microplastics in the Marine Environment. Mar. Pollut. Bull., 62(8), 1596–1605. https://doi.org/10.1016/j.marpolbul.2011.05.030

Arthur, C., Baker, J. E., & Bamford, H. A. (2009). Proceedings of the International Research Workshop on the Occurrence, Effects, and Fate of Microplastic Marine Debris, September 9-11, 2008, University of Washington Tacoma, Tacoma, WA, USA.

Avio, C. G., Gorbi, S., & Regoli, F. (2017). Plastics and microplastics in the oceans: From emerging pollutants to emerged threat. Mar. Environ. Res., 128, 2–11. https://doi.org/10.1016/j.marenvres.2016.05.012

Axworthy, J. B., & Padilla-Gamiño, J. L. (2019). Microplastics ingestion and heterotrophy in thermally stressed corals. Sci. Rep., 9(1). https://doi.org/10.1038/s41598-019-54698-7

Babichuk, I. S., Lin, C., Qiu, Y., Zhu, H., Ye, T. T., Gao, Z., & Yang, J. (2022). Raman mapping of piezoelectric poly(l-lactic acid) films for force sensors. RSC Adv., 12(43), 27687–27697. https://doi.org/10.1039/d2ra04241j

Bagheri, G., & Bonadonna, C. (2016). Aerodynamics of Volcanic Particles. Elsevier eBooks, 39–52. https://doi.org/10.1016/b978-0-08-100405-0.00005-7

Baier, R. E. (1980). Substrata Influences on the Adhesion of Microorganisms and Their Resultant New Surface Properties. eds K. C. Marshall and G. Bitton (New York, NY: Willey), 59–104.

Bakker, D. P., Busscher, H. J., van Zanten, J., de Vries, J., Klijnstra, J. W., & van der Mei, H. C. (2004). Multiple linear regression analysis of bacterial deposition to polyurethane coatings after conditioning film formation in the marine environment. Microbiology (Reading), 150(6), 1779–1784. https://doi.org/10.1099/mic.0.26983-0

Barnes, D. K. A., Galgani, F., Thompson, R. C., & Barlaz, M. (2009). Accumulation and Fragmentation of Plastic Debris in Global Environments. Phil. Trans. R. Soc. B, 364(1526), 1985–1998. https://doi.org/10.1098/rstb.2008.0205

Bergmeyer, H. U., & Grassl, M. (1983). Methods of enzymatic analysis, Metabolites 1: Carbohydrates (Vol. IV).

Bhagwat, G., Carbery, M., Anh Tran, T. K., Grainge, I., O'Connor, W., & Palanisami, T. (2021). Fingerprinting Plastic-Associated Inorganic and Organic Matter on Plastic Aged in the Marine Environment for a Decade. Environ. Sci. Technol., 55(11), 7407–7417. https://doi.org/10.1021/acs.est.1c00262

Caruso, M. M., Davis, D. A., Shen, Q., Odom, S. A., Sottos, N. R., White, S. R., & Moore, J. S. (2009). Mechanically-Induced Chemical Changes in Polymeric Materials. Chem. Rev., 109(11), 5755–5798. https://doi.org/10.1021/cr9001353

Chen, Y.-T., Ding, D.-S., Lim, Y. C., Singhania, R. R., Hsieh, S., Chen, C.-W., Hsieh, S.-L., & Dong, C.-D. (2022). Impact of polyethylene microplastics on coral Goniopora columna causing oxidative stress and histopathology damages. Sci. Total Environ., 828, 154234. https://doi.org/10.1016/j.scitotenv.2022.154234

Cole, M., Lindeque, P., Halsband, C., & Galloway, T. S. (2011). Microplastics as contaminants in the marine environment: A review. Mar. Pollut. Bull., 62(12), 2588–2597. https://doi.org/10.1016/j.marpolbul.2011.09.025

Compère, C., Bellon-Fontaine, M.-N., Bertrand, P., Costa, D. C., Marcus, P. M., Poleunis, C., Pradier, C., Rondot, B., & Walls, M. (2001). Kinetics of conditioning layer formation on stainless steel immersed in seawater. Biofouling, 17(2), 129–145. https://doi.org/10.1080/08927010109378472

Conkle, J. L., Báez Del Valle, C. D., & Turner, J. W. (2017). Are We Underestimating Microplastic Contamination in Aquatic Environments? Environ. Manag., 61(1), 1–8. https://doi.org/10.1007/s00267-017-0947-8

Corinaldesi, C., Canensi, S., Dell'Anno, A., Tangherlini, M., Di Capua, I., Varrella, S., Willis, T. J., Cerrano, C., & Danovaro, R. (2021). Multiple Impacts of Microplastics Can Threaten Marine habitat-forming Species. Commun. Biol., 4(1). https://doi.org/10.1038/s42003-021-01961-1

Costanza, R., de Groot, R., Sutton, P., van der Ploeg, S., Anderson, S. J., Kubiszewski, I., Farber, S., & Turner, R. K. (2014). Changes in the global value of ecosystem services. Glob. Environ. Change, 26, 152–158. https://doi.org/10.1016/j.gloenvcha.2014.04.002

De Kee, D., & Wissbrun, K. F. (1998). Polymer Rheology. Phys. Today, 51(6), 24–29. https://doi.org/10.1063/1.882283

Doyotte, A., Cossu, C., Jacquin, M. C., Babut, M., & Vasseur, P. (1997). Antioxidant enzymes, glutathione and lipid peroxidation as relevant biomarkers of experimental or field exposure in the gills and the digestive gland of the freshwater bivalve Unio tumidus. Aquat. Toxicol., 39(2), 93–110. https://doi.org/10.1016/s0166-445x(97)00024-6

Feng, L., He, L., Jiang, S., Chen, J., Zhou, C., Qian, Z.-J., Hong, P., Sun, S., & Li, C. (2020). Investigating the composition and distribution of microplastics surface biofilms in coral areas. Chemosphere, 252, 126565. https://doi.org/10.1016/j.chemosphere.2020.126565

Fridovich, I. (2022). Reprint of: Biological Effects of the Superoxide Radical. Arch. Biochem. Biophys., 726, 109228–109228. https://doi.org/10.1016/j.abb.2022.109228

Gardner, S. G., Nielsen, D. A., Laczka, O., Shimmon, R., Beltran, V. H., Ralph, P. J., & Petrou, K. (2016). Dimethylsulfoniopropionate, superoxide dismutase and glutathione as stress response indicators in three corals under short-term hyposalinity stress. Proc. R. Soc. B, 283(1824), 20152418. https://doi.org/10.1098/rspb.2015.2418

Garra, S., Hall, A., & Kingsford, M. J. (2020). The effects of predation on the condition of soft corals. Coral Reefs, 39(5), 1329–1343. https://doi.org/10.1007/s00338-020-01967-x

Gerard-Monnier, D., Erdelmeier, I., Régnard, K., Moze-Henry, N., Yadan, J.-C., & Chaudiere, J. (1998). Reactions of 1-Methyl-2-phenylindole with Malondialdehyde and 4-Hydroxyalkenals. Analytical Applications to a Colorimetric Assay of Lipid Peroxidation. Chem. Res. Toxicol., 11(10), 1176–1183. https://doi.org/10.1021/tx9701790

Gewert, B., Plassmann, M. M., & MacLeod, M. (2015). Pathways for degradation of plastic polymers floating in the marine environment. Environ. Sci.: Processes Impacts, 17(9), 1513–1521. https://doi.org/10.1039/c5em00207a

Global plastic production | Statista. (2018). Statista; Statista. https://www.statista.com/statistics/282732/global-production-of-plastics-since-1950

Graham, N. A. J., & Nash, K. L. (2012). The importance of structural complexity in coral reef ecosystems. Coral Reefs, 32(2), 315–326. https://doi.org/10.1007/s00338-012-0984-y

Gustus, R., & Wegewitz, L. (2025). Modification of polylactic acid (PLA) surfaces by argon DBD plasma jet treatment and x–ray irradiation. Appl. Surf. Sci., 162589–162589. https://doi.org/10.1016/j.apsusc.2025.162589

Hartmann, N. B., Rist, S., Bodin, J., Jensen, L. H., Schmidt, S. N., Mayer, P., Meibom, A., & Baun, A. (2017). Microplastics as vectors for environmental contaminants: Exploring sorption, desorption, and transfer to biota. Integr. Environ. Assess. Manag., 13(3), 488–493. https://doi.org/10.1002/ieam.1904

Hayes, J. D., & McLellan, L. I. (1999). Glutathione and glutathione-dependent enzymes represent a co-ordinately regulated defence against oxidative stress. Free Radic. Res., 31(4), 273–300. https://doi.org/10.1080/10715769900300851

Hayes, J. D., & Strange, R. C. (2000). Glutathione S-Transferase Polymorphisms and Their Biological Consequences. Pharmacology, 61(3), 154–166. https://doi.org/10.1159/000028396

Hutchings, P. (2019). The Great Barrier Reef : biology, environment and management. CSIRO Publishing.

Isa, V., Seveso, D., Diamante, L., Montalbetti, E., Montano, S., Gobbato, J., Lavorano, S., Galli, P., & Louis, Y. D. (2024). Physical and cellular impact of environmentally relevant microplastic exposure on thermally challenged Pocillopora damicornis (Cnidaria, Scleractinia). Sci. Total Environ., 170651–170651. https://doi.org/10.1016/j.scitotenv.2024.170651

Jeffrey, S. W., & Humphrey, G. F. (1975). New spectrophotometric equations for determining chlorophylls a, b, c1 and c2 in higher plants, algae and natural phytoplankton. Biochem. Physiol. Pflanz., 167(2), 191–194. https://doi.org/10.1016/s0015-3796(17)30778-3

Jeong, C.-B., Kang, H.-M., Lee, M.-C., Kim, D.-H., Han, J., Hwang, D.-S., Souissi, S., Lee, S.-J., Shin, K.-H., Park, H. G., & Lee, J.-S. (2017). Adverse effects of microplastics and oxidative stress-induced MAPK/Nrf2 pathway-mediated defense mechanisms in the marine copepod Paracyclopina nana. Sci. Rep., 7(1), 1–11. https://doi.org/10.1038/srep41323

Jiang, S., Zhang, Y., Feng, L., He, L., Zhou, C., Hong, P., Sun, S., Zhao, H., Liang, Y.-Q., Ren, L.,

Zhang, Y., Chen, J., & Li, C. (2020). Comparison of Short- and Long-Term Toxicity of Microplastics with Different Chemical Constituents on Button Polyps. (Protopalythoa sp.). ACS Earth Space Chem., 5(1), 12–22. https://doi.org/10.1021/acsearthspacechem.0c00213

Jiang, Y., Tang, X., Zhou, B., Sun, T., Chen, H., Zhao, X., & Wang, Y. (2017). The ROS-mediated pathway coupled with the MAPK-p38 signalling pathway and antioxidant system plays roles in the responses of Mytilus edulis haemocytes induced by BDE-47. Aquat. Toxicol., 187, 55–63. https://doi.org/10.1016/j.aquatox.2017.03.011

Jin, F.-L., Hu, R.-R., & Park, S.-J. (2019). Improvement of thermal behaviors of biodegradable poly(lactic acid) polymer: A review. Compos. B. Eng., 164, 287–296. https://doi.org/10.1016/j.compositesb.2018.10.078

Kaiser, D., Kowalski, N., & Waniek, J. J. (2017). Effects of biofouling on the sinking behavior of microplastics. Environ. Res. Lett., 12(12), 124003. https://doi.org/10.1088/1748-9326/aa8e8b

Kefer, S., Miesbauer, O., & Langowski, H. C. (2021). Environmental microplastic particles vs. engineered plastic microparticles—a comparative review. Polymers, 13(17), 2881. https://doi.org/10.3390/polym13172881

Kowalski, N., Reichardt, A. M., & Waniek, J. J. (2016). Sinking rates of microplastics and potential implications of their alteration by physical, biological, and chemical factors. Mar. Pollut. Bull., 109(1), 310–319. https://doi.org/10.1016/j.marpolbul.2016.05.064

Krueger, T., Hawkins, T. D., Becker, S., Pontasch, S., Dove, S., Hoegh-Guldberg, O., Leggat, W., Fisher, P. L., & Davy, S. K. (2015). Differential coral bleaching—Contrasting the activity and response of enzymatic antioxidants in symbiotic partners under thermal stress. Comp. Biochem. Physiol. A, 190, 15–25. https://doi.org/10.1016/j.cbpa.2015.08.012

Kushwaha, M., Shankar, S., Goel, D., Singh, S., Rahul, J., Rachna, K., & Singh, J. (2024). Microplastics pollution in the marine environment: A review of sources, impacts and mitigation. Mar. Pollut. Bull., 209, 117109. https://doi.org/10.1016/j.marpolbul.2024.117109.

Lawrence, J. R., Neu, T. R., Paule, A., Korber, D. R., & Wolfaardt, G. M. (2015). Aquatic Biofilms: Development, Cultivation, Analyses, and Applications. Manual Environ. Microbiol., 4.2.3-14.2.3-33. https://doi.org/10.1128/9781555818821.ch4.2.3

Lesser, M. P. (2006). Oxidative stress in marine environment: Biochemistry and Physiological Ecology. Annu. Rev. Physiol., 68(1), 253–278. https://doi.org/10.1146/annurev.physiol.68.040104.110001

Levy, O., Achituv, Y., Yacobi, Y. Z., Stambler, N., & Dubinsky, Z. (2006). The impact of spectral composition and light periodicity on the activity of two antioxidant enzymes (SOD and CAT) in the coral Favia favus. J. Exp. Mar. Bio. Ecol., 328(1), 35–46. https://doi.org/10.1016/j.jembe.2005.06.018

Li, T., Sun, H., Han, H., Zhang, C., Li, B., Huang, J., & Sun, D. (2022). Ultrafast bulk degradation of polylactic acid by artificially cultured diatom frustules. Compos. Sci. Technol., *223*, 109410. https://doi.org/10.1016/j.compscitech.2022.109410

Liao, B., Wang, J., Xiao, B., Yang, X., Xie, Z., Li, D., & Li, C. (2021). Effects of acute microplastic exposure on physiological parameters in Tubastrea aurea corals. Mar. Pollut. Bull., 165, 112173. https://doi.org/10.1016/j.marpolbul.2021.112173

Loeb, G. I., & Neihof, R. A. (1975). Marine Conditioning Films. Adv. Chem. Ser., 319–335. https://doi.org/10.1021/ba-1975-0145.ch016

Maddison, C., Sathish, C. I., Lakshmi, D., Wayne, O. C., & Palanisami, T. (2023). An advanced analytical approach to assess the long-term degradation of microplastics in the marine environment. NPJ Materials Degradation, 7(1), 59. https://doi.org/10.1038/s41529-023-00377-y

Manju Sudheer, M., Fazli, A., Sganga, S., Tirelli, N., Carzino, R., Veronesi, M., Khabarov, K., Athanassiou, A., & Fragouli, D. (2025). Poly(lactic acid) nanoplastics through laser ablation: Establishing a reference model for mimicking biobased nanoplastics in aquatic environments. Environ. Sci.: Nano. https://doi.org/10.1039/d4en00891j

Martin, C., Corona, E., Mahadik, G. A., & Duarte, C. M. (2019). Adhesion to coral surface as a potential sink for marine microplastics. Environ. Pollut., 255, 113281. https://doi.org/10.1016/j.envpol.2019.113281

Meaurio, E., López-Rodríguez, N., & Sarasua, J. R. (2006). Infrared Spectrum of Poly(l-lactide): Application to Crystallinity Studies. Macromolecules, 39(26), 9291–9301. https://doi.org/10.1021/ma061890r

Mkuye, R., Gong, S., Zhao, L., Masanja, F., Ndandala, C., Bubelwa, E., Yang, C., & Deng, Y. (2022). Effects of microplastics on physiological performance of marine bivalves, potential impacts, and enlightening the future based on a comparative study. Sci. Total Environ., 838, 155933. https://doi.org/10.1016/j.scitotenv.2022.155933

Montalbetti, E., Biscéré, T., Ferrier-Pagès, C., Houlbrèque, F., Orlandi, I., Forcella, M., Galli, P., Vai, M., & Seveso, D. (2021). Manganese Benefits Heat-Stressed Corals at the Cellular Level. Front. Mar. Sci., 8. https://doi.org/10.3389/fmars.2021.681119

Montalbetti, E., Cavallo, S., Azzola, A., Montano, S., Galli, P., Montefalcone, M., & Seveso, D. (2023). Mucilage-induced necrosis reveals cellular oxidative stress in the Mediterranean gorgonian Paramuricea clavata. J. Exp. Mar. Bio. Ecol., 559, 151839–151839. https://doi.org/10.1016/j.jembe.2022.151839

Montalbetti, E., Isa, V., Vencato, S., Louis, Y., Montano, S., Lavorano, S., Maggioni, D., Galli, P., & Seveso, D. (2022). Short-term microplastic exposure triggers cellular damage through oxidative stress in the soft coral Coelogorgia palmosa. Mar. Biol. Res., 18(7-8), 495–508. https://doi.org/10.1080/17451000.2022.2137199

Montalbetti, E., Cavallo, S., Azzola, A., Montano, S., Galli, P., Montefalcone, M., & Seveso, D. (2023). Mucilage-induced necrosis reveals cellular oxidative stress in the Mediterranean gorgonian Paramuricea clavata. J. Exp. Mar. Bio. Ecol., 559, 151839–151839. https://doi.org/10.1016/j.jembe.2022.151839

Montilla, L., Ramos, R., García, E., & Cróquer, A. (2016). Caribbean yellow band disease compromises the activity of catalase and glutathione S-transferase in the reef-building coral Orbicella faveolata exposed to anthracene. Dis. Aquat. Org., 119(2), 153–161. https://doi.org/10.3354/dao02980

Pan, P., Kai, W., Zhu, B., Dong, T., & Inoue, Y. (2007). Polymorphous Crystallization and Multiple Melting Behavior of Poly(l-lactide): Molecular Weight Dependence. Macromolecules, 40(19), 6898–6905. https://doi.org/10.1021/ma071258d

Paul-Pont, I., Lacroix, C., González Fernández, C., Hégaret, H., Lambert, C., Le Goïc, N., Frère, L., Cassone, A.-L., Sussarellu, R., Fabioux, C., Guyomarch, J., Albentosa, M., Huvet, A., & Soudant, P. (2016). Exposure of marine mussels Mytilus spp. to polystyrene microplastics: Toxicity and influence on fluoranthene bioaccumulation. Environ. Pollut., 216, 724–737. https://doi.org/10.1016/j.envpol.2016.06.039

PlasticsEurope. (2018). https://www.plasticseurope.org/en/resources/publications/619-plastics-facts-2018

Qi, X., Ren, Y., & Wang, X. (2017). New advances in the biodegradation of Poly(lactic) acid. Int. Biodeterior. Biodegrad., 117, 215–223. https://doi.org/10.1016/j.ibiod.2017.01.010

Qin, D., & Kean, R. (1998). Crystallinity Determination of Polylactide by FT-Raman Spectrometry. Appl. Spectrosc., 52(4), 488–495. https://doi.org/10.1366/0003702981943950

Rades, M., Schubert, P., Wilke, T., & Reichert, J. (2022). Reef-Building Corals Do Not Develop Adaptive Mechanisms to Better Cope With Microplastics. Front. Mar. Sci., 9. https://doi.org/10.3389/fmars.2022.863187

Ramos, R., & García, E. (2007). Induction of mixed-function oxygenase system and antioxidant enzymes in the coral Montastraea faveolata on acute exposure to benzo(a)pyrene. Comp. Biochem. Physiol. C, 144(4), 348–355. https://doi.org/10.1016/j.cbpc.2006.11.006

Ramsperger, A. F. R. M., Stellwag, A. C., Caspari, A., Fery, A., Lueders, T., Kress, H., Löder, M. G. J., & Laforsch, C. (2020). Structural Diversity in Early-Stage Biofilm Formation on Microplastics Depends on Environmental Medium and Polymer Properties. Water, 12(11), 3216. https://doi.org/10.3390/w12113216

Ravishankar, K., Ramesh, P. S., Sadhasivam, B., & Raghavachari, D. (2018). Wear-induced mechanical degradation of plastics by low-energy wet-grinding. Polym. Degrad. Stab., 158, 212–219. https://doi.org/10.1016/j.polymdegradstab.2018.10.026

Regoli, F., & Giuliani, M. E. (2014). Oxidative pathways of chemical toxicity and oxidative stress biomarkers in marine organisms. Mar. Environ. Res., 93, 106–117. https://doi.org/10.1016/j.marenvres.2013.07.006

Reichert, J., Arnold, A. L., Hoogenboom, M. O., Schubert, P., & Wilke, T. (2019). Impacts of microplastics on growth and health of hermatypic corals are species-specific. Environ. Pollut., 254, 113074. https://doi.org/10.1016/j.envpol.2019.113074

Rittle, K. H., Helmstetter, C. E., Meyer, A. E., & Baier, R. E. (1990). Escherichia coliretention on solid surfaces as functions of substratum surface energy and cell growth phase. Biofouling, 2(2), 121–130. https://doi.org/10.1080/08927019009378138

Rocha, R. J. M., Rodrigues, A. C. M., Campos, D., Cícero, L. H., Costa, A. P. L., Silva, D. A. M., Oliveira, M., Soares, A. M. V. M., & Patrício Silva, A. L. (2020). Do microplastics affect the zoanthid Zoanthus sociatus? Sci. Total Environ., 713, 136659. https://doi.org/10.1016/j.scitotenv.2020.136659

Smith, P. B., Leugers, A., Kang, S., Yang, X., & Hsu, S. L. (2001). Raman characterization of orientation in poly(lactic acid) films. Macromol. Symp., 175(1), 81–94. https://doi.org/10.1002/1521-3900(200110)175:1%3C81::aid-masy81%3E3.0.co;2-1

Song, X., Lan, D., Liu, Z., Wang, J., & Ma, Y. (2025). Microbial colonization and succession on polylactic acid microplastics (PLA MPs) in mangrove forests-the role of environmental conditions and plastic properties. Environ. Res., 121662. https://doi.org/10.1016/j.envres.2025.121662

Soriano-Santiago, O. S., Liñán-Cabello, M. A., Delgadillo-Nuño, M. A., Ortega-Ortiz, C., & Cuevas-Venegas, S. (2013). Physiological responses to oxidative stress associated with pH variations in host tissue and zooxanthellae of hermatypic coral Pocillopora capitata. Mar. Freshw. Behav. Physiol., 46(5), 275–286. https://doi.org/10.1080/10236244.2013.827877

Spalding, M., Burke, L., Wood, S. A., Ashpole, J., Hutchison, J., & zu Ermgassen, P. (2017). Mapping the global value and distribution of coral reef tourism. Mar. Policy, 82(1), 104–113. https://doi.org/10.1016/j.marpol.2017.05.014

Statista. (2025, February 28). Annual Production of Plastics Worldwide from 1950 to 2020. Statista. https://www.statista.com/statistics/282732/global-production-of-plastics-since-1950/

Stow, D. A. V. (2005). Sedimentary Rocks in the Field: A Colour Guide. CRC Press.

Sutton, R., Mason, S. A., Stanek, S. K., Willis-Norton, E., Wren, I. F., & Box, C. (2016). Microplastic contamination in the San Francisco Bay, California, USA. Mar. Pollut. Bull., 109(1), 230–235. https://doi.org/10.1016/j.marpolbul.2016.05.077

Syakti, A. D., Jaya, J. V., Rahman, A., Hidayati, N. V., Raza'i, T. S., Idris, F., Trenggono, M., Doumenq, P., & Chou, L. M. (2019). Bleaching and necrosis of staghorn coral (Acropora formosa) in laboratory assays: Immediate impact of LDPE microplastics. Chemosphere, 228, 528–535. https://doi.org/10.1016/j.chemosphere.2019.04.156

Tang, J., Ni, X., Zhou, Z., Wang, L., & Lin, S. (2018). Acute microplastic exposure raises stress response and suppresses detoxification and immune capacities in the scleractinian coral Pocillopora damicornis. Environ. Pollut., 243, 66–74. https://doi.org/10.1016/j.envpol.2018.08.045

Taylor, G. T., Zheng, D., Lee, M., Troy, P. J., Gyananath, G., & Sharma, S. K. (1997). Influence of surface properties on accumulation of conditioning films and marine bacteria on substrata exposed to oligotrophic waters. Biofouling, 11(1), 31–57. https://doi.org/10.1080/08927019709378319

Vance, P. G., Keele, B. B., & Rajagopalan, K. V. (1972). Superoxide Dismutase from Streptococcus mutans. J. Biol. Chem., 247(15), 4782–4786. https://doi.org/10.1016/s0021-9258(19)44979-x

Veal, C. J., Carmi, M., Fine, M., & Hoegh-Guldberg, O. (2010). Increasing the accuracy of surface area estimation using single wax dipping of coral fragments. Coral Reefs, 29(4), 893–897. https://doi.org/10.1007/s00338-010-0647-9

Vencato, S., Isa, V., Seveso, D., Saliu, F., Galli, P., Lavorano, S., & Montano, S. (2021). Soft corals and microplastics interaction: first evidence in the alcyonacean species Coelogorgia palmosa. Aquat. Biol., 30, 133–139. https://doi.org/10.3354/ab00747

Verma, D., Lakhanpal, N., & Singh, K. (2019). Genome-wide identification and characterization of abiotic-stress responsive SOD (superoxide dismutase) gene family in Brassica juncea and B. rapa. BMC Genomics, 20(1). https://doi.org/10.1186/s12864-019-5593-5

Voolstra, C. R., Buitrago-López, C., Perna, G., Cárdenas, A., Hume, B. C. C., Rädecker, N., & Barshis, D. J. (2020). Standardized short-term acute heat stress assays resolve historical differences in coral thermotolerance across microhabitat reef sites. Glob. Change Biol., 26(8), 4328–4343. https://doi.org/10.1111/gcb.15148

Wang, J., Tan, Z., Peng, J., Qiu, Q., & Li, M. (2016). The behaviors of microplastics in the marine environment. Mar. Environ. Res., 113, 7–17. https://doi.org/10.1016/j.marenvres.2015.10.014

Wang, Y., Oberley, L. W., & Murhammer, D. W. (2001). Antioxidant defense systems of two lipidopteran insect cell lines. Free Radic. Biol. Med., 30(11), 1254–1262. https://doi.org/10.1016/s0891-5849(01)00520-2

Wright, R. J., Erni-Cassola, G., Zadjelovic, V., Latva, M., & Christie-Oleza, J. A. (2020). Marine Plastic Debris: A New Surface for Microbial Colonization. Environ. Sci. Technol., 54(19), 11657–11672. https://doi.org/10.1021/acs.est.0c02305

Wright, S. L., Thompson, R. C., & Galloway, T. S. (2013). The Physical Impacts of Microplastics on Marine organisms: a Review. Environ. Pollut., 178, 483–492. https://doi.org/10.1016/j.envpol.2013.02.031

Xiao, B., Li, D., Liao, B., Zheng, H., Yang, X., Xie, Y., Xie, Z., & Li, C. (2021). Effects of Microplastics Exposure on the Acropora sp. Antioxidant, Immunization and Energy Metabolism Enzyme Activities. Front. Microbiol., 12. https://doi.org/10.3389/fmicb.2021.666100

Xiao, B., Wang, J., Liao, B., Zheng, H., Yang, X., Xie, Z., Li, D., & Li, C. (2021). Combined effects of copper and microplastics on physiological parameters of Tubastrea aurea corals. Environ. Sci. Pollut. Res., 29(10), 14393–14399. https://doi.org/10.1007/s11356-021-16665-6

Zettler, E. R., Mincer, T. J., & Amaral-Zettler, L. A. (2013). Life in the “Plastisphere”: Microbial Communities on Plastic Marine Debris. Environ. Sci. Technol., 47(13), 7137–7146. https://doi.org/10.1021/es401288x

Zhu, Z., Bian, Y., Zhang, X., Zeng, R., & Yang, B. (2022). Study of Crystallinity and Conformation of Poly(lactic acid) by Terahertz Spectroscopy. Anal. Chem., 94(31), 11104–11111. https://doi.org/10.1021/acs.analchem.2c02652

3.7 Supporting Information

Table S3.1. Atomic composition (At%) obtained from XPS wide scan spectra of the samples before the incubation in *Artemia* salina water medium (MPs neat), after 1h of incubation in *Artemia salina* water medium (MPs + Artemia), and after 1h of incubation in *Artemia salina* water medium and washed with deionized water (MPs + Artemia washed).

	C	O	N	S	Cl	Si	Na	Mg	Ca	In
MPs Neat (At%)	88.5	8.6	2.4	-	-	-	-	-	-	0.5
MPs + Artemia (At%)	70.7	15.2	1.8	0.7	5.9	-	0.4	3.3	1.5	0.5
MPs + Artemia washed) (At%)	83.5	11.4	3.9	0.1	0.3	0.7	-	-	-	0.1

Table S3.2 . Overview of enzymatic and oxidative stress responses (SOD, CAT, GST, GSH, GR, and LPO) induced by PLA MPs in comparison with synthetic MPs from previous studies

Study	Tang et al. 2018	Rocha et al. 2020	Jiang et al. 2020	Xiao et al. 2021	Xiao et al. 2021	Chen et al. 2022	Our study
Type of MPs	PS	PVC, LDPE	PVC, PE, PMMA	PVC	PET, PA66, PE	PE	PLA
Type of polymer	Synthetic	Synthetic	Synthetic	Synthetic	Synthetic	Synthetic	Biobased
Size of MPs	1 µm	63-125 µm	1-20 µm	5-10 µm	10-40 µm	40-48 µm	150-300 µm
Concentration of MPs	50 mg/L	1, 10 mg/L	50 mg/L	1, 30 mg/L	50 mg/L	5, 10, 50, 100, 300 mg/L	5, 15, 50 mg/L
Exposure time	24 h	96 h	96h	72h	96 h	168 h	72h
Coral species	P. damicornis	Z. sociatus	Protopalythoa sp.	T. aurea	A. pruinosa	G. columna	P. damicornis
SOD response	↑	/	↑ (PVC)	↓	↑	↑	–

CAT response	↑	↑ (PVC)	/	↑	/	↑	–
GST response	↓	–	↑ (PVC, PE, PMMA)	/	/	↑	–
GHS response	/	/	↑ (PVC, PE, PMMA)	↑	↑	↑	/
GR response	/	/	/	/	/	/	↑
LPO response	/	↑ (PVC)	↑ (PVC, PE, PMMA)	↓	/	↑ (PVC, PE, PMMA)	–
Chl (a+c2)	↑	/	↑	/	↓	/	–

Notes on abbreviations:
MP:Microplastics
PS:Polystyrene
PVC:Polyvinyl chloride
PE:Polyethylene
PMMA:Polymethyl methacrylate
LDPE: Low-density polyethylene
PLA:Poly(lactic)acid
SOD:Superoxide dismutase
CAT:Catalase
GST:Glutathione S-transferase
GSH: Reduced glutathione
GR:Glutathion reductase
LPO: Lipid peroxidation
Chl(a+c2):Chlorophyll a+c2
↑:Significant increase
↓:Significant decrease
–: No significant change
/: Parameter not investigated in the study

4

Ciliary Dynamics and Mucus Mechanisms of Microplastic Trapping in Porites lutea (Cnidaria, Scleractinia)

Giorgia Ferrari[1,2], Cesar O. Pacherres[3], Michael Kühl[3], Despina Fragouli[1]

[1] Smart Materials, Istituto Italiano di Tecnologia (IIT), Genoa, Italy

[2]Department of Earth and Environmental Science, University of Milano Bicocca, Milano, Italy

[3]Marine Biology Section, Department of Biology, University of Copenhagen, Helsingør, Denmark

Manuscript in preparation

4.1 Abstract

Microplastic (MP) pollution represents a serious threat to marine ecosystems, as these particles originate from multiple sources and eventually accumulate on the seafloor. This is supported by evidence showing that, although millions of tons of plastic enter the oceans each year, floating debris constitutes only about 1% of the total plastic input. This discrepancy is particularly evident for microplastics smaller than 1 mm, which are largely absent from surface waters due to removal processes such as ingestion by marine organisms, biofouling, and sinking. Among the various marine habitats, coral reefs play a particularly important role in trapping microplastics. Their complex morphology allows them to intercept MPs carried by surrounding water flows, and their surface mucus can effectively capture particles. Consequently, the adhesion of microplastics to coral reef surfaces has been proposed as a key mechanism contributing to the retention and accumulation of these pollutants within reef ecosystems. Using microscopic particle image velocimetry (PIV), we demonstrate that the common scleractinian coral *Porites lutea* generates vortical currents in the surrounding water, which draw particles near coral surface. Within this region, particles become trapped in mucus filaments and subsequently aggregate, forming particle-rich mucus clusters. Furthermore, our results show that corals actively enhance the removal of PLA MPs from the surrounding water compared to control conditions, and that this process occurs over relatively short time scales.

4.2 Introduction

Marine plastic pollution is now ubiquitous, extending from densely populated coastal regions to some of the most remote islands on Earth (Mishra et al., 2021; Pradit et al., 2020). Owing to their versatility, durability, light weight, and low production costs, plastics are widely employed across industries (Khan et al., 2020). However, when mismanaged plastic waste reaches the ocean, it gradually fragments into microplastics (<5 mm; Moore, 2008) that enter global circulation and may persist for centuries in diverse marine habitats, including coral reef ecosystems (Barnes et al., 2009; Lartaud et al., 2020; Soares et al., 2020). Despite the continuous input of plastics, floating debris observed at the ocean surface accounts for only ~1% of the expected quantities (Van Sebille et al., 2015; Law, 2017). While theoretical models predict an exponential increase in particle abundance with decreasing size (Timár et al., 2010), microplastics <1 mm remain underrepresented in surface waters (Cozar et al., 2014; Eriksen et al., 2014). Several processes may explain this discrepancy, including plastic fragmentation, ingestion by marine organisms, shoreline deposition, biofouling, and subsequent sinking (Cozar et al., 2014). Such removal mechanisms suggest the existence of multiple sinks for microplastics, including Arctic sea ice (Obbard et al., 2014; Peeken et al., 2018), deep-sea sediments (Barrett et al., 2020; Kane et al., 2020; Woodall et al., 2014), coastal sediments (de Smit et al., 2021; Martin et al., 2020; Van Cauwenberghe et al., 2015), and marine biota, particularly organisms feeding on particles <1 mm (Cozar et al., 2014). In fact, microplastics are ingested across diverse taxa (Karlsson et al., 2017; Pagter et al., 2020), raising concerns due to their potential toxicological effects, including the transport of harmful chemicals (Karlsson et al., 2017; Pagter et al., 2020; Huang et al., 2023).

The capacity of marine environments to retain and accumulate microplastics varies considerably (Näkk i et al., 2019; Woodall et al., 2014; Zamprogno et al., 2021). Coral reefs, in particular, have been identified as potential sinks (de Smit et al., 2021; Reichert et al., 2022). Globally, reefs cover approximately 250,000 km² and consist of biologically accreted calcium carbonate structures (Reichert et al., 2021). Reef-building corals are the primary architects of these complex three-dimensional frameworks, which provide essential ecosystem services such as shoreline protection, livelihoods for over 500 million people, and habitat for a high diversity of marine organisms (Fisher et al., 2015). Due to their intricate morphology (Bradbury and Reichelt, 1983), coral reefs can intercept microplastics transported by surrounding water flows, making them capable of trapping substantial amounts of microplastics (Burke et al., 2011). Adhesion of microplastics to reef surfaces has therefore been proposed as a potential trapping mechanism (Martin et al., 2019).

Laboratory experiments have frequently shown that corals can trap microplastics on their surfaces (Allen et al., 2017; Reichert et al., 2018). However, adhesion has only recently been confirmed as an effective sink in three Red Sea coral species—*Acropora hemprichii*, *Goniastrea retiformis*, and *Pocillopora verrucosa* (Martin et al., 2019). That study reported that surface adhesion removes microplastics from the water column with an efficiency up to 40-fold higher than ingestion (Corona et al., 2021), although the mechanistic basis for this enhanced retention remains unclear. Mitigating the exposure of coral reef ecosystems to plastic pollution requires, as a primary measure, a substantial reduction in plastic production and mismanaged waste. In parallel, elucidating the processes driving microplastic accumulation on corals is crucial to design effective, site-specific remediation and cleaning strategies (Kim et al., 2024). Whereas most previous investigations have concentrated on microplastic ingestion and its associated impacts, the present study focuses on passive trapping mechanisms, with particular attention to the roles of mucus, ciliary activity, and vortex generation in the capture of Poly(lactic) acid (PLA) MPs produced by mechanical grinding.

Using the reef-building coral *Porites lutea* as a model organism, we employed a Particle Image Velocimetry (PIV) system equipped with either LED or laser light sheets to visualize the interaction of ciliary vortices, mucus secretion and MPs at the coral surface, and to assess the efficiency of particle capture for suspended PLA MPs ≤50 µm.

4.2 Materials and Methods

4.3.1 Materials

Semi-crystalline poly (lactic acid) (PLA) in the form of pellets with 4 mm average size produced by NatureWorks LLC (U.S.A) (commercial name: PLA4043D) were used.

4.3.2 Particles preparation

PLA MPs with size from 50 µm to low were produced via mechanical grinding. PLA MPs with a size ≤ 50 µm were produced by using Dry mill – IKA – PILOTINA MC and an electrical sieve with VWR Test Sieve 200 x 50 mm (mesh size 300 and 50 µm).

4.3.3 Coral fragments

Colonies of the massive coral *Porites lutea* reared at the aquaria facilities of the University of Copenhagen were used as fragment source. Before the start of the experiments, small fragments (area of ~ 400-600 cm^2) were cut out from source colonies and allowed to heal for at least two weeks.

4.3.4 PLA MPs characterization

Morphological analysis on the surface of the MPs was conducted by scanning electron microscopy (SEM) (JEOL JSM-6490LA SEM) using the secondary electrons detector with a 10 kV accelerating voltage and a load current of 78 µA. The MPs were attached to aluminum stubs by using carbon tape and coated with a 10 nm gold layer through a high-resolution sputter coater (Cressington 208 HR). Infrared spectra of the PLA pellets and MPs were acquired with a Fourier Transform Infrared (FTIR) spectrometer (Vertex 70v FT-IR, Bruker) coupled to a single-reflection attenuated total reflection (ATR) accessory (MIRacle ATR, PIKE Technologies) (ATR-FTIR). All the spectra presented were the average of 32 repetitive scans in the range of 4000-600 cm^{-1} at a resolution of 2 cm^{-1}.

4.3.5 Particle Image Velocimetry (PIV)

To resolve the flow field around the coral fragment, Particle Image Velocimetry (PIV) was used. The PIV technique enables the visualization and quantification of fluid velocity fields through optical tracking of tracer particles. The process involves several key steps. First, the fluid is seeded with tracer particles that faithfully follow the flow motion. A thin light sheet (laser of LED) is then used to illuminate a defined plane within the flow, allowing the particles within this plane to scatter light. A high-speed camera records two consecutive images of the illuminated particles, separated by a short and precisely controlled time interval (typically in the microsecond-to-millisecond range). Image processing algorithms subsequently analyze pairs of images to determine the displacement of particle ensembles within small interrogation areas. The local velocity vector is then calculated as the ratio between particle displacement (Δx) and the time delay between frames (Δt), thereby providing a quantitative map of the instantaneous flow field (Raffael et al., 2018). Water inside the flow through system was first seeded with PLA MPs (size $\leq$ 50 µm). Particle concentration was 1 mg L^{-1}. Illumination was achieved using a LED (LPS3, iLA_5150, Germany)and Laser Pulsing System (Optolution GmbH, Germany) according to the experiment, in particular, for the *en face* observations, LED illumination was employed to minimize stress on the coral. In contrast, laser light was used for lateral observations of particle flow, as it provided clearer visualization of the movement of PLA particles. In this case, the coral was not subjected to stress, since the laser exposure was limited to significantly shorter durations compared to the *en face* imaging, which was required to monitor the entrapment of PLA MPs within the coral mucus. Images were captured using a OPTOcam 2/80 (Optolution GmbH, Germany) recording pictures at 25 frames per second (fps).

The obtained images were analysed with the freely available software PIVlab v2.56 (Thielicke & Stamhuis, 2014). To obtain velocity fields, the image sample size was set to 64 x 64 with 50% overlap and a multigrid sampling window of 128 x 128 px. The velocity map was smothed using a 3 x 3 median filter.

4.3.6 Flow-cytometer

The quantification of PLA MPs in the experimental samples was performed using a CytoFLEX flow cytometer (Beckman Coulter, Brea, CA, USA). Samples were analyzed with a flow rate of 10 µL/min, and instrument settings were optimized to detect and count PLA particles based on their forward and side scatter properties. For each measurement, events were recorded for 5 minutes, ensuring consistency across all replicates and experimental conditions. Data acquisition and analysis were carried out using the CytExpert software and MatLab.

4.3.7 Experimental design

To assess the ability of the coral to remove PLA MPs, a fragment of *Porites lutea*, previously acclimated, was placed inside a PIV chamber (Pacherres et al., 2025) filled with seawater maintained at 25–26 °C and supplemented with PLA MPs. The chamber was connected to a pump (Ismatec® Reglo-Z,Cole-Parmer GmbH, Germany) providing a continuous flow of 10 mL/min. A control was set up under identical experimental conditions but without coral. All measurements were performed in triplicate. For each replicate, nine time points were collected at 15-minute intervals over a period of 2 hours. A second experiment was performed to complement and deepen the understanding of the findings from the first experiment. In this case, a tank filled with seawater was maintained at 25–26 °C. The tank was placed on a six-position plate stirrer (Thermo Scientific Cimarec™ i Telesystem Multipoint Stirrers, Waltham, MA, USA).

Six chambers were placed inside the tank, each consisting of a perforated double bottom and equipped with a stirrer to promote water movement (Dellisanti et al., 2024). Each chamber contained acclimated fragments of *Porites lutea* and seawater with PLA MPs at a concentration of 50 mg/mL. A control was set up under identical experimental conditions but without coral. Measurements were performed in nine replicates. For each replicate, two time points were collected: one at time zero and one after 2 hours. The aliquots obtained at each time point were analyzed using flow cytometry, and the data were subsequently processed with MATLAB for statistical analysis.

4.4 Results and Discussion

4.4.1 PLA MPs production

PLA MPs were produced by using Dry mill – IKA – PILOTINA MC and an electrical siever with VWR Test Sieve 200 x 50 mm (mesh size 300 and 150 µm). Initially, the 4 mm pellets were reduced to grains with size lower than 1 mm by the dry mill operating at 1500 rpm, equipped with a 1 mm sieve. The obtained powder was further processed through a finer sieve to obtain powder grain size lower than 750 µm. To isolate particles lower µm than 50 µm, the powder was subsequently sieved using an electrical siever (VWR Test Sieve, 200 x 50 mm) with a 300 µm mesh size, followed by a second sieving step with a 150 µm mesh size, and followed by a third sieving step with a 50 µm mesh size. Particles that passed through the final sieve were collected for further use. A total of 50 mg of PLA microplastics (≤50 µm) were suspended in 50 mL of seawater collected from the aquarium tank and pre-filtered through a hydrophilic cellulose acetate membrane (200 nm pore size). The resulting suspension was sonicated for 1 minute prior to experimental use.

4.4.2 PLA MPs physical and chemical characterization

The surface morphology of the PLA MPs after the grinding and sieving processes was examined using SEM analysis. The PLA MPs exhibited a rough surface texture (Figure 4.1), indicating that the mechanical fragmentation of larger PLA pieces resulted in surface fractures and cavities. The obtained MPs were polydisperse, displaying irregular shapes. As shown in Figure 4.1, the particles appeared either as flakes or as more rounded yet uneven fragments. The presence of particles larger than 50 µm can be attributed to the fact that the sieve allows the passage of particles with one dimension ≤50 µm, while the other may be elongated.

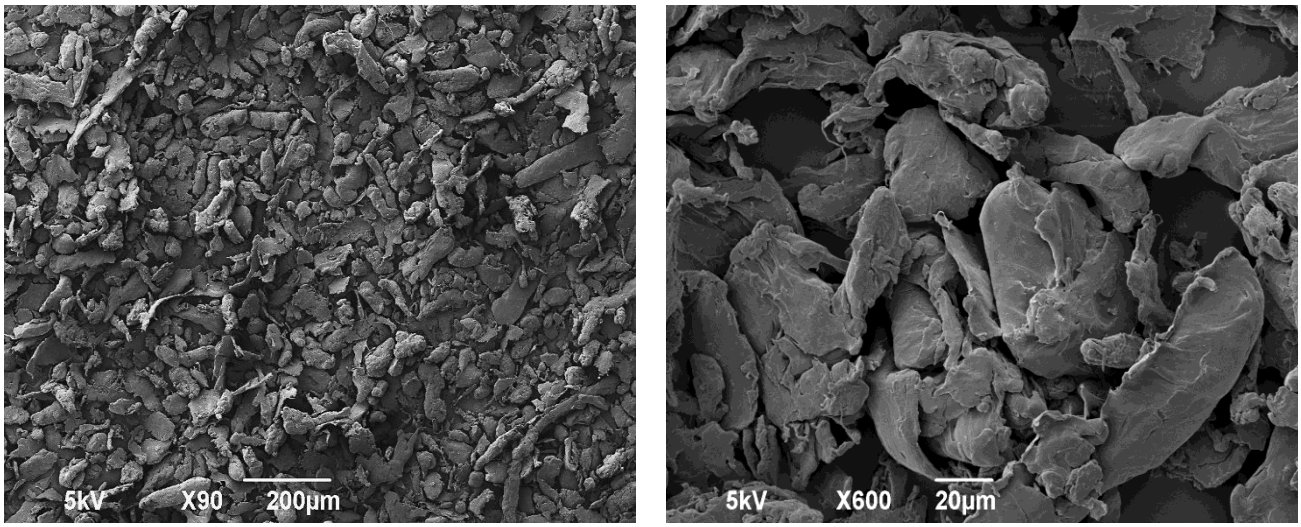

Figure 4.1. SEM images at two different magnification of PLA MPs after the grinding and sieving processes.

To assess potential compositional variations and structural modifications in PLA induced by the grinding process, ATR-FTIR spectroscopy was conducted. Figure 4.2 presents the normalized spectra of the PLA pellets and PLA MPs. The characteristic absorption bands of PLA were detected at comparable wavenumbers in both materials, corresponding to the C=O stretching of lactic acid ester groups, the asymmetric deformation of CH_3 groups, and the C–O–C stretching vibrations of ester linkages (1749–1747 cm^{-1}, 1454–1452 cm^{-1}, and within 1300–1000 cm^{-1}, respectively) (Kister et al., 1998; Urayama et al., 2003). Additional absorption peaks at 956 and 921 cm^{-1} were also present, with the former attributed to the amorphous phase and the latter associated with the crystalline α-phase (Meaurio et al., 2006).

However, distinct differences between the spectra were evident. In particular, the intensity of the 921 cm^{-1} band—corresponding to the flexural C–H vibration typical of the crystalline domains of PLA (Carrasco et al., 2010)—was markedly lower in the ground and milled PLA MPs than in the original pellets.

A similar reduction was observed for the 1210 cm^{-1} peak, which represents the ester C–O stretching of the crystalline structure (Meaurio et al., 2006). In the MPs spectrum, this feature appeared only as a minor shoulder, reflecting the reduced crystalline organization compared with the pristine material. Overall, these spectral variations indicate that the mechanical grinding process disrupts the ordered molecular structure of PLA, leading to a decrease in crystallinity.

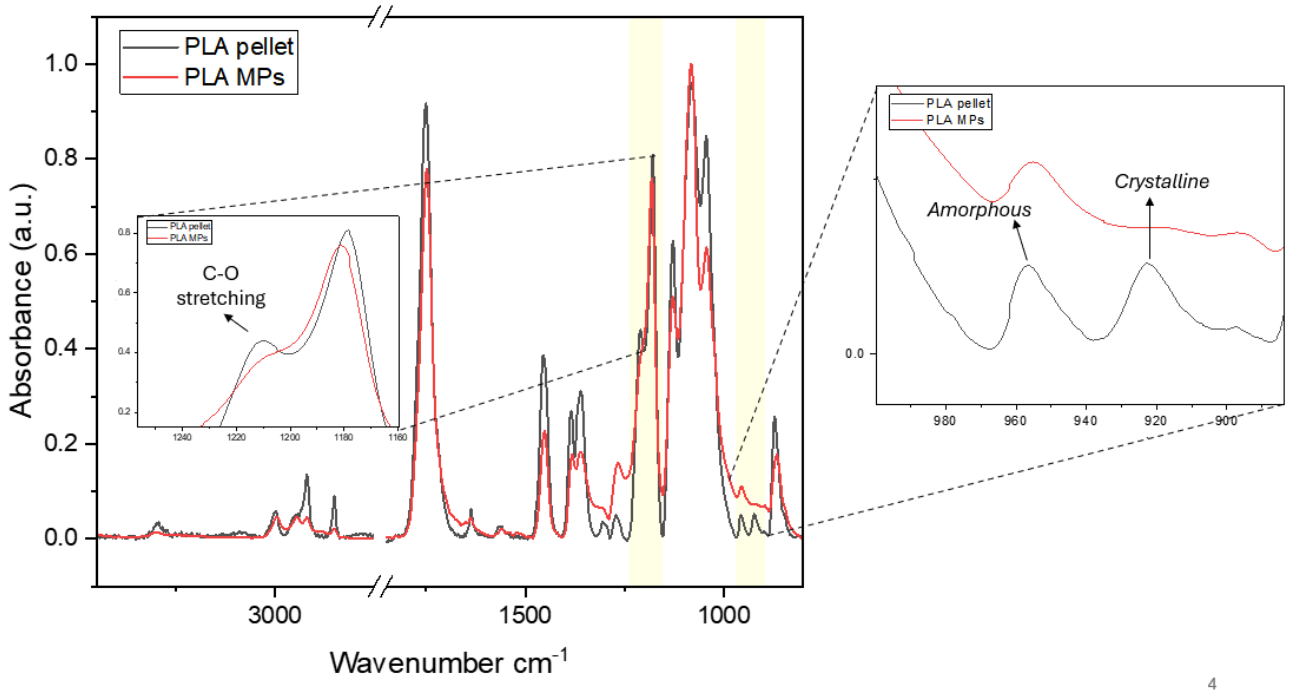

Figure 4.2. FTIR spectra of PLA MPs samples before the enzymatic treatment. Insets present the spectra magnifications of specific wavenumber areas.

4.4.3 Particle trapping by mucus and ciliary vortices

To perform PIV and investigate the interaction between *Porites lutea* and the PLA MPs (≤ 50 µm), we employed a setup combining light-sheet microscopy with a laminar flow chamber, which enabled high-resolution observations from both lateral and *en face* perspectives. Our observations revealed that the coral actively secreted mucus filaments (Figure 4.3a). Streamline analysis of the acquired images revealed that the coordinated beating of cilia generated vortical structures in the surrounding water (Figure 4.4), consistent with previous observations (Shapiro et al. 2014; Pacherres et al. 2020)

demonstrating that such vortical flows can enhance oxygen exchange and mitigate oxidative stress. PIV analyses further showed that, within these vortices, water was alternately directed toward and away from the coral surface, suggesting a dynamic control of local fluid transport. The ciliary beating at the coral surface appeared to drive vortices that transported particle-laden water toward the mucus-covered tissue, thereby promoting particle entrapment. Over time, we observed that mucus filaments progressively trapped suspended particles, which were subsequently either released back into the water column or consolidated into compact, particle-rich aggregates (Figure 4.3b). This process highlights the dual role of mucus secretion and ciliary activity in mediating particle capture and removal by the coral.

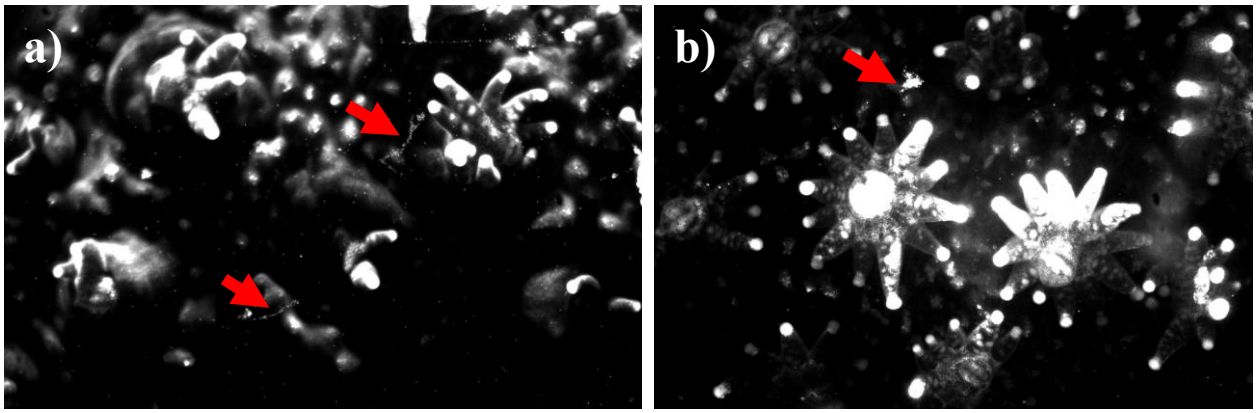

Figure 4.3. Particles trapped by mucus filaments in *en face* experiments. Red arrows indicate **a)** mucus filaments with entrapped PLA MPs and **b)** PLA MPs – mucus aggregates.

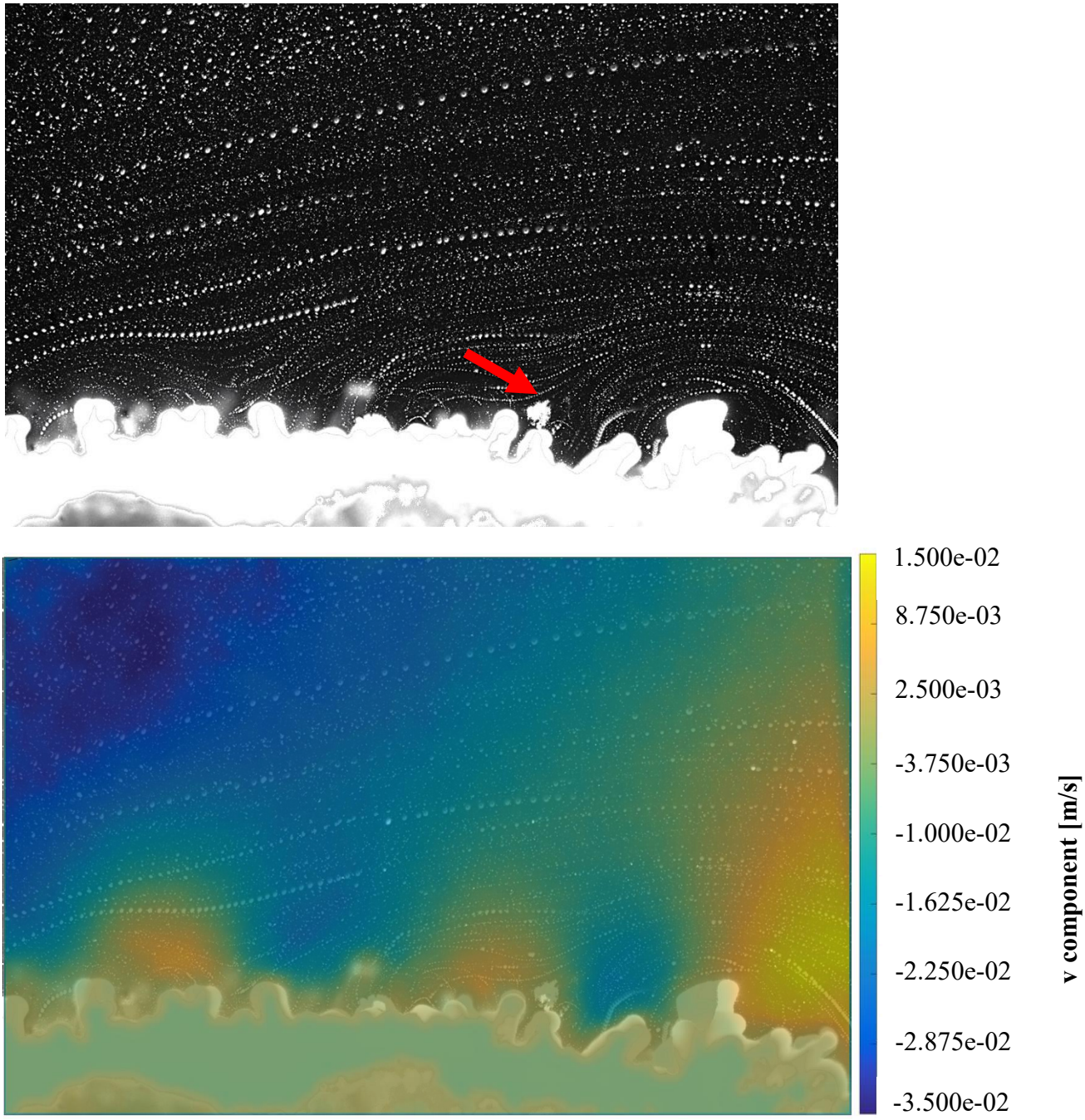

Figure 4.4. Particle trajectories at the coral-water interface under active cilia activity, showing the formation of vortices and their interaction with mucus filaments leading to particle aggregation and formation of mucus balls. Red arrow indicates mucus ball and detailed vertical velocity component of a vortex extracted from the PIV results under 10 mL/min flow speed, positive values indicate movement towards the coral while negative values indicate water moving away from the coral.

4.4.4 PLA MPs removal by Porites lutea - experiment with PIV chamber

To confirm the coral's effective removal and capture of PLA MPs, we measured MPs concentrations over a two-hour exposure, taking samples at nine time points every 15 minutes using flow cytometry. The comparison between the two experimental conditions (Control and Treatment) showed a clear difference in the temporal trend of PLA MPs removal (Figure 4.5). In both groups, the normalized number of particles decreased progressively over time; however, the decline was more pronounced in the presence of coral. After 120 minutes, the treatment group exhibited a significantly lower particle concentration compared to the control, indicating a more efficient removal of MPs.

Repeated measures ANOVA confirmed these observations. The analysis revealed a significant effect of Group ($p < 0.05$, Table 4.1), demonstrating that the presence of coral influenced particle dynamics. A highly significant effect of Time ($p < 0.05$, Table 4.1) was also detected, consistent with a gradual decrease in particle abundance over the course of the experiment. Moreover, the significant Group × Time interaction ($p < 0.05$, Table 4.1) indicates that the two groups followed distinct temporal patterns, with the treatment group showing a steeper decline.

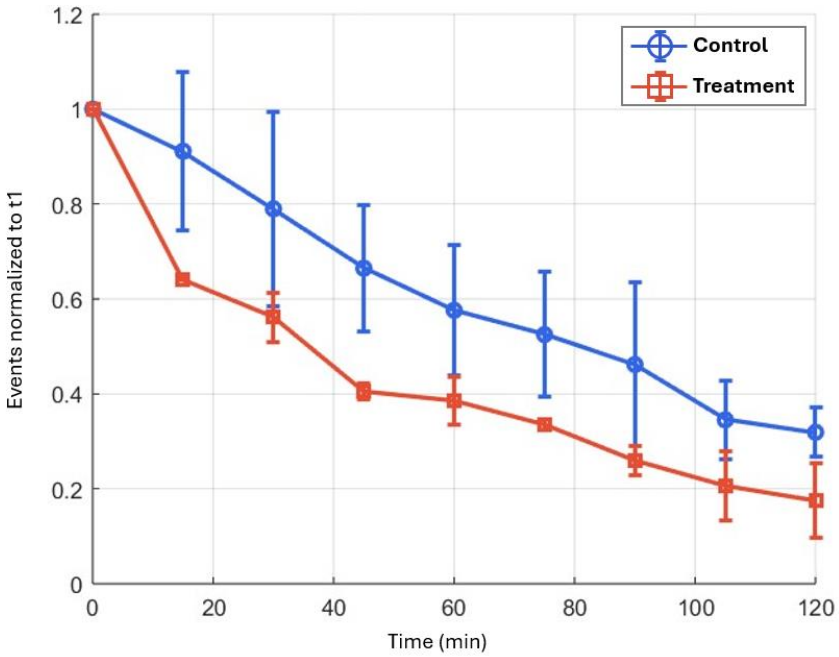

Figure 4.5. Temporal dynamics of normalized PLA MPs concentrations in the treatment and control groups over a 120-minute period. Data are expressed as mean ± SE, normalized to the initial time point (t1).

4.4.5 PLA MPs removal by Porites lutea - experiment with tank

To validate the findings of the previous experiment, we conducted an additional study to evaluate the coral's efficiency in removing and capturing PLA MPs, measuring MPs concentrations at two time points—at time zero and after two hours—using flow cytometry.

The two-way repeated measures ANOVA revealed significant main effects of both Group and Time, as well as a significant Group × Time interaction. The significant Group effect ($p < 0.05$, Table 4.1) indicates that overall MP removal differed between the treatment group and the control group, suggesting that the presence of coral substantially enhanced MP clearance. The significant effect of Time ($p < 0.05$, Table 4.1) highlights that MPs concentrations changed markedly over the two-hour experimental period, reflecting a strong temporal dynamic.

Importantly, the significant Group × Time interaction ($p < 0.05$, Table 4.1) shows that the temporal patterns of MP removal differed between

the two groups, indicating that changes in MPs concentrations were driven by the coral treatment rather than time alone.

Normalized MPs concentrations illustrate these trends clearly. In the treatment, MPs levels declined sharply over time, whereas in the control group, concentrations remained largely stable, producing non-parallel trajectories. This differential pattern confirms that coral actively contributes to MPs reduction, supporting the observed interaction between Group and Time.

The rapid decline in MP levels in the treatment suggests that corals may employ both passive filtration and active ingestion mechanisms to remove PLA MPs, whereas in the absence of coral, MPs persist in the water, as observed in the control (Figure 4.6).

TABLE 4.1. Results of the repeated measures ANOVA and two-way repeated measures ANOVA for the experiments described in Sections *4.3.4* and *4.3.5*. Main effects of the tested factors and their interaction are reported, together with the corresponding p-values.

Experiment with PIV chamber			**Experiment with tank**	
Effect	**p-value**		**p-value**	
Group	0.044089	*Significative* → difference between Treatmenr and Control groups.	0.0017	*Significative* → difference between Treatment and Control groups.
Time	0.00028	*Highly Signicative* → the number of particles clearly changes with time.	8.0338e-6	*Highly Signicative* → the number of particles clearly changes with time.
Group x Time	0.04723	*Significative* → The two curves display distinct temporal trends.	0.0017	*Significative* → The two curves display distinct temporal trends.

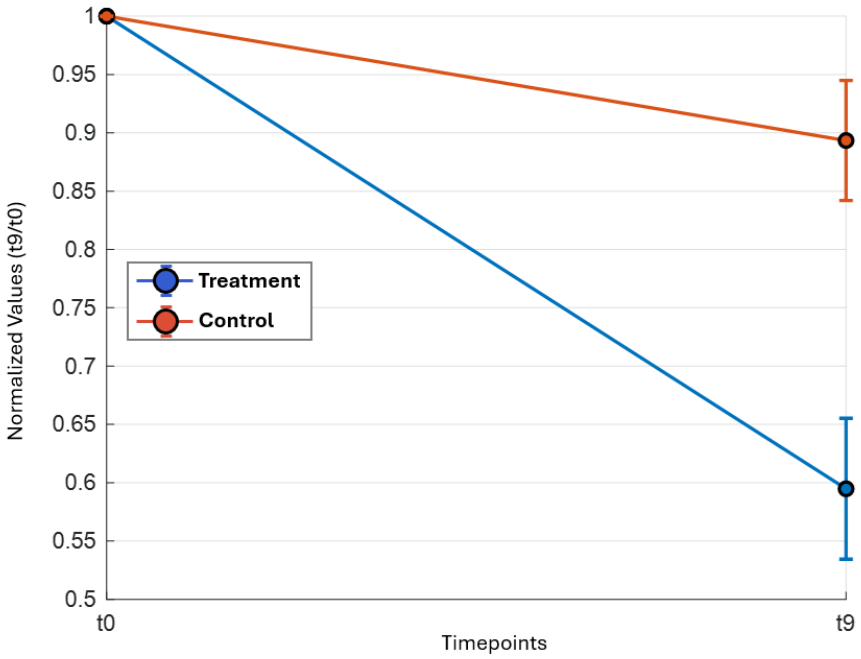

Figure 4.6. Temporal variation of normalized values in the treatment and control groups between the initial (t0) and final (t9) time points. Data are expressed as mean ± SE, normalized to t0.

To the best of our knowledge, this study represents the first comprehensive investigation into the roles of cilia and mucus in the capture of microplastics by a reef-building coral exposed to ground PLA MPs. Our findings indicate that vortices generated by ciliary motion, together with mucus filaments, can significantly enhance the retention of microplastics suspended in the water column. Corals are known to employ mucus filaments to trap fine particulate matter, which can subsequently be ingested (Muscatine, 1973; Ferrier-Pagès and Gattuso, 1998). In our experiments, ciliary beating at the coral surface produced localized water currents that directed particles toward the mucus-coated coral, thereby promoting their entrapment (Figure 4).

Additionally, as illustrated in Figure 3a–b, an intricate mucus network formed on the coral surface, effectively capturing PLA particles. The ability of corals to generate feeding currents to capture small planktonic particles may have significant ecological implications. Corals utilize ciliary currents to organize mucus filaments into particle-laden mucus balls, which are then transported to the mouth for ingestion—a mechanism also observed in earlier studies (Yonge, 1930; Lewis and Price, 2009). As demonstrated in this study and confirmed by previous work (Kim et al., 2024; Hall et al., 2015), corals can employ the same mechanism to capture microplastics suspended in the water column, potentially causing harm to the coral and acting as a sink for microplastic debris.

4.5 Conclusion

Taken together, these results demonstrate that corals actively contribute to the removal of PLA MPs from the surrounding water with respect to the control. These findings align with previous studies reporting the capacity of corals to capture particles from the water column. Overall, our results suggest that corals interact with microplastics over relatively short time scales, which could represent a concern in natural environments given how quickly these interactions occur. The contrast between treatment and control groups underscores that MPs reduction is not a passive phenomenon but depends on coral activity, emphasizing the importance of considering biological interactions in assessments of MPs dynamics.

4.6 References

Allen, A. S., Seymour, A. C., & Rittschof, D. (2017). Chemoreception drives plastic consumption in a hard coral. Mar. Pollut. Bull., 124(1), 198–205. https://doi.org/10.1016/j.marpolbul.2017.07.030

Barnes, D. K. A., Galgani, F., Thompson, R. C., & Barlaz, M. (2009). Accumulation and Fragmentation of Plastic Debris in Global Environments. Philos. Trans. R. Soc. B Biol. Sci., 364(1526), 1985–1998. https://doi.org/10.1098/rstb.2008.0205

Barrett, J., Chase, Z., Zhang, J., Holl, M. M. B., Willis, K., Williams, A., Hardesty, B. D., & Wilcox, C. (2020). Microplastic Pollution in Deep-Sea Sediments From the Great Australian Bight. Front. Mar. Sci., 7. https://doi.org/10.3389/fmars.2020.576170

Bradbury, R., & Reichelt, R. (1983). Fractal Dimension of a Coral Reef at Ecological Scales. Mar. Ecol. Prog. Ser., 10, 169–171. https://doi.org/10.3354/meps010169

Burke, L., Reytar, K., Spalding, M., & Perry, A. (2011). Reefs at Risk Revisited. In bvearmb.do. Washington, DC: World Resources Institute. https://bvearmb.do/handle/123456789/1787

Carrasco, F., Pagès, P., Gámez-Pérez, J., Santana, O. O., & Maspoch, M. L. (2010). Processing of poly(lactic acid): Characterization of chemical structure, thermal stability and mechanical properties. Polym. Degrad. Stab., 95(2), 116–125. https://doi.org/10.1016/j.polymdegradstab.2009.11.045

Corona, E., Martin, C., Marasco, R., & Duarte, C. M. (2020). Passive and Active Removal of Marine Microplastics by a Mushroom Coral (Danafungia scruposa). Front. Mar. Sci., 7. https://doi.org/10.3389/fmars.2020.00128

Cozar, A., Echevarria, F., Gonzalez-Gordillo, J. I., Irigoien, X., Ubeda, B., Hernandez-Leon, S., Palma, A. T., Navarro, S., Garcia-de-Lomas, J., Ruiz, A., Fernandez-de-Puelles, M. L., & Duarte, C. M. (2014). Plastic Debris in the Open Ocean. Proc. Natl. Acad. Sci. U. S. A., 111(28), 10239–10244. https://doi.org/10.1073/pnas.1314705111

Dellisanti, W., Zhang, Q., Ferrier-Pagès, C., & Kühl, M. (2024). Contrasting effects of increasing dissolved iron on photosynthesis and O2 availability in the gastric cavity of two Mediterranean corals. *PeerJ*, *12*, e17259. https://doi.org/10.7717/peerj.17259

de Smit, J. C., Anton, A., Martin, C., Rossbach, S., Bouma, T. J., & Duarte, C. M. (2021). Habitat-forming species trap microplastics into coastal sediment sinks. Sci. Total Environ., 772, 145520. https://doi.org/10.1016/j.scitotenv.2021.145520

Eriksen, M., Lebreton, L. C. M., Carson, H. S., Thiel, M., Moore, C. J., Borerro, J. C., Galgani, F., Ryan, P. G., & Reisser, J. (2014). Plastic Pollution in the World's Oceans: More than 5 Trillion Plastic Pieces Weighing over 250,000 Tons Afloat at Sea. PLoS One, 9(12), e111913. https://doi.org/10.1371/journal.pone.0111913

Ferrier-Pagès, C., & Gattuso, J.-P. (1998). Biomass, Production and Grazing Rates of Pico- and Nanoplankton in Coral Reef Waters (Miyako Island, Japan). Microb. Ecol., 35(1), 46–57. https://doi.org/10.1007/s002489900059

Fisher, R., O'Leary, R. A., Low-Choy, S., Mengersen, K., Knowlton, N., Brainard, R. E., & Caley, M. J. (2015). Species Richness on Coral Reefs and the Pursuit of Convergent Global Estimates. Curr. Biol., 25(4), 500–505. https://doi.org/10.1016/j.cub.2014.12.022

Hall, N. M., Berry, K. L. E., Rintoul, L., & Hoogenboom, M. O. (2015). Microplastic ingestion by scleractinian corals. Mar. Biol., 162(3), 725–732. https://doi.org/10.1007/s00227-015-2619-7

Huang, W., Deng, J., Liang, J., & Xia, X. (2023). Comparison of lead adsorption on the aged conventional microplastics, biodegradable microplastics and environmentally-relevant tire wear particles. Chem. Eng. J., 460, 141838. https://doi.org/10.1016/j.cej.2023.141838

Kane, I. A., Clare, M. A., Miramontes, E., Wogelius, R., Rothwell, J. J., Garreau, P., & Pohl, F. (2020). Seafloor microplastic hotspots controlled by deep-sea circulation. Science, 368(6495), eaba5899. https://doi.org/10.1126/science.aba5899

Karlsson, T. M., Vethaak, A. D., Almroth, B. C., Ariese, F., van Velzen, M., Hassellöv, M., & Leslie, H. A. (2017). Screening for microplastics in sediment, water, marine invertebrates and fish: Method development and microplastic accumulation. Mar. Pollut. Bull., 122(1-2), 403–408. https://doi.org/10.1016/j.marpolbul.2017.06.081

Khan, S., & Iqbal, A. (2023). Organic polymers revolution: Applications and formation strategies, and future perspectives. *J. Polym. Sci. Eng*, *6*(1), 3125. https://doi.org/10.24294/jpse.v6i1.3125

Kim, A.-R., Mitra, S. K., & Zhao, B. (2024). Unlocking Passive Collection of Microplastics in Coral Reefs by Adhesion Measurements. ACS ES&T Water. https://doi.org/10.1021/acsestwater.4c00650

Kister, G., Cassanas, G., & Vert, M. (1998). Effects of morphology, conformation and configuration on the IR and Raman spectra of various poly(lactic acid)s. Polymer, 39(2), 267–273. https://doi.org/10.1016/S0032-3861(97)00229-2

Lartaud, F., Meistertzheim, A. L., Reichert, J., Ziegler, M., Peru, E., & Ghiglione, J. F. (2020). Plastics: An Additional Threat for Coral Ecosystems. Perspect. Mar. Anim. For. World, 469–485. https://doi.org/10.1007/978-3-030-57054-5_14

Law, K. L. (2017). Plastics in the marine environment. Annu. Rev. Mar. Sci., 9(1), 205–229. https://doi.org/10.1146/annurev-marine-010816-060409

Lewis, J. B., & Price, W. S. (2009). Patterns of ciliary currents in Atlantic reef corals and their functional significance. J. Zool., 178(1), 77–89. https://doi.org/10.1111/j.1469-7998.1976.tb02264.x

Martin, C., Baalkhuyur, F., Valluzzi, L., Saderne, V., Cusack, M., Almahasheer, H., Krishnakumar, P. K., Rabaoui, L., Qurban, M. A., Arias-Ortiz, A., Masqué, P., & Duarte, C. M. (2020). Exponential increase of plastic burial in mangrove sediments as a major plastic sink. Sci. Adv., 6(44), eaaz5593. https://doi.org/10.1126/sciadv.aaz5593

Martin, C., Corona, E., Mahadik, G. A., & Duarte, C. M. (2019). Adhesion to coral surface as a potential sink for marine microplastics. Environ. Pollut., 255, 113281. https://doi.org/10.1016/j.envpol.2019.113281

Meaurio, E., López-Rodríguez, N., & Sarasua, J. R. (2006). Infrared Spectrum of Poly(l-lactide): Application to Crystallinity Studies. Macromolecules, 39(26), 9291–9301. https://doi.org/10.1021/ma061890r

Mishra, A. K., Singh, J., & Mishra, P. P. (2021). Microplastics in polar regions: An early warning to the world's pristine ecosystem. Sci. Total Environ., 784, 147149. https://doi.org/10.1016/j.scitotenv.2021.147149

Moore, C. J. (2008). Synthetic polymers in the marine environment: A rapidly increasing, long-term threat. Environ. Res., 108(2), 131–139. https://doi.org/10.1016/j.envres.2008.07.025

Muscatine, L. (1973). Nutrition of corals. Biol. Geol. Coral Reefs, 77–115. https://doi.org/10.1016/B978-0-12-395526-5.50012-2

Näkki, P., Setälä, O., & Lehtiniemi, M. (2019). Seafloor sediments as microplastic sinks in the northern Baltic Sea – Negligible upward transport of buried microplastics by bioturbation. Environ. Pollut., 249, 74–81. https://doi.org/10.1016/j.envpol.2019.02.099

Obbard, R. W., Sadri, S., Wong, Y. Q., Khitun, A. A., Baker, I., & Thompson, R. C. (2014). Global warming releases microplastic legacy frozen in Arctic Sea ice. Earth's Future, 2(6), 315–320. https://doi.org/10.1002/2014ef000240

Pacherres, C. O., Ahmerkamp, S., Schmidt-Grieb, G. M., Holtappels, M., & Richter, C. (2020). Ciliary vortex flows and oxygen dynamics in the coral boundary layer. Sci. Rep., 10(1), 7541. https://doi.org/10.1038/s41598-020-64420-7

Pacherres, C. O., Huber, A. A., Murthy, S., & Kühl, M. (2025). A scanning particle image velocimetry system for spatial mapping of steady flow and O2 concentration fields around aquatic organisms. *Methods Ecol. Evol*. https://doi.org/10.1111/2041-210X.70073

Pagter, E., Frias, J., Kavanagh, F., & Nash, R. (2020). Differences in microplastic abundances within demersal communities highlight the importance of an ecosystem-based approach to microplastic monitoring. Mar. Pollut. Bull., 160, 111644. https://doi.org/10.1016/j.marpolbul.2020.111644

Peeken, I., Primpke, S., Beyer, B., Gütermann, J., Katlein, C., Krumpen, T., Bergmann, M., Hehemann, L., & Gerdts, G. (2018). Arctic sea ice is an important temporal sink and means of transport for microplastic. Nat. Commun., 9(1), 1–12. https://doi.org/10.1038/s41467-018-03825-5

Pradit, S., Towatana, P., Nitiratsuwan, T., Jualaong, S., Jirajarus, M., Sornplang, K., Noppradit, P., Darakai, Y., & Weerawong, C. (2020). Occurrence of microplastics on beach sediment at Libong, a pristine island in Andaman Sea, Thailand. ScienceAsia, 46(3), 336. https://doi.org/10.2306/scienceasia1513-1874.2020.042

Raffel, M., Willert, C. E., Scarano, F., Kähler, C. J., Wereley, S. T., & Kompenhans, J. (2018). *Particle image velocimetry: a practical guide*. springer.

Reichert, J., Arnold, A. L., Hammer, N., Miller, I. B., Rades, M., Schubert, P., Ziegler, M., & Wilke, T. (2021). Reef-building corals act as long-term sink for microplastic. Glob. Change Biol., 28(1), 33–45. https://doi.org/10.1111/gcb.15920

Reichert, J., Schellenberg, J., Schubert, P., & Wilke, T. (2018). Responses of reef building corals to microplastic exposure. Environ. Pollut., 237, 955–960. https://doi.org/10.1016/j.envpol.2017.11.006

Shapiro, O. H., Fernandez, V. I., Garren, M., Guasto, J. S., Debaillon-Vesque, F. P., Kramarsky-Winter, E., ... & Stocker, R. (2014). Vortical ciliary flows actively enhance mass transport in reef corals.Proc. Natl. Acad. Sci. 111(37),13391-13396. https://doi.org/10.1073/pnas.1323094111

Soares, M. O., Matos, E., Lucas, C., Rizzo, L., Allcock, L., & Rossi, S. (2020). Microplastics in corals: An emergent threat. Mar. Pollut. Bull., 161, 111810. https://doi.org/10.1016/j.marpolbul.2020.111810

Thielicke, W., & Sonntag, R. (2021). Particle Image Velocimetry for MATLAB: Accuracy and enhanced algorithms in PIVlab. *Journal of Open Research Software*, *9*(1). https://doi.org/10.5334/jors.334

Timár, G., Blömer, J., Kun, F., & Herrmann, H. J. (2010). New Universality Class for the Fragmentation of Plastic Materials. Phys. Rev. Lett., 104(9). https://doi.org/10.1103/physrevlett.104.095502

Urayama, H., Moon, S., & Kimura, Y. (2003). Microstructure and Thermal Properties of Polylactides with Different L- and D-Unit Sequences: Importance of the Helical Nature of the L-Sequenced Segments. Macromol. Mater. Eng., 288(2), 137–143. https://doi.org/10.1002/mame.200390006

Van Cauwenberghe, L., Devriese, L., Galgani, F., Robbens, J., & Janssen, C. R. (2015). Microplastics in sediments: A review of techniques, occurrence and effects. Mar. Environ. Res., 111, 5–17. https://doi.org/10.1016/j.marenvres.2015.06.007

van Sebille, E., Wilcox, C., Lebreton, L., Maximenko, N., Hardesty, B. D., van Franeker, J. A., Eriksen, M., Siegel, D., Galgani, F., & Law, K. L. (2015). A global inventory of small floating plastic debris. Environ. Res. Lett., 10(12), 124006. https://doi.org/10.1088/1748-9326/10/12/124006

Woodall, L. C., Sanchez-Vidal, A., Canals, M., Paterson, G. L. J., Coppock, R., Sleight, V., Calafat, A., Rogers, A. D., Narayanaswamy, B. E., & Thompson, R. C. (2014). The deep sea is a major sink for microplastic debris. R. Soc. Open Sci., 1(4), 140317–140317. https://doi.org/10.1098/rsos.140317

Yonge, C. M. (1930). Studies on the physiology of corals: i. feeding mechanisms and food. Biol. Geol. Coral Reefs, 1, 13–57.

Zamprogno, G. C., Caniçali, F. B., dos Reis Cozer, C., Otegui, M. B. P., Graceli, J. B., & da Costa, M. B. (2021). Spatial distribution of microplastics in the superficial sediment of a mangrove in Southeast Brazil: A comparison between fringe and basin. Sci. Total Environ., 146963. https://doi.org/10.1016/j.scitotenv.2021.146963

5

Enzymatic Degradation of Poly(lactic) Acid Microplastics: Influence of the Fabrication Method

Giorgia Ferrari[1,2] , Christina N. Economou[1], Sergio Marras[3], Stefania Sganga[4,5], Nicola Tirelli[4], Athanassia Athanassiou[1], Despina Fragouli[1,*]

[1] Smart Materials, Istituto Italiano di Tecnologia (IIT), Genova, Italy

[2] Department of Earth and Environmental Science, University of Milano Bicocca, Milano, Italy

[3] Materials Characterization Facility, Istituto Italiano di Tecnologia (IIT), Genova, Italy

[4] Polymers and Biomaterials, Istituto Italiano di Tecnologia (IIT), Genova, Italy

[5] Nanobiointeractions & Nanodiagnostics, Istituto Italiano di Tecnologia (IIT), Genova, Italy

Manuscript submitted

5.1 Abstract

This study explores the enzymatic degradation of poly(lactic) acid microplastics, produced through different manufacturing protocols, by a commercial lipase enzyme from the fungus *Aspergillus oryzae*. After 28 days of enzymatic hydrolysis at pH 8.0, noticeable changes on the surface morphology of microplastics were observed, due to the emergence of micrometric pores. Detailed characterizations reveal that the microplastics fabrication process affects the performance of the enzymatic treatment. Specifically, the carbonyl index and crystallinity were increased and the polymer's molecular weight decreased in different degrees depending on the type of poly(lactic acid) microplastics. This study confirms the capability of the lipase enzyme to degrade poly(lactic acid) and underscores that the degradation performance is influenced by the production method of the polymeric particles. The latter highlights the importance of evaluating and carefully considering the microplastics formation procedure, which affects the specific characteristics of particles of the same pristine composition, when studies on the biodegradation processes are involved.

5.2 Introduction

To address global plastic pollution, research is increasingly focused on eco-friendly biopolymers that degrade through microbial activity in the environment (Iwata, 2015). Among them, poly(lactic) acid (PLA), a biodegradable polyester from renewable resources, offers environmental advantages along with mechanical and physical properties comparable to conventional plastics. These qualities have broadened its applications and driven its growing use (Qi et al., 2017; Taib et al., 2023). Despite being biodegradable, PLA requires industrial composting with controlled temperature and humidity to degrade efficiently, posing challenges for infrastructure- and energy-limited countires (Steiner et al., 2022). In natural environments, especially seawater, PLA degrades slowly, behaving similarly to conventional synthetic plastics (Nampoothiri et al., 2010; Goswami et al., 2020; Upadhyay et al., 2020). Environmental exposure causes plastic to weather and fragment into micro- and nanoplastics (MPs and NPs) via biotic and abiotic processes (Andrady, 2011; Gewert et al., 2015). These particles, recognized as emerging contaminants, pose ecological and health risks due to their mobility, pollutant-carrying capacity, and bioaccumulation through food webs (Geissen et al., 2015; Jiang et al., 2020).-To mitigate their impact, various remediation strategies have been explored, including physical, chemical, and biochemical treatments. Techniques such as rapid sand filtration, dissolved air flotation, and membrane bioreactors have shown high removal efficiency (Ahmed et al., 2024). However, their energy demands, limited particle-size removal, and low selectivity restrict large-scale application (Badola et al., 2022).-As an alternative, biodegradation is increasingly recognized as an effective and eco-friendly solution, relying on the natural breakdown of polymers by microorganisms like bacteria, fungi, and algae (Chen et al., 2020).

One of the main biodegradation mechanisms is biochemical degradation, where enzymes secreted by microorganisms—such as hydrolases, including esterases, depolymerases, and lipases—hydrolyze chemical bonds or side chains of non-water-soluble polymer macromolecules. This breakdown results in shorter polymer chains, which are then absorbed or consumed by the microorganisms, ultimately converting them into low-molecular-weight compounds, which eventually turn into CO_2, H_2O, biomass, and energy (Yuan et al., 2020). Microbial degradation of MPs generally occurs in several stages: initial colonization of the plastic surface, enzymatic oxidation that leads to polymer fragmentation, and subsequent microbial assimilation. Among biological degradation methods, fungi have garnered significant attention for their ability to secrete extracellular enzymes capable of breaking down complex polymeric structures (Zhang et al., 2020; Lucas et al., 2008). Fungal hydrolases, such as esterases, cutinases, lipases, and proteases, can directly target the hydrolysable functional groups of polyesters and polyamides, facilitating their effective degradation (Gao et al., 2022; Ogunbayo et al., 2019). The fungus *Aspergillus flavus*, for example, has been shown to degrade PE MPs via laccase-like multicopper oxidase enzymes, breaking down polymer chains into smaller, oxygenated compounds (Zhang et al., 2020). Furthermore, certain bacterial genera, such as *Bacillus* and *Rhodococcus*, contribute to MPs degradation by utilizing oxidative and hydrolytic enzymes to break down plastic polymers (Bacha et al., 2021).-Despite promising advances, the main challenges concerning the biodegradation of MPs are their chemical structure, molecular weight, crystallinity, shape and size as well as their surface chemistry, as they play a crucial role in determining their biodegradation efficiency and rate. Even though plastics are often thought of as chemically homogenous on a molecular level, MPs may present altered physicochemical characteristics compared to pristine polymer counterparts, which may hinder the in-depth aspects of the degradation mechanism from being discovered.

In fact, although recent studies are driving the attention of biodegradation towards MPs, their presented findings are largely based on the degradation of the corresponding plastics films (Thakur et al., 2023; Wei et al., 2019; Sarkhel et al., 2019). Nonetheless, MPs may be produced by the aging of larger plastic components exposed to environmental conditions (secondary MPs) or may be directly formed in their micrometric form for various applications (primary MPs), and in both cases MPs may undergo various biotic and abiotic aging processes, impacting their chemical and physical structure and consequently their environmental fate and interactions. In the few studies involving MPs biodegradation, insufficient consideration is taken on how manufacturing and processing methods alter the MPs' pristine physicochemical characteristics, which can significantly influence their degradation behavior. For instance, Paço et al. (2017) and Auta et al. (2018) explore various bioremediation strategies for PE and PP MPs produced through mechanical cutting, yet they do not assess the properties of the pristine materials. Auta et al. (2017) investigates the biodegradation of different UV-treated MPs, including PE, PP, PET, and PS, by bacteria isolated from mangrove sediments. However, the lack of comparative studies with the pristine MPs, and the effects of the MPs fabrication process and UV treatment on the physicochemical properties of the polymeric components and on the biodegradation performance are still unexplored. Focusing on PLA, microorganisms and enzymes capable of degrading the polymer are mainly focused on the α/β-hydrolase family, including proteases, lipases, cutinases, and esterases (Qi et al., 2017; Xu et al., 2022a). These enzymes share common characteristics with other polyester depolymerases—the ability to interact with highly hydrophobic substrates and efficiently hydrolyze ester bonds (Shalem et al., 2024). So far, to the best of our knowledge, the enzymatic degradation of PLA particles has been explored in a limited number of studies (Lee et al., 2014; Nakajima-Kambe et al., 2012; Williams, 1981).

These investigations are primarily focused on the activity of enzymes on PLA of various physical forms and size ranges, including nonwoven fibers (thickness: 0.126 mm), emulsions, and powders. Nonetheless, it has been recently proved that microbial activity, and therefore the biodegradation process is affected by the shape and size of MPs (Thapliyal et al., 2024; Schlundt et al., 2019), with smaller MPs to exhibit greater heterotrophic activity (Cheng et al. 2021), due to their higher surface area-to-volume ratio, which facilitates microbial colonization and metabolic processes. Similarly, for the same mass of material, an irregular, rough, surface provides more available area than a smooth one, promoting greater microbial colonization and, consequently, higher metabolic activity (Cheng et al., 2021). Lee et al. (2014) examined PLA nonwoven fibers with an average thickness of 0.126 mm and reported significant alterations in surface morphology after 21 days of exposure to a lipase enzyme. Nakajima-Kambe et al. (2012) investigated emulsified PLA solutions, observing a rapid decrease in turbidity within three days when treated with a purified *Aspergillus niger* lipase. Williams (1981) studied the enzymatic degradation of PLA powders in the form of fibrous polymeric particles. The findings demonstrated that enzymes such as pronase, proteinase K, and bromelain significantly enhanced PLA degradation. A comprehensive evaluation of PLA degradability requires considering both the polymer's intrinsic properties and the impact of manufacturing processes on the final physicochemical characteristics of the MPs. The enantiomeric composition, for instance, plays a key role in determining crystallinity and thermal behavior, with enantiomerically pure PLA (PLLA or PDLA) typically exhibiting semi-crystalline structures, while PDLLA tends to be more amorphous (Taib et al., 2023). Additionally, variations in manufacturing processes can significantly modify key physicochemical characteristics, ultimately influencing the material's degradation rate and efficiency.

A thorough evaluation of these aspects is vital to optimize enzymatic degradation pathways and to ensure effective materials' breakdown, crucial for developing appropriate bioremediation strategies and assessing the environmental fate of MPs.

This study aims to fill some gaps exploring how variations in MPs fabrication method, applied to industrially available PLA pellets, can produce particles with distinct physicochemical properties, even when processing methods appear similar. These differences in fabrication can lead to variations in the material's susceptibility to enzymatic degradation, emphasizing the need to consider production methods when evaluating MPs biodegradation. In particular, the depolymerization of PLA MPs, fabricated following different routes, utilizing a commercial lipase enzyme from *Aspergillus oryzae* under mild conditions is explored. The PLA MPs studied were the original pellets, MPs obtained via mechanical grinding, and MPs prepared using a combined process of mechanical grinding and wet or dry ball milling. Comprehensive analyses reveal that after 28 days of enzymatic treatment, processed PLA MPs exhibit increased surface porosity and crystallinity, with a consequent reduction in their molecular weight, and the formation of oxidized organic groups, confirming the effectiveness of lipase enzymes in degrading the particles. These structural and chemical changes are differentiated dependent on the MPs fabrication route, highlighting the importance of effectively evaluating the MPs reference model prior to the enzymatic treatment process and suggesting caution when results from different research groups on the same type of MPs are compared.

5.3 Materials and Methods

5.3.1 Materials

A commercial lipase enzyme produced from *Aspergillus oryzae*, chemicals for preparing culture media, enzyme assay, and the other reagents were purchased from Sigma–Aldrich. All chemicals were analytical grade and used as received. Deionized water was obtained from Milli-Q Advantage A10 purification system. Semi-crystalline poly (lactic acid) (PLA) in the form of pellets with 4 mm average size was purchased by NatureWorks LLC (U.S.A) (commercial name: PLA4043D, Mn = 160.000 g/mol, density:1.24 g/cm^3).

5.3.2 PLA MPs production

PLA MPs with size lower than 300 µm were produced via mechanical grinding. Initially, 4 mm pellets – which is the first type of MPs used in this study – (denoted hereafter as MPs_{pel}) were reduced to powder with grains size lower than 1 mm using a Dry mill – IKA – PILOTINA MC (accessorized with 1 mm PILOTINA sieve) operating at 1500 rpm. The resulting powder was further grinded and collected through a finer PILOTINA sieve (750 mm) to obtain PLA powder with grain sizes lower than 750 mm. To isolate particles with a size lower than 300 µm, the produced PLA powder was sieved using an electrical siever (VWR Test Sieve, 200x50 mm) equipped with a 300 µm mesh. This process yielded the second type of MPs used in the study, referred to, hereafter, as MPs_0.

The PLA MPs_0 were subsequently used to produce two additional types of PLA MPs, designated as MPs_{Wet} and MPs_{Dry}, depending on whether water was present or absent during their processing. To do so a PM100 Retsch® planetary ball mill was used. MPs_{Dry} were produced through the ball milling of 2g of MPs_0 placed in a zirconia (ZrO_2) jar (50 mL), using 50g zirconia balls (⌀= 1 mm) while MPs_{Wet} were formed under the same conditions but with the presence also of 6 mL of MilliQ water in the jar. In both cases the milling protocol involved pauses of 7 min each 3 min of milling operating at 650 rpm, for a total duration of 5 hours. The pause time was applied for limiting the temperature increase inside the jar, and therefore for preventing the polymer melting.

To collect the samples after wet ball milling, additional Milli-Q water was added, and a hydrophilic cellulose acetate filter (5 µm cut off) was used to collect the particles. The remaining material, consisting of PLA MPs and zirconia balls, is then left to dry. Once dried, the electrical siever (VWR Test Sieve, 200x50 mm) equipped with a 300 µm mesh was used to separate the zirconia balls from the MPs and collect the material intended for the experiments.

The final step of the process is the same also for samples obtained through dry ball milling. Indeed, since this technique is performed without water, neither filtration to remove liquid nor the subsequent drying phase is required before the application of the final sieving step.

5.3.3 Biodegradation process

PLA MPs (weighing about 16 mg each) were placed in tubes containing 3 mL Tris-HCl buffer solution 20 mM with pH 8.0 and lipase enzyme activity of 11,250 ± 177 U/mL. The lipase (EC 3.1.1.3) activity was assayed by the Sigma lipase assay (Sigma in-house procedure) using olive oil as substrate. Briefly, the reaction mixture consisted of 3 mL olive oil, 1.0 mL of 200 mM Tris-HCl buffer solution (pH 8), 2.5 mL deionized water and 1.0 mL lipase enzyme solution was incubated at 37 °C for 30 min. Thereafter, 3 mL of 95% (v/v) ethanol was added to terminate the reaction followed by addition of 4 drops of 0.9% (w/v) thymolphthalein solution. Then, the titration of the mixture with NaOH solution 50 mM until the pH reached 10.0 was performed. One unit (U) of lipase activity is defined as the hydrolysis of 1.0 microequivalent of fatty acid from a triglyceride in 30 min at pH 8 at 37°C. The pH values were measured with a pH meter (Hanna Edge instrument).

Before adding lipase enzyme, the mixture of PLA MPs and Tris-HCl buffer solution was sterilized under UV light in a biohazard hood (VBH 48, ANGELANTONI LIFE SCIENCE Srl) for 1 hour to avoid any microbial contamination. Experiments were carried out in triplicate at 37 °C in a rotary incubator (100 rpm) for 28 days. Control experiments (without lipase enzyme addition) were performed under the same conditions. At the end of experiments, the solution of buffer and lipase enzyme was removed from the tubes and PLA MPs rinsed thoroughly with deionized water. Then, the PLA MPs were dried at 37°C until a constant weight was achieved.

5.3.4 PLA MPs charcterization

Morphological analysis on the surface of the MPs was conducted by scanning electron microscopy (SEM, JEOL JSM-6490LA) at an acceleration voltage of 10 kV after coating the samples with a 10-nm Au layer using a high-resolution sputter coater (Cressington 208 HR).

A differential scanning calorimeter (DSC) (Discovery DSC 250 TA Instruments) was used to explore structural modifications of the polymer, and to determine the degree of crystallinity (X_{C_DSC}) before and after the enzymatic treatment. To do so, the treated and non-treated PLA MPs (3-5 mg) were placed in a Tzero aluminum pans and after their accurate weighing the measurements were performed under N_2 flow (50 mL min^{-1}) using conventional heating-cooling-heating scan cycles (from -20 °C to 200 °C) with a heating-cooling rate of 10 °C min^{-1}. X_{C_DSC} was calculated using the following equation:

$$X_{C_{DSC}} = \frac{(\Delta H_m - \Delta H_c)}{\Delta H_m{}^0} 100\% \qquad \text{Equation 5.1}$$

where ΔH_c is the enthalpy of cold crystallization, ΔH_m is the enthalpy of fusion, and $\Delta H_m{}^0$ is the enthalpy of fusion of crystalline PLA (~ 93 $J\ g^{-1}$) (Fischer et al., 1973). All parameters were determined by the integration of the corresponding transition peaks in the second heating DSC thermograms.

X-ray diffraction analysis of the samples before and after the enzymatic treatment was carried out on a Malvern-PANalytical 3rd generation Empyrean X-ray powder diffractometer. The instrument was equipped with a 1.8kW CuKα ceramic X-ray tube operating at 45 kV and 40 mA, iCore and dCore automated PreFIX optical modules, motorized Eulerian Cradle (chi, phi,x,y and z movements) and solid-state hybrid pixel PIXcel^{3D} area detector operating in 0D mode. The XRD patterns were collected from 5° to 35° with a step size of 0.05°.

A parallel beam configuration, including 0.04rad soller slits and 0.28° parallel plate collimator (PPC) on the diffracted beam and specific for samples characterized by an extremely irregular surface, was used. The acquisition was carried out in air at room temperature, using a zero-diffraction silicon substrate.

The degree of crystallinity $X_{c_{XRD}}$ was calculated using the equation:

$$X_{C_{XRD}} = \frac{A_c}{A_c + A_a} 100\% \qquad \text{Equation 5.2}$$

where $\boldsymbol{A_c}$ and $\boldsymbol{A_a}$ denote the integrated intensity of crystalline peaks and amorphous halo respectively, on the X-ray diffractograms. Data analysis was performed using HighScore Plus 5.2 software from Malvern Panalytical.

Gel permeation chromatography (GPC) was performed using an integrated OMNISEC system (Malvern Panalytical Ltd., UK) equipped with a PLgel 5 µm MIXED-D column in series with a PLgel 3 µm MIXED-E operating online at 35 °C and connected to a refractive index and light scattering detectors (Omnisec reveal, Malvern, UK). As eluent, tetrahydrofuran (THF) with 250ppm of butylated hydroxytoluene (BHT) is used. The instrument is calibrated using PS (PolyCal standards, Malvern Panalytical Ltd., UK) 105 kDa narrow standard of known dispersity, intrinsic viscosity, and dn/dc. The analysis was conducted by injecting three times with a flow rate of 0.8 mL/min for 35 min. Data analysis was performed using OMNISEC software V11.32. The PLA samples were dissolved in chloroform for 4 hours and then diluted 4 times in THF with 250 ppm of BHT to reach a concentration of 10 mg/mL. The samples were mixed in a thermos-shaker at 35°C for 24 hours and finally filtered with a 0.2 µm pore size PTFE filter. The weight average molecular weight M_w, the number average molecular weight M_n, and the molar-mass dispersity ($Đ = M_w/M_n$) were obtained from the average of triplicate measurements.

Infrared spectra were acquired with a Fourier transform infrared (FTIR) spectrometer (Vertex 70v FT-IR, Bruker) coupled to a single-reflection attenuated total reflection (ATR) accessory (MIRacle ATR, PIKE Technologies). All the spectra presented were the average of 32 repetitive scans in the range of 4000-600 cm^{-1} at a resolution of 2 cm^{-1}, and they were normalized to the reference peak at 1452 cm^{-1}, attributed to CH_3 asymmetric deformation vibrational modes ($\delta_{as}CH_3$), which serve as an internal standard for PLA (Kister et al., 1998; Oliveira et al., 2016). For all samples, the average of triplicate measurements is presented. Spectral analysis was performed with OriginPro 2022 software. The changes in the carbonyl band, characteristic of the degradation of the PLA polymer chain, were detected through the calculation of the carbonyl index (CI) (Gomes et al., 2024), i.e. the ratio between the intensity (I) of the carbonyl (C═O) peak at 1747 cm^{-1} and that of the methylene (C-H) peak at 1452 cm^{-1} as expressed in the following equation:

$$CI = \frac{I_{C=O}}{I_{C-H}} \qquad \text{Equation 5.3}$$

5.4 Results and Discussion

5.4.1 Chemical and Physical Characterization of the MPs

The surface morphology of the PLA MPs before and after the enzymatic treatment was examined through SEM analysis. Prior to enzymatic treatment, MPs_0, MPs_{wet}, and MPs_{dry} exhibit similar surface characteristics, indicating that the different grinding and milling methods do not result in significant morphological alterations at the micrometric scale. However, compared to MPs_{pel} the ground and milled samples present a rougher surface (Figure 5.1), indicating that the mechanical breakdown of bigger PLA particles leads to surface fractures, cavities and enhanced roughness on the processed MPs, increasing their overall surface area.

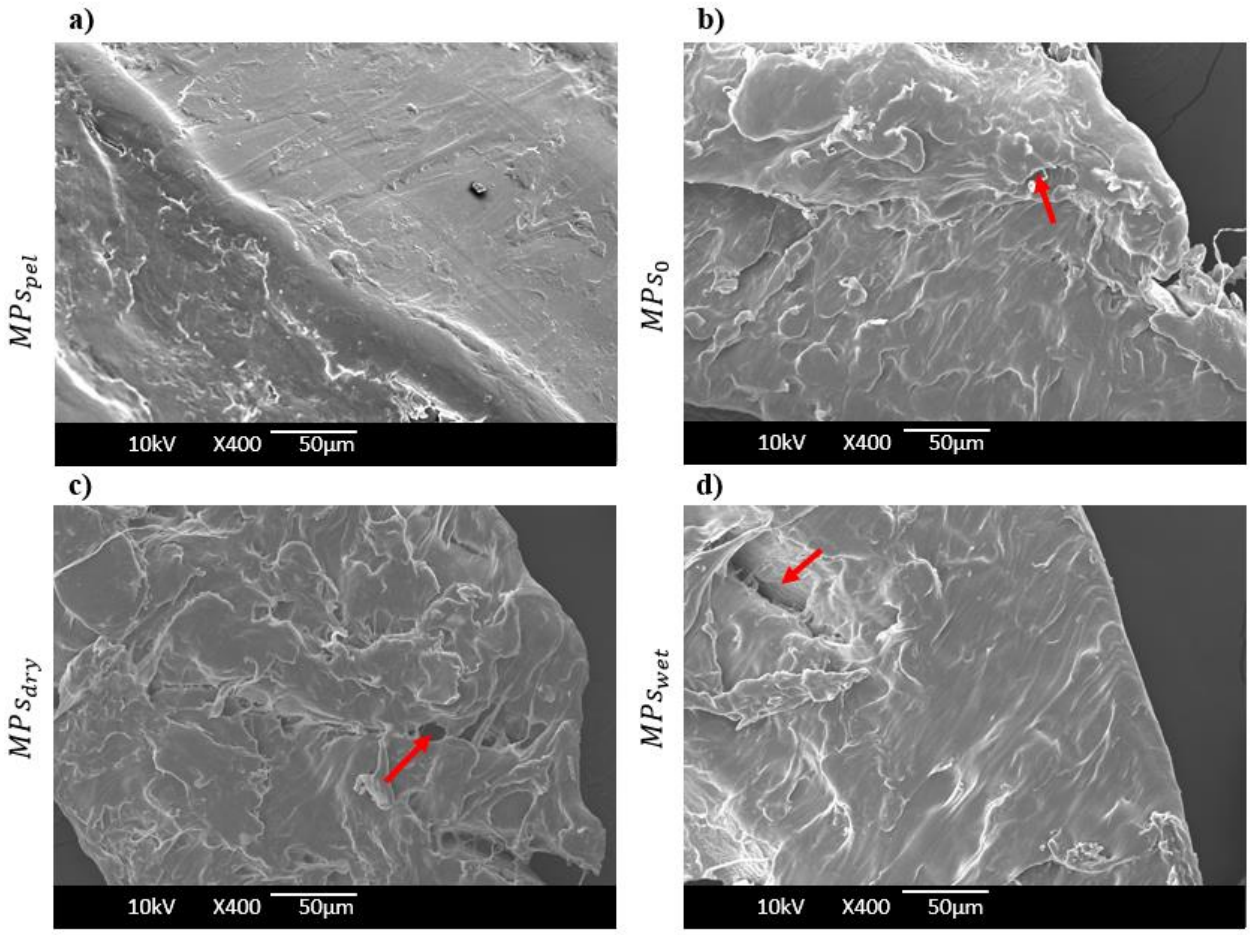

Figure 5.1. SEM images of PLA (**a**) MPs_{pel}, (**b**) MPs_0, (**c**) MPs_{dry}, and (**d**) MPs_{wet} before the enzymatic treatment. The arrows highlight the cavity on MPs' surface after grinding and milling processes.

As shown in Figure 5.2, after 28 days of enzymatic treatment, the surface of the MPs_0, MPs_{wet}, and MPs_{dry} show significant modifications, with an increased roughness. Noticeable, the formation of pores is also observed, with a size ranging from hundreds of nanometers to less than two micrometers, with no significant variation among the samples. As evident from the images, distinguishing differences in pore structure between the samples is challenging. However, a significant overall increase in porosity is evident, indicating a successful initiation of biodegradation (Tham et al., 2014). In fact, during enzymatic polymer degradation, enzymes primarily target the surface, altering the structure and morphology, as also confirmed in a previous study on PLA fibers treated with lipase from the yeast Candida cylindracea (Lee et al., 2014). The creation of pores facilitates enzyme and water diffusion into the particles, leading to the polymer chain scission and subsequent biodegradation (Araújo et al., 2013). It should be mentioned that surface changes in MPs_{pel} seemed less pronounced (Figure 5.3) at the studied scale, because their spherical three-dimensional structure posed challenges for their SEM morphological analysis at enhanced magnifications. It is important also to highlight that in the control experiments (without lipase enzyme) the surface of all MPs remained intact, with no porosity observed after 28 days of treatment (Figure 5.4).

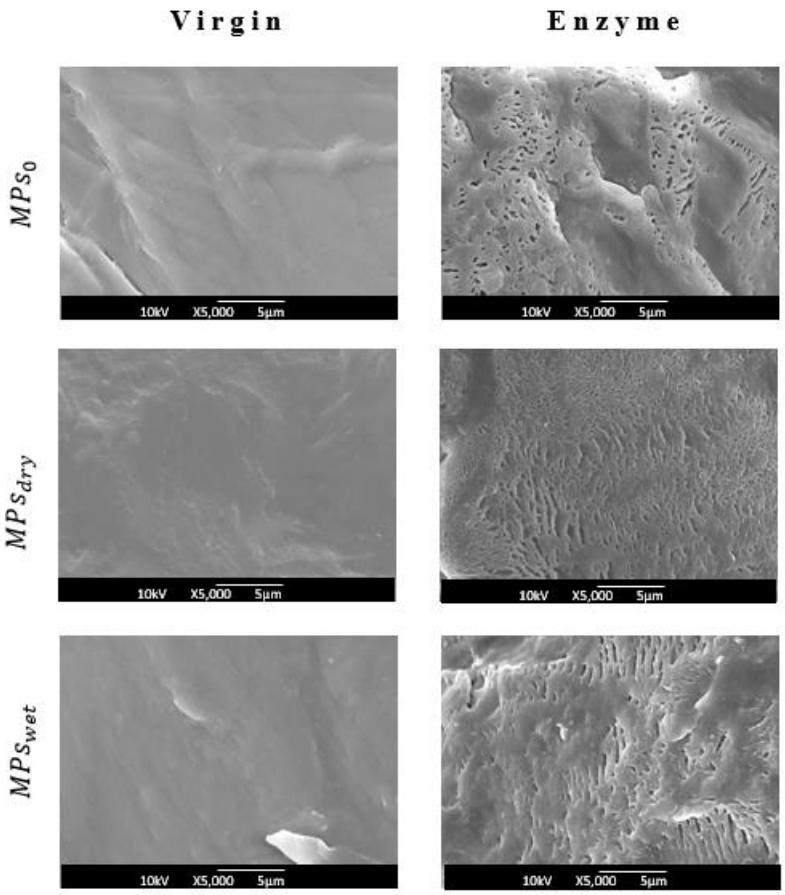

Figure 5.2. SEM images of PLA MPs before (Virgin) and after (Enzyme) 28-days of enzymatic treatment.

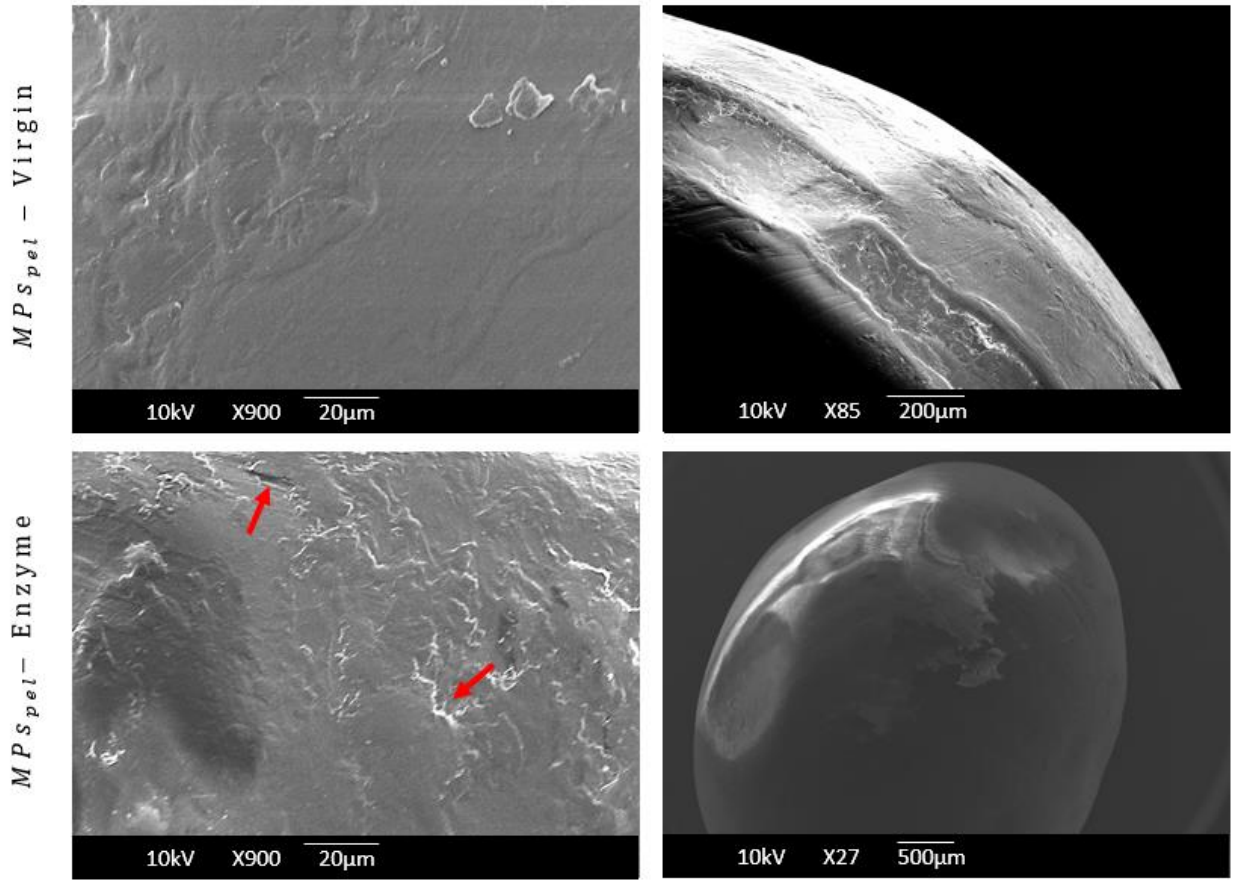

Figure 5.3. SEM images of PLA MPs_{pel}, before (Virgin) and after (Enzyme) 28-days of enzymatic treatment. The arrows highlight the surface roughness on MPs_{pla} after the enzymatic treatment.

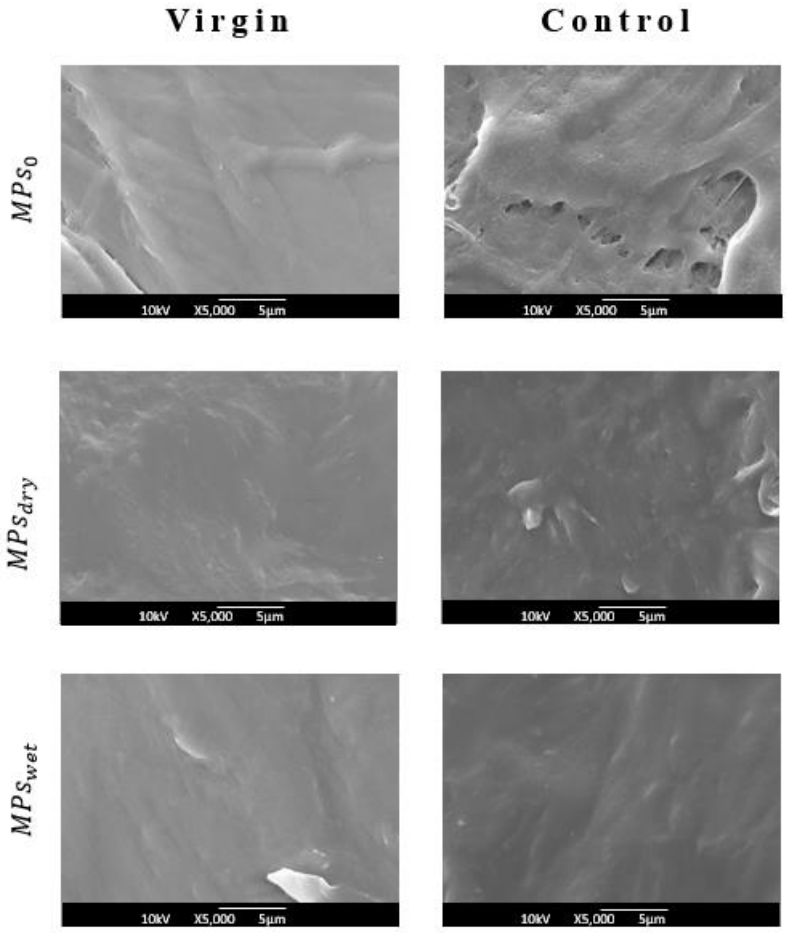

Figure 5.4. SEM images of PLA MPs before (Virgin) and after (Control**)** 28-days of exposure to solution at pH 8 without the enzyme.

To evaluate variations in composition and possible changes in the PLA structure following the different fabrication processes of MPs and their exposure to the enzymatic treatment, ATR-FTIR analysis was performed. Figure 5.5 shows the normalized spectra of untreated MPs. The characteristic absorption bands of PLA such as the C=O stretching vibrations of lactic acid esters, the CH_3 asymmetric deformation modes, and the C-O-C stretching vibrations of ester groups were identified in similar positions for all samples (1749-1747 cm^{-1}, 1454-1452 cm^{-1}, and within the 1300–1000 cm^{-1} range, respectively) (Kister et al., 1998; Urayama et al., 2003). The absorption bands at 956 and 921 cm^{-1} were also observed, with the former characteristic of the amorphous phase and the latter of the crystalline α-phase (Meaurio et al., 2006).

Nonetheless, variations between the spectra were also observed. Specifically, the intensity of the absorption band at 921 cm^{-1} of the MPs_{pel} (due to flexural C-H bond vibration) (Carrasco et al., 2010), associated with the crystalline phase of PLA, was significantly reduced after the grinding and milling processes. This is also the case for the peak at 1210 cm^{-1} representative of the crystalline structure of PLA (referring to the ester C-O stretching for PLA) (Meaurio et al., 2006) which reflects the higher crystallinity of the MPs_{pel} with respect to the other MPs in which only a small shoulder is present.

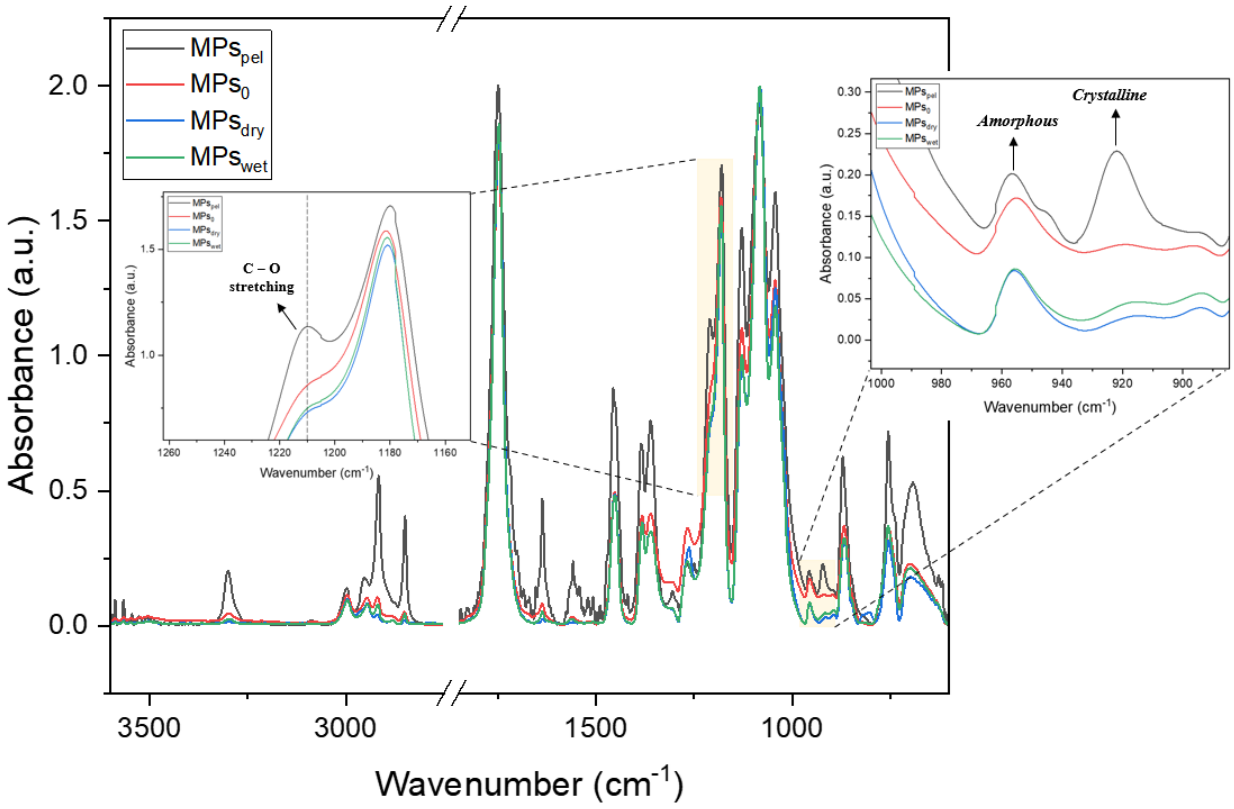

Figure 5.5. FTIR spectra of PLA MPs samples before the enzymatic treatment. Insets present the spectra magnifications of specific wavenumber areas.

The observed changes suggest that the preparation of MPs through mechanical grinding alters the polymer's molecular arrangement, decreasing its crystallinity.

This is further confirmed by the XRD analysis (Table 5.3), showing that MPs_{pel} exhibits the highest crystallinity ($X_{C_{XRD}}$), while after the mechanical processing a decrease was observed, with the MPs_{dry} presenting the highest modification.

Therefore, the mechanical breakdown of a semi-crystalline polymer such as PLA induces structural disruption, leading to increased amorphization (Cha et al., 2024). This process likely involves also mechanical degradation caused by shear forces during grinding processes resulting in molecular chain scission reflected by the reduction of the polymer's average molecular weight (Niaounakis, 2015; Lucas et al., 2008). To confirm this, the GPC analysis of the various MP samples was performed, revealing that both Mw, Mn, and Đ values, after grinding and milling, are lower than those of MPs_{pel} (Table 5.1 and Table 5.2). The post-mechanical processing decrease in molecular weight ranges from 17% for MPs_0 and MPs_{dry} to 27% for MPs_{wet}. This suggests that the mechanical fragmentation of PLA particles not only reduces their size and alters their surface morphology but also induces structural changes that may affect their physicochemical properties.

The slight decrease in Đ following mechanical grinding and milling suggests that a first degradation step occurred, resulting in a more uniform chain scission and leading to a narrower molecular weight distribution. This indicates that the polymer chains become more uniform in size, with reduced length variation after mechanical treatment. Typically, Đ values range between 1 and 2, with values closer to 1 signifying a more uniform molecular weight distribution. Ideally, upon prolonged degradation processes, Đ should continue to decrease until complete polymer degradation, ultimately approaching 1.00 (Stepto, 2009), where only polymer chain oligomers remain (Kale et al., 2006).

TABLE 5.1. Weight-average molecular weight (Mw) and average of molar-mass dispersity (Đ) of the different MPs before any enzymatic treatment, as determined by GPC.

Sample	$\overline{\mathbf{M_w}}$ **(kDa)**	$\overline{\mathbf{Đ}}$
MPs_{pel} virgin	**124.33 ± 18.03**	**1.33 ± 0.15**
MPs_0 virgin	**102.66 ± 7.75**	**1.27 ± 0.15**
MPs_{dry} virgin	**103.00 ± 3.00**	**1.23 ± 0.05**
MPs_{wet} virgin	**91.33 ± 2.30**	**1.27 ± 0.05**

Table 5.2. Weight-average molecular weight (Mw), number-average molecular weight (Mn), and average of molar-mass dispersity (Đ) concerning MPs samples before and after 28-days of enzymatic treatment. All the values are represented as mean ± SD.

Sample	$\overline{\boldsymbol{M_n}}$ **(kDa)**	$\overline{\boldsymbol{M_w}}$ **(kDa)**	$\overline{\mathbf{Đ}}$
MPs_{pel} virgin	**92.66 ± 3.05**	**124.33 ± 18.03**	**1.33 ± 0.15**
MPs_{pel} enzyme	**83.33 ± 9.60**	**112.33 ± 25.00**	**1.33 ± 0.05**
MPs_0 virgin	**83.66 ± 2.51**	**102.66 ± 7.57**	**1.27 ± 0.15**
MPs_0 enzyme	**68.33 ± 2.51**	**89.00 ± 6.24**	**1.27 ± 0.05**
MPs_{dry} virgin	**83.00 ± 2.00**	**103.00 ± 3.00**	**1.23 ± 0.05**
MPs_{dry} enzyme	**70.33 ± 2.08**	**84.66 ± 6.80**	**1.23 ± 0.05**
MPs_{wet} virgin	**71.33 ± 2.30**	**91.33 ± 2.30**	**1.27 ± 0.05**
MPs_{wet} enzyme	**64.00 ± 1.73**	**81.33 ± 4.50**	**1.27 ± 0.11**

The chemical modification of the samples was analyzed after 28 days of enzymatic treatment. As shown in the ATR-FTIR spectra of Figure 5.6 (a-d), and Figures 5.7 and 5.8, significant changes were observed at the 1637 cm^{-1} and 1558 cm^{-1} bands indicating modifications induced by the enzymatic treatment. The peak at 1637 cm^{-1} is attributed to the $C=O_{Hbond}$, which likely corresponds to the C=O stretching vibration of the intermolecular hydrogen-bonded acid groups of lactic acid (LA) (Lee et al., 2016), while the peak at 1558 cm^{-1}, is attributed to the C=O stretching of carboxylic acid salts (labeled as $C=O_{RCO_2H}$ salts) (Lee et al., 2016). To substantiate these findings, the ratio of the intensity of these peaks to the reference peak at 1452 cm^{-1} (the CH_3 asymmetric deformation mode) was calculated before and after the enzymatic treatment (Figure 9). As shown in Figure 9a, all treated samples exhibit an increase in the intensity of the $C=O_{Hbond}$ peak (1637 cm^{-1}) compared to the untreated corresponding samples. Therefore, LA likely formed from the degradation of PLA MPs interacts with the polymer through hydrogen bonding, and the resulting chemical entity (polymer + LA) generates a signal whose intensity enables the monitoring of polymer degradation (Lee et al., 2016). The peak at 1558 cm^{-1} ($C=O_{RCO_2H}$ salts) can be attributed to the hydrolysis of ester bonds and the subsequent formation of carboxylic acid and alcohol (Figure 5.6) (Kawai et al., 2011) which may undergo deprotonation, forming its carboxylate salt. For all treated samples, the presence of this peak (Figure 5.6 a-d) further confirms successful biodegradation, consistent with previous findings (Lee et al., 2016). Overall, the rise in both carboxylic acid and carboxylate salt levels indicates significant hydrolysis of PLA chains over the 28-day treatment period. It should be mentioned that for all samples the presence of these peaks, also before the enzymatic treatment, may be attributed to residual LA already present in the original PLA pellets and/or formed during mechanical degradation through grinding and milling.

In both cases, after the treatment the smallest increase of the bonds intensities are observed for PLA MPs_0, while although all the rest of the treated samples present similar values in the ratios after treatment, the largest relative changes were observed for PLA MPs_{wet}. This is attributed to the lower initial intensity of the peak observed in MPs_{wet}, possibly due to the production process, which involves milling in an aqueous environment, during which a portion of the residual LA entrapped in the polymer may have been dissolved in the water medium.

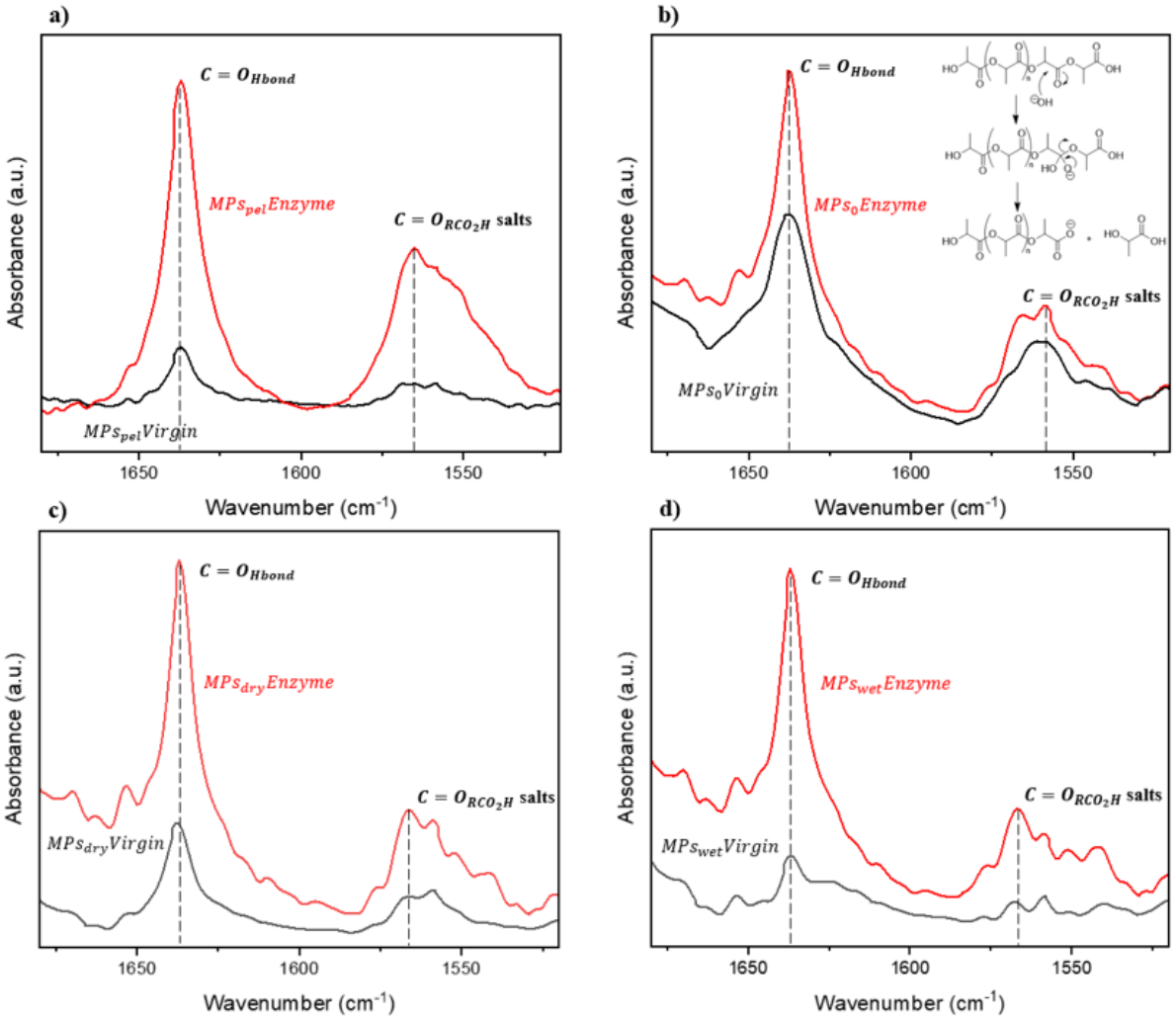

Figure 5.6 (a-d). FTIR spectra magnification of the 1700 – 1500 cm^{-1} region, representative of hydroxyl and carboxyl groups, respectively, of PLA MPs samples before (Black) and after (Red) 28-days of enzymatic treatment. **Inset of b)** Schematic mechanism of PLA hydrolysis.

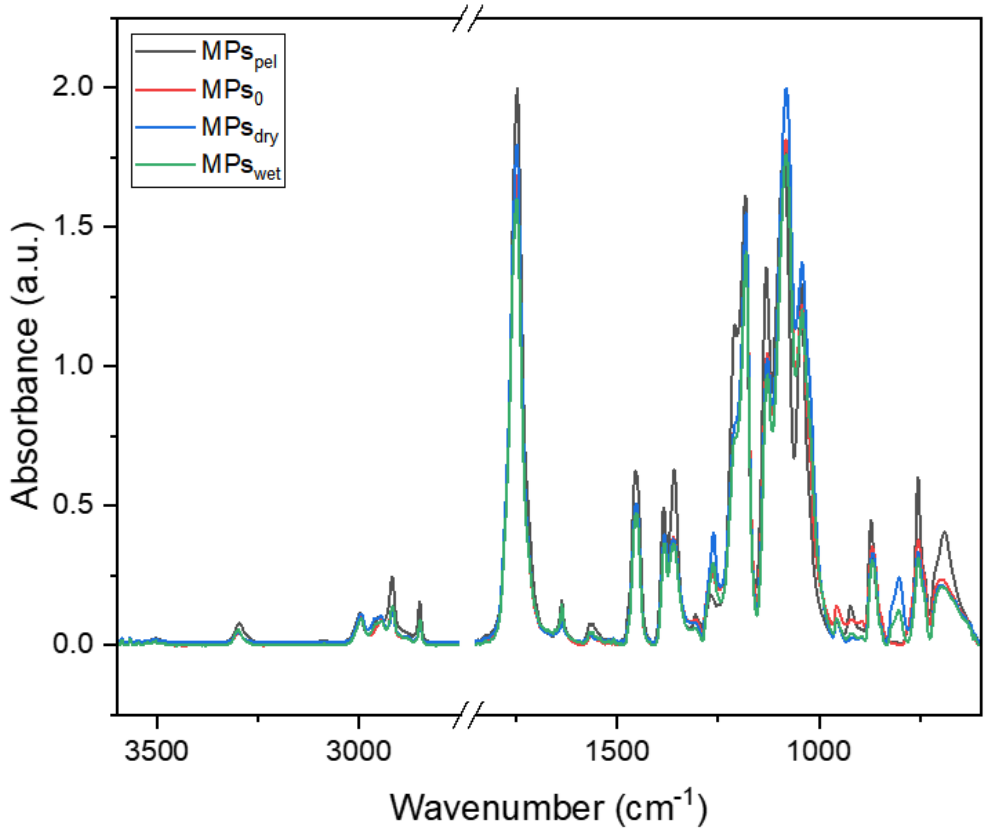

Figure 5.7. FTIR spectra of PLA MPs after 28-days of enzymatic treatment.

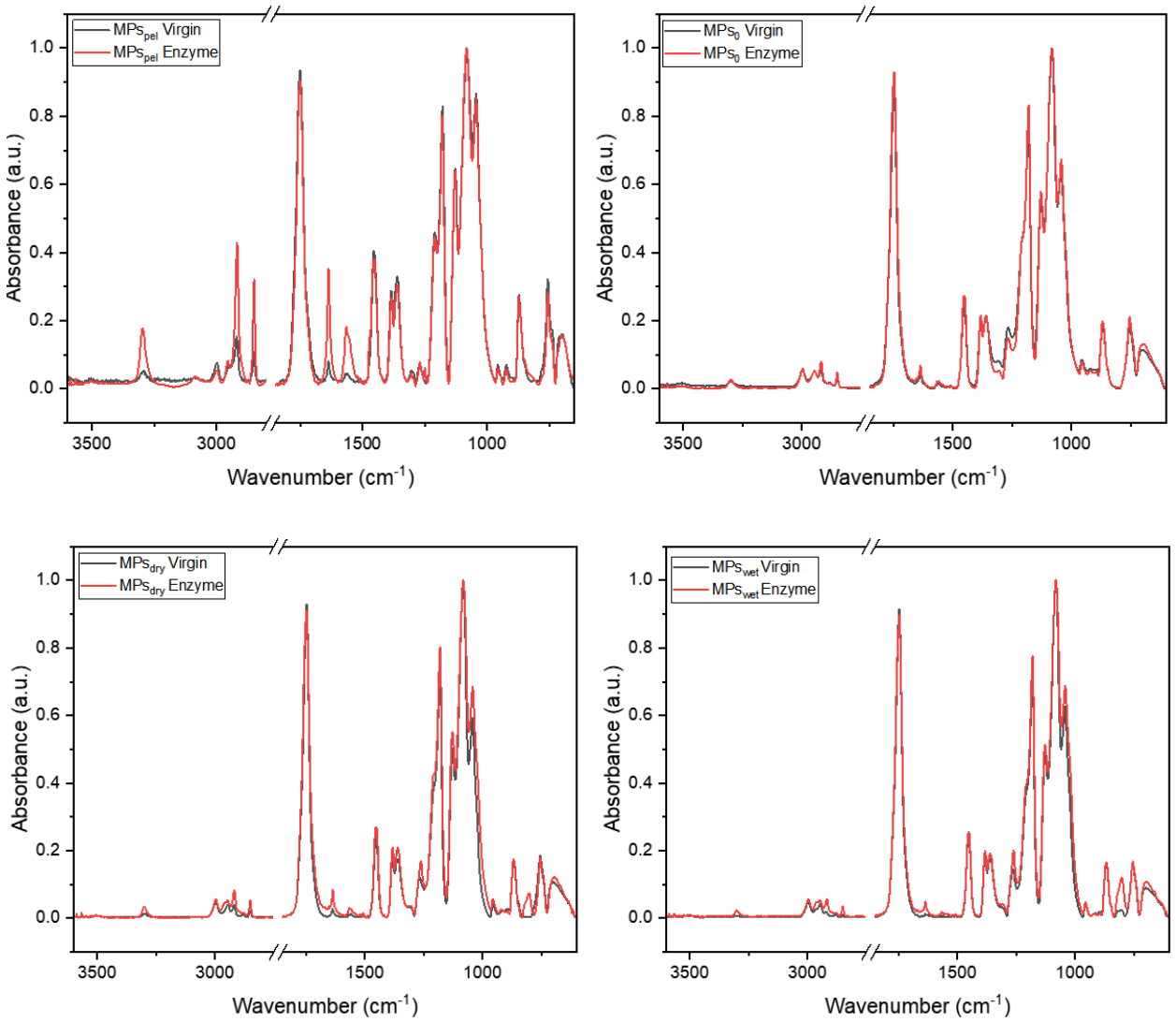

Figure 5.8. FTIR spectra of PLA MPs before (Virgin) and after (Enzyme) 28-days of enzymatic treatment.

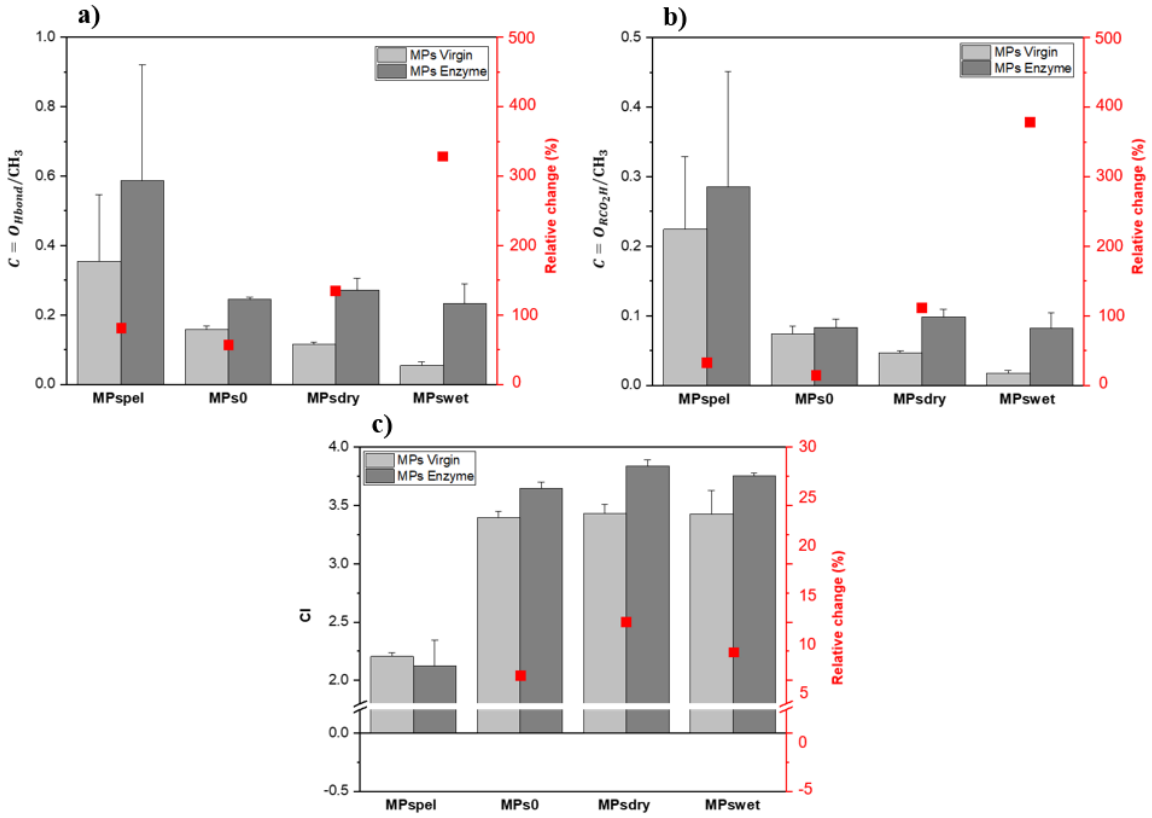

Figure 5.9. Plots showing the modification of the peaks of interest for PLA MPs before and after the enzymatic treatment. **a)** Absorbance ratio of the $C = O_{Hbond}$ (1637 cm^{-1}) relative to the CH_3 (1452 cm^{-1}) (bars) and the relative intensity increase (scatters); **b)** absorbance ratio of the $C = O_{RCO_2H}$ salts (1558 cm^{-1}) relative to the CH_3 (1452 cm^{-1}) (bars) and the relative increase (scatters); and **c)** Carbonyl index (bars) and the relative percentage change (scatters).

To further confirm the degradation of PLA samples following exposure to the lipase enzyme, the variations in carbonyl index (CI) as indicator of polymer degradation were also evaluated, following Eq. 5.2. As shown in Figure 9c, an increase in the CI is observed in the untreated $MPs_{0,}$ MPs_{wet}, and MPs_{dry} compared to the $MPs_{pel.}$ This is likely attributed to the onset of degradation caused by the MPs manufacturing processes, as suggested by the GPC results. A further increase in the CI for all mechanical fragmented MPs exposed to 28 days of enzymatic treatment was observed.

The largest CI increase was observed for PLA MPs_{dry} (~12%), suggesting that the enzyme effectively initiated the polymer degradation, while for the PLA MPs_{pel} no significant changes were observed. As suggested by Chamas et al. (2020), samples with identical compositions but differing surface areas exhibit significant differences in the degradation behavior. This observation highlights that degradation is not solely governed by the fundamental properties of plastics, such as molecular weight, additives, polymer type, but is also significantly influenced by its surface properties, including shape, size and surface features (Corcoran, 2022). Indeed, smaller or rougher MPs degrade faster with respect to larger or smoother due to their higher surface-to-volume ratio.

Accordingly, as already presented in Figure 5.2 and Figure 5.1, MPs_0, MPs_{wet}, and MPs_{dry} present an exposed larger surface area not only due to their smaller size, but also due to the presence of rougher and more irregular surface, and the presence of cracks, all of which facilitate enzymatic accessibility. On the other hand, the negligible modification of the CI values for the PLA MPs_{pel} may be attributed to the fact that the pellet, having never undergone any processing, presents a more uniform, smoother, and more compact surface making it less susceptible to external agents, such as enzymes (Figures 5.1-5.3).

To further evaluate the changes in PLA MPs following the enzymatic treatment and provide valuable insights into potential polymer degradation, crystallinity, structural and molecular weight variations were assessed. As shown in the representative XRD patterns of Figure 5.10, at least 5 peaks characteristic of PLA a-phase with orthorhombic cell are present and in agreement with the reference card 00-064-1624 of ICDD crystallographic database (Babichuk et al., 2022). The two most intense peaks at $2\theta \sim 16.6°$ (200/110 planes) and ~18.9° (203 plane) are flanked by 3 peaks of significantly lower intensity at $2\theta \sim 12.4°$ (103), $2\theta \sim 14.8°$ (010) and ~22.2° (015).

Along with the crystalline peaks, the presence of a broad amorphous halo can also be seen in all patterns. Following enzymatic treatment, all MPs showed increased crystallinity, with MPs_{dry} to exhibit the largest (43.02%) and MPs_{pel} the smallest (7.98%) relative percentage increase (Table 3).

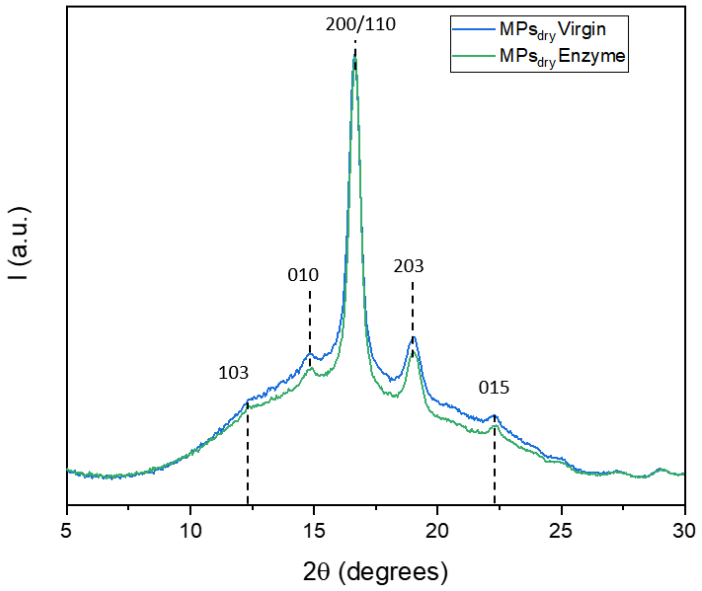

Figure 5.10. XRD diffractogram of PLA MPs_{dry} before (Virgin) and after (Enzyme) 28-days of enzymatic treatment. The patterns of the rest of the MPs present similar behavior as the one presented herein.

TABLE 5.3. Crystallinity ($X_{C_{XRD}}$) and the relative Xc increase of the MPs before (virgin) and after (enzyme) 28-days of enzymatic treatment based on XRD data.

Sample	**X_c (%)**	**% Change of X_c**
MPs_{pel} virgin	**44.73**	**7.98**
MPs_{pel} enzyme	**48.30**	
MPs_0 virgin	**20.63**	**15.07**
MPs_0 enzyme	**23.74**	
MPs_{dry} virgin	**17.20**	**43.02**
MPs_{dry} enzyme	**24.60**	
MPs_{wet} virgin	**21.30**	**18.54**
MPs_{wet} enzyme	**25.24**	

Since thermal properties, including melting temperature (Tm) and cold crystallization temperature (Tc), are strongly influenced by the polymer's molecular weight and structure (Velghe et al., 2023), DSC was employed to monitor process-induced alterations of the MPs. As shown in the corresponding thermograms (Figure 5.11 and 5.12), a glass transition (Tg) occurs around 54 °C, corresponding to the transition of the amorphous fraction, a cold crystallization (Tc) is observed between 120 and 117 °C, and a melting event (Tm) between 149 and 154 °C, depending on the specific sample.

In particular, the Tm and Tc of untreated MPs are slightly higher than that of the other enzymatically untreated MPs (Table 5.4), indicating a molecular weight reduction upon the mechanical fragmentation process, due to chain scissions, which disrupt the polymer's crystalline structure and lower its thermal stability (Pan et al., 2007; Lim et al., 2008) in accordance with the data presented so far. After enzymatic treatment, a further decrease in Tc was observed (Table 5.4) due to the chain scissions caused by polymer degradation during the treatment (Velghe et al., 2023), which increase polymer chain mobility, thereby facilitating crystallization at lower temperatures.

Since PLA is known to crystallize slowly, and its crystallization behavior is significantly influenced by its molecular weight (Velghe et al., 2023), the degree of crystallinity was also determined through the calculation of the melting and crystallization enthalpies as described in the experimental section. In fact, although XRD provides a direct and reliable method for determining polymer crystallinity it may underestimate crystallinity for more amorphous samples (Tretinnikov and Zagorskaya, 2012). On the other hand DSC is a complementary technique for the crystallinity evaluation, even though it is destructive and less precise in comparison (Doumeng et al., 2021). In the second heating cycle—used for more accurate analysis after eliminating the thermal history of the sample during the first heating—it was observed that the crystallinity values increased for all PLA MPs samples following enzymatic treatment (Table 5.4). It should be mentioned that the distinct melting peak observed in the first heating ramp of PLA MPs_{pel} suggests the presence of a crystalline fraction (Figure 5.13). However, the absence of a clear melting peak in the second heating ramp indicates that recrystallization does not occur during cooling at a rate of 10 °C/min, likely due to the insufficient time for polymer chains to reorganize into crystalline structures (Cuadri and Martín-Alfonso, 2018).

On the other hand, a clear melting peak appears in the second heating ramp of the other PLA MPs (MPs_0, MPs_{dry}, and MPs_{wet}), likely due to the grinding and milling process, which induces polymer degradation and reduces molecular chain length, as evidenced by the decrease in molecular weight. This chain scission results in shorter molecular chains, promoting the reorganization of amorphous domains into crystalline structures and increasing molecular flexibility and mobility (Oliveira et al., 2016), thereby enhancing the polymer's crystallization ability as degradation progresses (Bruster et al., 2018).

TABLE 5.4. DSC parameters for the thermal transitions observed (considering 2nd heating) and weight-average molecular weight (Mw) concerning MPs samples before and after 28-days of enzymatic treatment.

Sample	Heating	Glass transition T_g (°C)	Cold crystallization T_c (°C)	Melting T_m (°C)	Crystallinity X_c (%)	$\overline{M_w}$ (kDa)
MPs_{pel} virgin	2nd	**54.86**	-	**153.57**	**1.12**	**124.33 ± 18.03**
MPs_{pel} enzyme	2nd	**54.62**	-	**151.81**	**1.42**	**112.33 ± 25.00**
MPs_0 virgin	2nd	**54.08**	**119.73**	**149.82**	**2.88**	**102.66 ± 7.57**
MPs_0 enzyme	2nd	**53.53**	**117.34**	**149.57**	**3.85**	**89.00 ± 6.24**
MPs_{dry} virgin	2nd	**53.94**	**120.57**	**149.81**	**2.55**	**103.00 ± 3.00**
MPs_{dry} enzyme	2nd	**53.33**	**117.03**	**149.08**	**6.5**	**84.66 ± 6.80**
MPs_{wet} virgin	2nd	**54.03**	**120.42**	**150.01**	**3.2**	**91.33 ± 2.30**
MPs_{wet} enzyme	2nd	**53.27**	**117.13**	**149.19**	**4.99**	**81.33 ± 4.50**

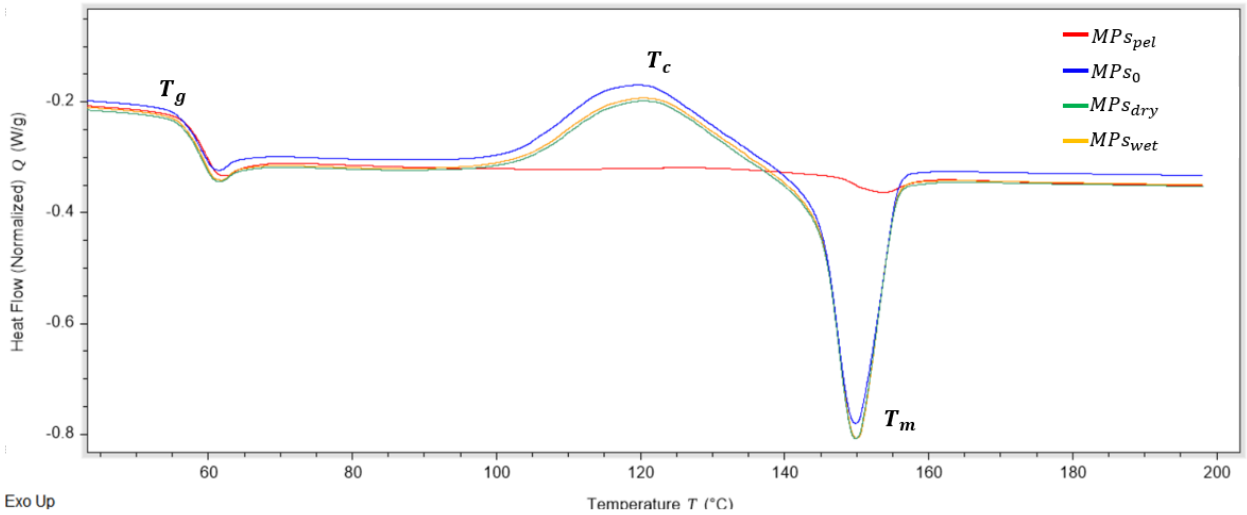

Figure 5.11. DSC thermogram (2° heating) of PLA MPs before the 28-days of enzymatic treatment.

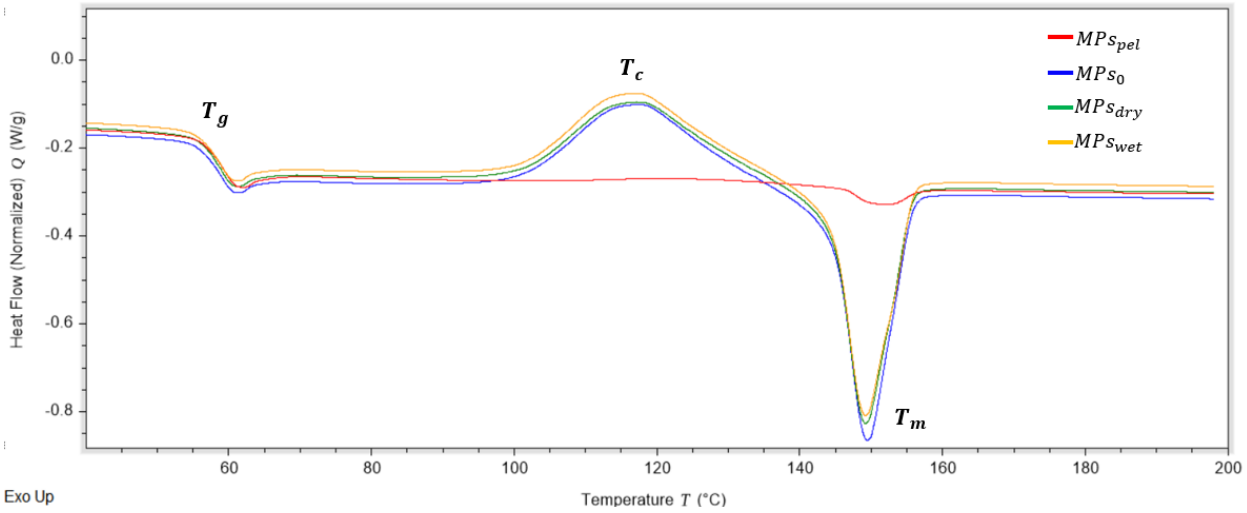

Figure 5.12. DSC thermogram (2° heating) of PLA MPs after the 28-days of enzymatic treatment

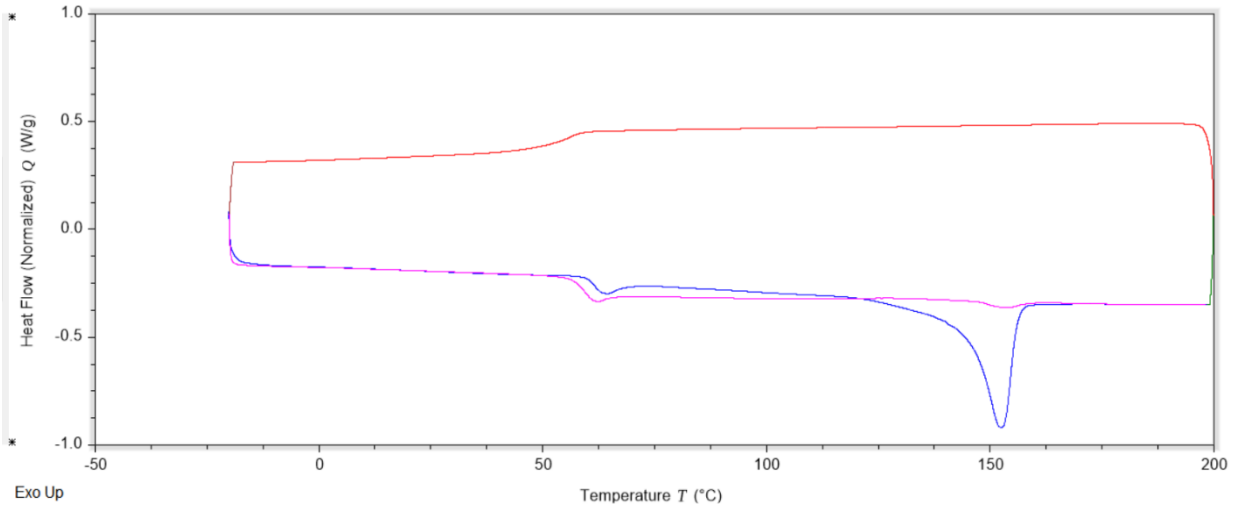

Figure 5.13. DSC thermogram of PLA MPs_{pel}. Blue curve represents the first heating, a distinct melting peak at around 152°C is present suggesting the presence of a crystalline fraction.

Although the absolute crystallinity values do not align with those obtained through the XRD method, it is noteworthy that in both cases the dry grinding process led to the formation of MPs with lower crystallinity compared to the original pellets and to the other MPs fabrication approaches presented herein. This suggests a modification in the configuration of the polymer chains and their interactions within the bulk structure. Moreover, although thermal analysis showed an increase in crystallinity in all the samples after the enzymatic treatment, the largest increase was observed for the PLA MPs_{dry} with a final value more than 2.5 times higher after the enzymatic treatment.

To further confirm the molecular chain scissions after enzymatic treatment, and the effect on the crystallinity, GPC analysis on the treated samples was also conducted. As shown in Table 5.3 all samples exhibited a reduction in weight-average molecular weight (Mw) after enzymatic treatment. Among them, PLA MPs_{dry} showed the greatest decrease (14.47%). The more pronounced change compared to the other samples aligns with previous chemical analyses, which identified it as the most susceptible to degradation by the lipase enzyme.

This is attributed to the fact that the specific way of mechanical fragmentation for the MPs induces more intense polymer chain scissions, therefore, lower molecular weight and crystallinity, making the material more susceptible to enzymatic attack.

5.5 Conclusions

With this study, the degradative effectiveness of a lipase enzyme from Aspergillus oryzae on PLA-based MPs is evaluated. After 28 days of enzymatic hydrolysis at 37°C and pH 8.0, noticeable changes in surface morphology were observed in the MP samples, characterized by the emergence of porosity on their surfaces. Chemical changes were also observed as the increase in the CI, the presence of lactic acid-based by-products in the polymers bulk structure, and the decrease in the molecular weight of the treated samples. A clear dependence on the MPs' fabrication process of the degradation effectiveness was observed, with the dry milling to result in particles more susceptible to enzymatic degradation than the others. This can be attributed to the lower crystallinity, and to the higher presence of monomer components in their pristine structure making the polymer more prone to enzymatic attack and its subsequent degradation. In conclusion, this study confirms the capability of lipase enzyme to degrade PLA MPs and underscores that the degradation efficiency is influenced by the production method of the MPs. This highlights the importance of evaluating how the formation procedure affects the structural properties of MPs of the same pristine composition, as well as the need for consistent and comparable production methods when assessing biodegradation, to ensure meaningful comparisons across studies.

5.6 References

Ahmed, S. F., Islam, N., Tasannum, N., Mehjabin, A., Momtahin, A., Chowdhury, A. A., Almomani, F., Mofijur, M. (2024). Microplastic removal and management strategies for wastewater treatment plants. Chemosphere, 347, 140648. https://doi.org/10.1016/j.chemosphere.2023.140648

Ainali, N. M., Kalaronis, D., Evgenidou, E., Kyzas, G. Z., Bobori, D. C., Kaloyianni, M., Yang, X., Bikiaris, D. N., Lambropoulou, D. A. (2022). Do poly(lactic acid) microplastics instigate a threat? A perception for their dynamic towards environmental pollution and toxicity. Sci. Total Environ., 832, 155014. https://doi.org/10.1016/j.scitotenv.2022.155014

Ali, W., Ali, H., Gillani, S., Zinck, P., Souissi, S. (2023). Polylactic acid synthesis, biodegradability, conversion to microplastics and toxicity: a review. Environ. Chem. Lett., 21. https://doi.org/10.1007/s10311-023-01564-8

Araújo, A., Oliveira, M., Oliveira, R., Botelho, G., Machado, A. V. (2013). Biodegradation assessment of PLA and its nanocomposites. Environ. Sci. Pollut. Res., 21(16), 9477–9486. https://doi.org/10.1007/s11356-013-2256-y

Ashrafy, A., Liza, A. A., Islam, M. N., Billah, M. M., Arafat, S. T., Rahman, M. M., Rahman, Sk. M. (2022). Microplastics Pollution: A Brief Review of Its Source and Abundance in Different Aquatic Ecosystems. J. Hazard. Mater. Adv., 9, 100215. https://doi.org/10.1016/j.hazadv.2022.100215

Auta, H. S., Emenike, C. U., Fauziah, S. H. (2017). Screening of Bacillus strains isolated from mangrove ecosystems in Peninsular Malaysia for microplastic degradation. Environ. Pollut., 231, 1552–1559. https://doi.org/10.1016/j.envpol.2017.09.043

Auta, H. S., Emenike, C. U., Jayanthi, B., Fauziah, S. H. (2018). Growth kinetics and biodeterioration of polypropylene microplastics by Bacillus sp. and Rhodococcus sp. isolated from mangrove sediment. Mar. Pollut. Bull., 127, 15–21. https://doi.org/10.1016/j.marpolbul.2017.11.036

Babichuk, I. S., Lin, C., Qiu, Y., Zhu, H., Ye, T. T., Gao, Z., Yang, J. (2022). Raman mapping of piezoelectric poly(l-lactic acid) films for force sensors. RSC Adv., 12(43), 27687–27697. https://doi.org/10.1039/d2ra04241j

Bacha, A.-U.-R., Nabi, I., Zhang, L. (2021). Mechanisms and the Engineering Approaches for the Degradation of Microplastics. ACS ES&T Eng., 1(11), 1481–1501. https://doi.org/10.1021/acsestengg.1c00216

Badola, N., Bahuguna, A., Sasson, Y., Chauhan, J. S. (2021). Microplastics removal strategies: A step toward finding the solution. Front. Environ. Sci. Eng., 16(1). https://doi.org/10.1007/s11783-021-1441-3

Bancin, L. J., Walther, B. A., Lee, Y.-C., Kunz, A. (2019). Two-dimensional distribution and abundance of micro- and mesoplastic pollution in the surface sediment of Xialiao Beach, New Taipei City, Taiwan. Mar. Pollut. Bull., 140, 75–85. https://doi.org/10.1016/j.marpolbul.2019.01.028

Bertolacci, L., Goldoni, L., Zych, A., Athanassiou, A. (2022). Biocatalytic oxidation of polyethylene by Agrocybe aegerita mycelium. Polym. Degrad. Stab., 199, 109911. https://doi.org/10.1016/j.polymdegradstab.2022.109911

Carrasco, F., Pagès, P., Gámez-Pérez, J., Santana, O. O., Maspoch, M. L. (2010). Processing of poly(lactic acid): Characterization of chemical structure, thermal stability and mechanical properties. Polym. Degrad. Stab., 95(2), 116–125. https://doi.org/10.1016/j.polymdegradstab.2009.11.045

Cha, S., Kim, J. G., Peterson, G. I. (2024). Influence of Crystallinity on the Mechanochemical Degradation of Poly(lactide) with Ball-Mill Grinding. Macromolecules, 57(21), 9960–9964. https://doi.org/10.1021/acs.macromol.4c02156

Chamas, A., Moon, H., Zheng, J., Qiu, Y., Tabassum, T., Jang, J. H., Abu-Omar, M., Scott, S. L., Suh, S. (2020). Degradation rates of plastics in the environment. ACS Sustain. Chem. Eng., 8(9), 3494–3511. https://doi.org/10.1021/acssuschemeng.9b06635

Cheng, J., Jacquin, J., Conan, P., Pujo-Pay, M., Barbe, V., George, M., Fabre, P., Bruzaud, S., Ter Halle, A., Meistertzheim, A.-L., Ghiglione, J.-F. (2021). Relative Influence of Plastic Debris Size and Shape, Chemical Composition and Phytoplankton-Bacteria Interactions in Driving Seawater Plastisphere Abundance, Diversity and Activity. Front. Microbiol., 11. https://doi.org/10.3389/fmicb.2020.610231

Corcoran, P. L. (2022). Degradation of Microplastics in the Environment. In Handbook of Microplastics in the Environment (pp. 531–542). https://doi.org/10.1007/978-3-030-39041-9_10

Cuadri, A. A., Martín-Alfonso, J. E. (2018). Thermal, thermo-oxidative and thermomechanical degradation of PLA: A comparative study based on rheological, chemical and thermal properties. Polym. Degrad. Stab., 150, 37–45. https://doi.org/10.1016/j.polymdegradstab.2018.02.011

Doumeng, M., Makhlouf, L., Berthet, F., Marsan, O., Delbé, K., Denape, J., Chabert, F. (2021). A comparative study of the crystallinity of polyetheretherketone by using density, DSC, XRD, and Raman spectroscopy techniques. Polym. Test., 93, 106878. https://doi.org/10.1016/j.polymertesting.2020.106878

Fischer, E. O., Sterzel, H. J., Wegner, G. (1973). Investigation of the structure of solution grown crystals of lactide copolymers by means of chemical reactions. Kolloid-Zeitschrift & Zeitschrift für Polymere, 251(11), 980–990. https://doi.org/10.1007/bf01498927

Gao, R., Liu, R., Sun, C. (2022). A marine fungus Alternaria alternata FB1 efficiently degrades polyethylene. J. Hazard. Mater., 431, 128617. https://doi.org/10.1016/j.jhazmat.2022.128617

Geissen, V., Mol, H., Klumpp, E., Umlauf, G., Nadal, M., van der Ploeg, M., van de Zee, S. E. A. T. M., Ritsema, C. J. (2015). Emerging pollutants in the environment: A challenge for water resource management. Int. Soil Water Conserv. Res., 3(1), 57–65. https://doi.org/10.1016/j.iswcr.2015.03.002

Gewert, B., Plassmann, M. M., MacLeod, M. (2015). Pathways for degradation of plastic polymers floating in the marine environment. Environ. Sci.: Process. Impacts, 17(9), 1513–1521. https://doi.org/10.1039/c5em00207a

Gomes, R. S., Fernandes, A. N., Waldman, W. R. (2024). How to Measure Polymer Degradation? An Analysis of Authors' Choices When Calculating the Carbonyl Index. Environ. Sci. Technol, 58 (17), 7609-7616 https://doi.org/10.1021/acs.est.3c10855

Goswami, P., Vinithkumar, N. V., Dharani, G. (2020). First evidence of microplastics bioaccumulation by marine organisms in the Port Blair Bay, Andaman Islands. Mar. Pollut. Bull., 155, 111163. https://doi.org/10.1016/j.marpolbul.2020.111163

Huang, M., Wang, D., Zhang, S., Weng, Y., Li, K., Huang, R., Guo, Y., Jiang, C., Wang, Z., Wang, H., Meng, H., Lin, Y., Fang, M., & Li, J. (2023). Impacts of Polylactic Acid Microplastics on Performance and Microbial Dynamics in Activated Sludge System. Sustain., *15*(19), 14332–14332. https://doi.org/10.3390/su151914332

Iwata, T. (2015). Biodegradable and Bio-Based Polymers: Future Prospects of Eco-Friendly Plastics. Angew. Chem. Int. Ed., 54(11), 3210–3215. https://doi.org/10.1002/anie.201410770

Jiang, B., Kauffman, A. E., Li, L., McFee, W., Cai, B., Weinstein, J., Lead, J. R., Chatterjee, S., Scott, G. I., Xiao, S. (2020). Health impacts of environmental contamination of micro- and nanoplastics: a review. Environ. Health Prev. Med., 25(1). https://doi.org/10.1186/s12199-020-00870-9

Kale, G., Auras, R., Singh, S. P. (2006). Degradation of Commercial Biodegradable Packages under Real Composting and Ambient Exposure Conditions. J. Polym. Environ., 14(3), 317–334. https://doi.org/10.1007/s10924-006-0015-6

Kawai, F., Nakadai, K., Nishioka, E., Nakajima, H., Ohara, H., Masaki, K., Iefuji, H. (2011). Different enantioselectivity of two types of poly(lactic acid) depolymerases toward poly(l-lactic acid) and poly(d-lactic acid). Polym. Degrad. Stab., 96(7), 1342–1348. https://doi.org/10.1016/j.polymdegradstab.2011.03.022

Kazour, M., Jemaa, S., Issa, C., Khalaf, G., Amara, R. (2019). Microplastics pollution along the Lebanese coast (Eastern Mediterranean Basin): Occurrence in surface water, sediments and biota samples. Sci. Total Environ., 696, 133933. https://doi.org/10.1016/j.scitotenv.2019.133933

Kister, G., Cassanas, G., Vert, M. (1998). Effects of morphology, conformation and configuration on the IR and Raman spectra of various poly(lactic acid)s. Polymer, 39(2), 267–273. https://doi.org/10.1016/s0032-3861(97)00229-2

Lee, J. C., Moon, J. H., Jeong, J.-H., Kim, M. Y., Kim, B. M., Choi, M.-C., Kim, J. R., Ha, C.-S. (2016). Biodegradability of poly(lactic acid) (PLA)/lactic acid (LA) blends using anaerobic digester sludge. Macromol. Res., 24(8), 741–747. https://doi.org/10.1007/s13233-016-4100-y

Lee, S. H., Kim, I. Y., Song, W. S. (2014). Biodegradation of polylactic acid (PLA) fibers using different enzymes. Macromol. Res., 22(6), 657–663. https://doi.org/10.1007/s13233-014-2107-9

Li, W., Zu, B., Yang, Q., Guo, J., & Li, J. (2023). Sources, distribution, and environmental effects of microplastics: a systematic review. RSC Adv., 13(23), 15566–15574. https://doi.org/10.1039/D3RA02169F

Liao, J., Chen, Q. (2021). Biodegradable plastics in the air and soil environment: Low degradation rate and high microplastics formation. J. Hazard. Mater., 418, 126329. https://doi.org/10.1016/j.jhazmat.2021.126329

Lim, L.-T., Auras, R., Rubino, M. (2008). Processing technologies for poly(lactic acid). Prog. Polym. Sci., 33(8), 820–852. https://doi.org/10.1016/j.progpolymsci.2008.05.004

Lucas, N., Bienaime, C., Belloy, C., Queneudec, M., Silvestre, F., Nava-Saucedo, J.-E. (2008). Polymer biodegradation: Mechanisms and estimation techniques – A review. Chemosphere, 73(4), 429–442. https://doi.org/10.1016/j.chemosphere.2008.06.064

Meaurio, E., López-Rodríguez, N., Sarasua, J. R. (2006). Infrared Spectrum of Poly(l-lactide): Application to Crystallinity Studies. Macromolecules, 39(26), 9291–9301. https://doi.org/10.1021/ma061890r

Microplastics. (n.d.). Environment.ec.europa.eu. https://environment.ec.europa.eu/topics/plastics/microplastics_en

Mühlschlegel, P., Hauk, A., Walter, U., Sieber, R. (2017). Lack of evidence for microplastic contamination in honey. Food Addit. Contam. Part A, 34(11), 1982–1989. https://doi.org/10.1080/19440049.2017.1347281

Nakajima-Kambe, T., Edwinoliver, N. G., Maéda, H., Thirunavukarasu, K., Gowthaman, M. K., Masaki, K., Mahalingam, S., Numbi Ramudu Kamini. (2012). Purification, cloning and expression of an Aspergillus niger lipase for degradation of poly(lactic acid) and poly(ε-caprolactone). Polym. Degrad. Stab., 97(2), 139–144. https://doi.org/10.1016/j.polymdegradstab.2011.11.009

Nampoothiri, K., Nair, N. R., John, R. P. (2010). An overview of the recent developments in polylactide (PLA) research. Bioresour. Technol., 101(22), 8493–8501. https://doi.org/10.1016/j.biortech.2010.05.092

Niaounakis, M., (2015). Biopolymers: Processing and Products Recycling. (16), pp. 481–530. doi:10.1016/B978-0-323-26698-7.00016-7

Ogunbayo, A. O., Olanipekun, O. O., Adamu, I. A. (2019). Preliminary Studies on the Microbial Degradation of Plastic Waste Using Aspergillus niger and Pseudomonas sp. J. Environ. Prot., 10(05), 625–631. https://doi.org/10.4236/jep.2019.105037

Oliveira, M. M., Santos, E., Araújo, A., Fechine, G. J. M., Machado, A. L., Botelho, G. (2016). The role of shear and stabilizer on PLA degradation. Polym. Test., 51, 109–116. https://doi.org/10.1016/j.polymertesting.2016.03.005

Paço, A., Duarte, K., da Costa, J. P., Santos, P. S. M., Pereira, R., Pereira, M. E., Freitas, A. C., Duarte, A. C., Rocha-Santos, T. A. P. (2017). Biodegradation of polyethylene microplastics by the marine fungus Zalerion maritimum. Sci. Total Environ., 586, 10–15. https://doi.org/10.1016/j.scitotenv.2017.02.017

Pan, P., Kai, W., Zhu, B., Dong, T., Inoue, Y. (2007). Polymorphous Crystallization and Multiple Melting Behavior of Poly(lactide): Molecular Weight Dependence. Macromolecules, 40(19), 6898–6905. https://doi.org/10.1021/ma071258d

Qi, X., Ren, Y., Wang, X. (2017). New advances in the biodegradation of Poly(lactic) acid. Int. Biodeterior. Biodegrad., 117, 215. https://doi.org/10.1016/j.ibiod.2017.01.010

Regulation - 2023/2055 – EN – EUR Lex. (2023). Europa.eu. http://data.europa.eu/eli/reg/2023/2055/oj

Rummel, C. D., Löder, M. G. J., Fricke, N. F., Lang, T., Griebeler, E.-M., Janke, M., Gerdts, G. (2016). Plastic ingestion by pelagic and demersal fish from the North Sea and Baltic Sea. Mar. Pollut. Bull., 102(1), 134–141. https://doi.org/10.1016/j.marpolbul.2015.11.043

Sarkhel, R., Sengupta, S., Das, P., Bhowal, A. (2019). Comparative biodegradation study of polymer from plastic bottle waste using novel isolated bacteria and fungi from marine source. J. Polym. Res., 27(1). https://doi.org/10.1007/s10965-019-1973-4

Schlundt, C., Mark Welch, J. L., Knochel, A. M., Zettler, E. R., Amaral-Zettler, L. A. (2019). Spatial structure in the “Plastisphere”: Molecular resources for imaging microscopic communities on plastic marine debris. Mol. Ecol. Resour., 20(3), 620–634. https://doi.org/10.1111/1755-0998.13119

Schymanski, D., Goldbeck, C., Humpf, H.-U., Fürst, P. (2018). Analysis of microplastics in water by micro-Raman spectroscopy: Release of plastic particles from different packaging into mineral water. Water Res., 129, 154–162. https://doi.org/10.1016/j.watres.2017.11.011

Shalem, A., Yehezkeli, O., Fishman, A. (2024). Enzymatic degradation of polylactic acid (PLA). Appl. Microbiol. Biotechnol., 108(1). https://doi.org/10.1007/s00253-024-13212-4

Steiner, T., Zhang, Y., Möller, J. N., Agarwal, S., Greiner, A., Laforsch, C., Freitag, R. (2022). Municipal biowaste treatment plants contribute to the contamination of the environment with residues of biodegradable plastics with putative higher persistence potential. Sci. Rep., 12(1). https://doi.org/10.1038/s41598-022-12912-z

Stepto, R. F. T. (2009). Dispersity in polymer science (IUPAC Recommendations 2009). Pure Appl. Chem., 81(2), 351–353. https://doi.org/10.1351/pac-rec-08-05-02

Taib, N.-A. A. B., Rahman, M. R., Huda, D., Kuok, K. K., Hamdan, S., Bakri, M. K. B., Julaihi, M. R. M. B., Khan, A. (2022). A review on poly lactic acid (PLA) as a biodegradable polymer. Polym. Bull., 80(2), 1179–1213. https://doi.org/10.1007/s00289-022-04160-y

Thakur, B., Singh, J., Singh, J., Angmo, D., Vig, A. P. (2023). Biodegradation of different types of microplastics: Molecular mechanism and degradation efficiency. Sci. Total Environ., 877, 162912. https://doi.org/10.1016/j.scitotenv.2023.162912

Tham, C. Y., Hamid, Z. A. A., Ahmad, Z. A., Ismail, H. (2014). Surface engineered poly (lactic acid)(PLA) microspheres by chemical treatment for drug delivery system. Key Eng. Mater., 594, 214-218. https://doi.org/10.4028/www.scientific.net/KEM.594-595.214

Thapliyal, C., Priya, A., Singh, S. B., Bahuguna, V., Daverey, A. (2024). Potential strategies for bioremediation of microplastic contaminated soil. Environ. Chem. Ecotoxicol., 6, 117–131. https://doi.org/10.1016/j.enceco.2024.05.001

Tretinnikov, O. N., Zagorskaya, S. A. (2012). Determination of the degree of crystallinity of poly(vinyl alcohol) by FTIR spectroscopy. J. Appl. Spectrosc., 79(4), 521–526. https://doi.org/10.1007/s10812-012-9634-y

Upadhyay, R. K., Mishra, A. K., Kumar, A. (2020). Mechanical Degradation of 3D Printed PLA in Simulated Marine Environment. Surf. Interfaces, 21, 100778. https://doi.org/10.1016/j.surfin.2020.100778

Urayama, H., Moon, S., Kimura, Y. (2003). Microstructure and Thermal Properties of Polylactides with Different L- and D-Unit Sequences: Importance of the Helical Nature of the L-Sequenced Segments. Macromol. Mater. Eng., 288(2), 137–143. https://doi.org/10.1002/mame.200390006

Velghe, I., Buffel, B., Vandeginste, V., Thielemans, W., Desplentere, F. (2023). Review on the Degradation of Poly(lactic acid) during Melt Processing. Polymers, 15(9), 2047–2047. https://doi.org/10.3390/polym15092047

Wei, R., Breite, D., Song, C., Gräsing, D., Ploss, T., Hille, P., Schwerdtfeger, R., Matysik, J., Schulze, A., Zimmermann, W. (2019). Biocatalytic Degradation Efficiency of Postconsumer Polyethylene Terephthalate Packaging Determined by Their Polymer Microstructures. Adv. Sci., 6(14), 1900491. https://doi.org/10.1002/advs.201900491

Williams, D. F. (1981). Enzymic Hydrolysis of Polylactic Acid. Eng. Med., 10(1), 5–7. https://doi.org/10.1243/emed_jour_1981_010_004_02

Wright, S. L., Thompson, R. C., Galloway, T. S. (2013). The physical impacts of microplastics on marine organisms: A review. Environ. Pollut., 178, 483–492. https://doi.org/10.1016/j.envpol.2013.02.031

Xu, B., Chen, Y., He, J., Cao, S., Liu, J., Xue, R., Xin, F., Qian, X., Zhou, J., Dong, W., Jiang, M. (2022). New insights into the biodegradation of polylactic acid: from degradation to upcycling. Environ. Rev., 30(1), 30–38. https://doi.org/10.1139/er-2020-0117

Yang, D., Shi, H., Li, L., Li, J., Jabeen, K., Kolandhasamy, P. (2015). Microplastic Pollution in Table Salts from China. Environ. Sci. Technol., 49(22), 13622–13627. https://doi.org/10.1021/acs.est.5b03163

Zhang, J., Gao, D., Li, Q., Zhao, Y., Li, L., Lin, H., Bi, Q., Zhao, Y. (2020). Biodegradation of polyethylene microplastic particles by the fungus Aspergillus flavus from the guts of wax moth Galleria mellonella. Sci. Total Environ., 704, 135931. https://doi.org/10.1016/j.scitotenv.2019.135931

6

Discussion and Conclusions

At the outset of this thesis, the global issue of microplastic pollution was discussed, highlighting its impacts on both the environment and human health, as well as the challenges associated with its study and management. Biodegradable plastics have been proposed as a potential solution, with the hope that they would be less persistent in natural environments. However, numerous studies have shown that, despite their biobased origin and "biodegradable" label, these materials can still persist, representing a significant ecological concern.

This chapter aims to discuss and synthesize the main findings of this research, focusing on two key aspects: the effects of MPs on corals and the assessment of their biodegradability through bioremediation processes using lipase from the fungus *Aspergillus oryzae*. The goal is to provide an integrated understanding of the environmental behavior of PLA MPs, their biological interactions, and their degradation potential, thereby contributing to a more comprehensive view of the ecological implications of bioplastics.

6.1 Feedback to the proposed research questions

Q.1. What are the effects of PLA MPs on overall coral health, including mortality, bleaching, and oxidative response?

The results indicate that short-term exposure to mechanically fragmented PLA MPs does not induce any detectable physiological alterations in corals. No mortality or signs of bleaching were observed, as further confirmed by the analysis of chlorophyll concentrations (Chl *a* and Chl c_2). Moreover, oxidative stress assessment revealed no evident activation of antioxidant responses following exposure (**Chapter 3**).

Q.2. Can PLA MPs interact with coral mucus and cilia? Can corals actively remove PLA MPs from the surrounding water?

Yes, coral cilia generate vortical currents capable of transporting particle-rich water toward the coral surface. Within this region, the particles are trapped by the mucus layer, which intercepts the vortices and promotes their aggregation within the mucus matrix. Importantly, statistical analyses revealed that corals actively facilitate the removal of PLA MPs from the surrounding water, acting as potential sinks for these particles (**Chapter 4**).

Q.3. Do different PLA MPs fabrication methods affect their susceptibility to enzymatic degradation?

Yes, different fabrication methods of PLA MPs can influence their susceptibility to enzymatic degradation. The fabrication process determines key physicochemical properties of the particles—such as morphology, crystallinity, and molecular weight—which in turn affect enzyme accessibility and degradation efficiency. The results clearly indicate that the effectiveness of enzymatic degradation depends on the microplastic fabrication method. Among the tested processes, dry milling produced particles that were more susceptible to enzymatic breakdown than those generated by other methodology.

This higher degradability can be attributed to their lower degree of crystallinity and the greater presence of monomeric components within the original polymer matrix, both of which increase the material's vulnerability to enzymatic attack. Consequently, even when produced from the same PLA source, differences in processing conditions can result in distinct degradation behaviors (**Chapter 5**).

Q.4. Which particle characteristics resulting from different fabrication processes determine the efficiency of enzymatic degradation?

The results indicate that particles with lower crystallinity are more susceptible to enzymatic attack, as amorphous regions are more easily degraded than highly ordered crystalline domains. Molecular weight also plays a key role: particles with lower molecular weight possess a greater number of chain ends and weaker intermolecular forces, making them more vulnerable to enzymatic cleavage. Therefore, this study demonstrates that the combined effects of crystallinity and molecular weight ultimately govern the susceptibility of PLA MPs to enzymatic degradation (**Chapter 5**).

6.2 General discussion and perspectives

This thesis provides an integrated assessment of PLA–derived MPs, from their production and characterization to their environmental interactions and degradation dynamics. The work contributes to bridging critical knowledge gaps regarding the environmental behavior of bioplastics, particularly those marketed as sustainable alternatives to conventional polymers.

Through the establishment of reproducible top-down fabrication protocols, this research demonstrates the feasibility of generating PLA MPs and NPs with environmentally relevant morphologies. These reference materials constitute valuable tools for future studies on the fate and biological effects of plastic contaminants under controlled conditions.

The exposure of *Pocillopora damicornis* to PLA MPs showed no signs of acute toxicity, mortality, or bleaching across the tested concentrations and duration. This outcome contrasts with the adverse responses commonly observed in corals exposed to synthetic plastics, indicating that bio-based polymers like PLA could have a comparatively milder impact on coral physiology. Complementary experiments on *Porites lutea* further revealed that corals play an active role in capturing and aggregating MPs through mucus secretion and ciliary movement. These findings indicate that coral reefs may act not only as vulnerable habitats but also as active sinks for microplastic particles, thereby influencing their distribution and accumulation in marine ecosystems.

Finally, the enzymatic degradation assays demonstrated that PLA MPs are susceptible to lipase enzyme, and in particular their degradation efficiency strongly depends on the physicochemical properties imparted by the fabrication method. This highlights that both the environmental fate and the potential biodegradability of PLA cannot be generalized, as particle characteristics such as crystallinity, molecular weight, and surface roughness significantly modulate degradation rates.

Overall, this work underscores the dual nature of bioplastics such as PLA: while offering a promising alternative to fossil-based polymers, they may still contribute to MPs pollution if improperly managed. The results emphasize the need for standardized protocols in particle production, and for further research on the long-term ecological implications of bioplastic-derived particles. Advancing our understanding of these processes is crucial for guiding the development of truly sustainable materials and for implementing effective strategies to mitigate plastic pollution in aquatic environments.

Looking ahead, future studies should extend this work to the nanoscale. Although technically more challenging, investigating the enzymatic degradation of PLA NPs would provide valuable insights into whether biodegradation remains effective at smaller particle sizes. In parallel, testing the effects of PLA NPs produced through the fabrication protocols developed in this thesis on corals would help determine whether nanosized fragments elicit similar or distinct physiological responses compared to MPs. Such research would be fundamental to better understand the environmental behavior, persistence, and potential risks associated with bioplastic-derived particles across different size scales.